Christoph Guger · Brendan Allison ·
Tomasz M. Rutkowski ·
Milena Korostenskaja  *Editors*

# Brain-Computer Interface Research

## A State-of-the-Art Summary 11

Springer

# SpringerBriefs in Electrical and Computer Engineering

SpringerBriefs present concise summaries of cutting-edge research and practical applications across a wide spectrum of fields. Featuring compact volumes of 50 to 125 pages, the series covers a range of content from professional to academic. Typical topics might include: timely report of state-of-the art analytical techniques, a bridge between new research results, as published in journal articles, and a contextual literature review, a snapshot of a hot or emerging topic, an in-depth case study or clinical example and a presentation of core concepts that students must understand in order to make independent contributions.

Christoph Guger • Brendan Allison •
Tomasz M. Rutkowski • Milena Korostenskaja
Editors

# Brain-Computer Interface Research

## A State-of-the-Art Summary 11

*Editors*
Christoph Guger
g.tec medical engineering GmbH
Schiedlberg, Oberösterreich, Austria

Brendan Allison
Cognitive Science Department
UC San Diego
La Jolla, CA, USA

Tomasz M. Rutkowski
RIKEN AIP
Tokyo Chuo-ku, Japan

Milena Korostenskaja
The Institute of Neuroapproaches
Winter Springs, FL, USA

Paper in this product is recyclable.

# Contents

# Brain-Computer Interface Research: A State-of-the-Art Summary 11

**Christoph Guger, Nuri Firat Ince, Milena Korostenskaja, and Brendan Z. Allison**

**Abstract** With brain-computer interfaces (BCIs), people can send information directly from their brains to computers. People can use BCIs to send messages or commands without moving. In 2010, we launched the Annual BCI Research Awards. People submit their projects to a jury that scores each project on many criteria and then selects the best projects from that year. This book contains project summaries written by most of the teams that were nominated for a BCI Research Award in 2022. Each annual book also contains introduction and discussion chapters written primarily by author BZA. This introduction chapter briefly overviews BCIs, the process and scoring criteria we use for each annual award, this year's jury, and the 12 projects that the jury nominated for an award.

**Keywords** Brain-computer interface · EEG · ECoG · BCI research awards · BCI foundation

## 1 Introduction

Brain-computer interface (BCI) systems are tools that allow people to send information just by thinking—without moving. Early BCIs were devoted to helping people with severe movement disabilities, but more recently, we've seen a lot of attention to mainstream BCIs from big companies like Neuralink and Facebook. As

C. Guger (✉)
g.tec medical engineering GmbH, Schiedlberg, Austria
e-mail: guger@gtec.at

N. F. Ince
Department of Biomedical Engineering, University of Houston, Houston, TX, USA

M. Korostenskaja
The Institute of Neuroapproaches, Orlando, FL, USA

B. Z. Allison
Cognitive Science Department, University of California at San Diego, San Diego, CA, USA

BCIs become more powerful, flexible, inexpensive, and practical, the future should see even more BCI research and BCI devices.

We've been organizing the Annual BCI Research Award every year since 2010 for a few reasons. Mainly, we want to recognize and reward the best BCI projects. The annual awards and book series provide tools that students and others can use to learn about different BCIs. We also want to publicize these projects and BCI research through the annual awards ceremony positive publicity, writing a book series that includes chapters about the nominated BCI projects, and other activities like our website.[1]

This book has a format similar to our prior books about each year's BCI Research Awards. The first chapter briefly describes BCIs and the procedures for each year's awards. Next, we present chapters written by the people responsible for the BCI projects that were nominated for a BCI Research Award in 2022. These chapters present background issues and challenges, their methods and results, and discussion.

## 2   What Is a BCI?

"A BCI is a communication system in which messages or commands that an individual sends to the external world do not pass through the brain's normal output pathways of peripheral nerves and muscles [1]." Instead, people perform mental activities like imagining movements or words while a system detects the brain signals associated with these mental activities. The BCI then translates these signals into commands for a speller, mobile robot, exoskeleton, or other device. Most BCIs help people with severe movement disability by replacing or restoring lost movements.

The "replace" function includes BCIs for control of prosthetic limbs or spelling systems [2–4]. Thus, people who are no longer able to perform different movements can replace some lost functions by using their brains to directly communicate and control devices. Early BCIs focused primarily on replacing functions that people lost due to Lou Gehrig's Disease, brainstem stroke, or other causes. Many such systems allowed users to slowly select letters by counting flashes or imagining movement. Newer work, such as the chapter from Metzger and colleagues, shows how BCIs can detect imagined letters or words, allowing them to literally "think and spell." [5, 6].

Other BCIs help restore lost movements, such as helping to restore movements lost due to a stroke [7–9]. These BCIs help people regain the ability to move, such as regaining the ability to grasp or walk. In this approach, patients typically participate in therapy with a licensed therapist for 2–3 sessions per week for about 10 weeks. This book includes chapters with new directions in BCIs for movement restoration [10].

---

[1] https://www.bci-award.com

BCIs are becoming better and better known for applications beyond helping patients, such as gaming or relaxation for mainstream users. High-profile BCI activities from Neuralink and Facebook have gained attention, and dozens of companies now sell consumer BCIs. During COVID, online schools and web-based training resources became more prominent. With the decline of COVID concerns, in-person activities like university classes about BCIs, BCI hackathons, and BCI conferences have returned.[2] The chapters in this book present several different types of BCIs that should interest students, teachers, makers, futurists, manufacturers, business experts and others.

## 3   The Annual BCI Research Award

The BCI Award Foundation organizes the Annual BCI Research Award. Drs. Christoph Guger and Dean Krusienski are both presidents of the BCI Award Foundation, which was founded in 2017. Figure 1 shows the two presidents and the other Board Members of the BCI Award Foundation. The BCI Research Award is open to researchers or teams (excluding members of the jury) around the world. Different projects have involved various combinations of hardware, software, algorithms, methods, and other components. The prizes were provided by the Austrian company g.tec medical engineering (author CG is the CEO) and IEEE Brain.

The awards procedure this year followed a procedure like prior years:

1. The BCI Award Foundation selects a Chairperson of the Jury from a top BCI research institute.
2. The Chairperson selects a jury of international BCI experts to evaluate all projects submitted for the Award.
3. The Award website[3] announces instructions, scoring criteria, and the submission deadline for projects.
4. After the deadline, the jury members judge each submitted project.
5. The jury chooses the nominees and the first, second, and third place winners.
6. The Award website announces the nominees, and we invite them to that year's Awards Ceremony within a major BCI conference.
7. At the Awards Ceremony, we announce the winners, provide prizes, and thank the jury and the conference organizers.

For the first several years of the BCI Research Award, each submission was a project description of up to two pages. We added another requirement to the submissions in 2018: a video with a 2-min project overview.

---

[2]https://bcisociety.org/bci-meeting/

[3]https://www.bci-award.com

Christoph Guger (AT)

President
g.tec medical engineering GmbH

Dean J. Krusienski (US)

Co-President
Virginia Commonwealth University

Tomasz M. Rutkowski (JP)

Treasurer
RIKEN AIP

Mikhail Lebedev (US)

Ambassador
Duke University Medical Center

Jing Jin (CN)

Ambassador
East China University of Science and
Technology

Nuri Firat Ince (US)

Ambassador
University of Houston

Brendan Allison (US)

Chief Editor, Book Series
University of California San Diego

Milena Korostenskaja (US)

Podcast Host
The Institute of Neuroapproaches

**Fig. 1** The BCI Award Foundation has eight board members. All of the board members have been active in BCI research for at least 15 years

The 2022 jury was chaired by Professor Nuri Firat Ince from University of Houston. The 2022 jury included Nicolas Opie, who won the 2021 BCI Research Award. The complete 2022 jury was (Fig. 2):

The scoring criteria that the jury used to select the nominees and winners were the same as all previous BCI Research Awards:

- Does the project include a novel application of the BCI?
- Is there any new methodological approach used compared to earlier projects?
- Is there any new benefit for potential users of a BCI?
- Is there any improvement in terms of speed of the system (e.g. bit/min)?
- Is there any improvement in terms of accuracy of the system?
- Does the project include any results obtained from real patients or other potential users?
- Is the used approach working online/in real-time?
- Is there any improvement in terms of usability?
- Does the project include any novel hardware or software developments?

After all of the jury members have scored all of the projects, the 12 projects with the highest scores are nominated for an award. These nominations are announced

Nuri Firat Ince
Chair 2022
University of Houston, USA

Nicolas Opie
Winner 2021
Synchron Inc., AU

Cynthia Chestek
University of Michigan, USA

Dora Hermes
Mayo Clinic, USA

Guiseppe Pellizer
University of Minnesota, USA

David Moses
University of California, San Francisco, USA

Abdelkader N. Belkacem
United Arab Emirates University, UAE
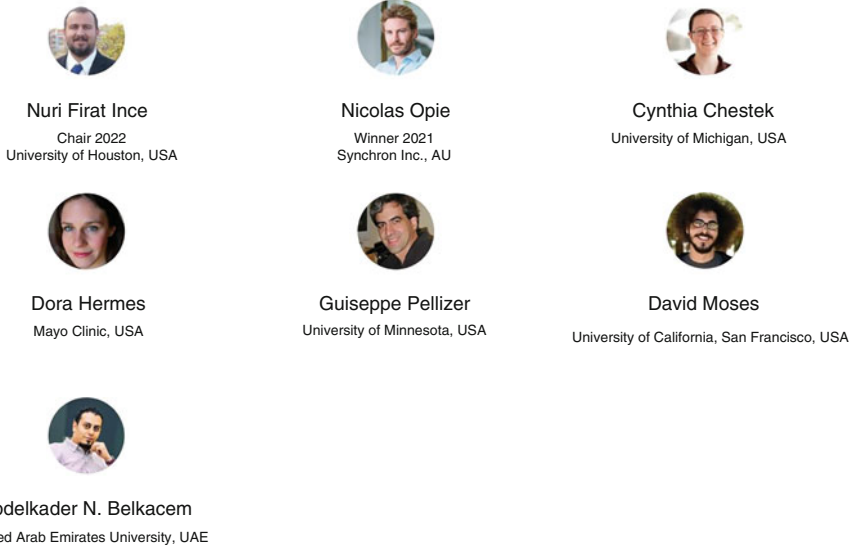
**Fig. 2** The jury for the 2022 BCI Research Award

through the BCI Award website and other means, and we invite the nominees to the Awards Ceremony.

Last year, the Awards Ceremony occurred online as part of the virtual IEEE Systems, Man, and Cybernetics conference on October 11, 2022 in Prague. We began hosting these ceremonies online with IEEE conferences in 2020 due to COVID. Before then, the ceremonies occurred in person, usually attached to a BCI Meeting or BCI conference with author BZA as the main emcee. The 2022 Ceremony included a friendly introduction by Dr. Guger, announcement of the nominees and winner, and videos or statements from some nominees (including brief interviews).

The 2020 Award Ceremony occurred online as part of the virtual IEEE Systems, Man, and Cybernetics conference organized in Toronto, Canada from October 11–14, 2020. The 2021 Award Ceremony was held along with the IEEE SMC 2021 in Melbourne, Australia from October 17–20, 2021. These conferences, like the 2022 IEEE SMC conference, had a lot of other BCI-related activities. including several BMI sessions and BR41N.IO hackathon.

The jury was asked to choose winners for first, second, and third place. We announced that these winners would receive $3000, $2000, and $1000, respectively, in addition to a certificate and other prizes. The authors of the winning project were also asked to contribute to this book by writing a chapter, and/or joining us for an interview, about their project and related work.

We recently added a new opportunity. We invited all nominees for a podcast interview by the Institute of Neuroapproaches.[4] This organization, managed by jury member Dr. Milena Korostenskaja, conducts podcasts along with education and consulting. Drs. Guger, Krusienski, and Allison from the BCI Foundation and former BCI Research Award winner Tomasz Rutkowski contributed to a podcast about the BCI Research Awards earlier this year.[5]

## 4   The BCI Research Award Book Series

The following section includes the timeline for the annual Award that ends with the announcement of the winners at the Awards Ceremony. That's when the work on these books begins:

1. We tell the nominees what we need in each chapter. We encourage images, reports about their newest research future directions, and discussion in addition to project details.
2. Read the project summary chapters when the authors submit them to us.
3. Edit the chapters as needed. Aside from fixing mistakes, we want chapters to be informative and clear.
4. Correspond with the authors to ask for clarification or new text, check on changes, get new references or figures, check copyright issues, and other details.
5. Develop the introduction and conclusion chapters.
6. Submit all chapters to the publisher.
7. The publisher then reviews the chapters and sends them to a typesetter.
8. A few months later, the typesetter sends us the proofs, which we share with the chapter authors.
9. Submit any corrections to the proofs and ask the publisher to finalize the book.

The book is always edited by a couple of people: Drs. Guger and Allison from the BCI Award Foundation, and the chair of the jury from that year. This year, our jury chair and co-author is Prof. Nuri Firat Ince from the University of Houston. Additionally, we invited Milena Korostenskaja, our podcast host, to edit the book with us. These four people are also responsible for the introduction and discussion chapters.

---

[4] https://www.neuroapproaches.org/

[5] https://www.neuroapproaches.org/podcast/episode/2810e9a1/bci-award-tips-and-tricks-from-the-pros-drs-guger-krusienski-rutkowski-and-allison

# 5    Projects Nominated for the BCI Award 2022

Twelve submissions with the highest scores were nominated for the BCI Research Award 2022. These 12 projects, followed by authors and affiliations, were:

**A High-Performance Intracortical Speech BCI**

Francis R. Willett[1,2], Chaofei Fan[1], Erin Kunz[1], Donald T. Avansino[1], Foram Kamdar[1], Leigh R. Hochberg[3], Krishna V. Shenoy[1,2], Jaimie M. Henderson[1]

*1 Stanford University, USA*

*2 Howard Hughes Medical Institute, USA*

*3 Brown University, Harvard Medical School, Massachusetts General Hospital, Providence VA Medical Center, USA*

**Digital Bridge To Restore Voluntary Control Of Leg Movements After Paralysis**

Andrea Galvez [1,2,3], Guillaume Charvet[4], Jocelyne Bloch[1,2,3], Grégoire Courtine[1,2,3], Henri Lorach[1,2,3]

*1 NeuroX Institute, School of Life Sciences, Ecole Polytechnique Fédérale de Lausanne (EPFL), Geneve, Switzerland*

*2 Department of Clinical Neuroscience, Lausanne University Hospital (CHUV) and University of Lausanne (UNIL), Lausanne, Switzerland*

*3 NeuroRestore, Defitech Center for Interventional Neurotherapies, EPFL/CHUV/ UNIL, Lausanne, Switzerland*

*4 University Grenoble Alpes, CEA, LETI, Clinatec, Grenoble, France*

**Highly Generalizable Spelling Using a Silent-Speech BCI in a Person With Severe Anarthria**

Sean L. Metzger[1,2,3], Jessie R. Liu[1,2,3], David A. Moses[1,2], Maximilian E. Dougherty[1], Margaret P. Seaton[1], Kaylo T. Littlejohn[1,2,4], Josh Chartier[1,2], Gopala K. Anumanchipalli[1,2,4], Adelyn Tu-Chan[5], Karunesh Ganguly[2,5], Edward F. Chang[1,2,3]

*1 Department. of Neurological Surgery University of California, San Francisco (UCSF), USA*

*2 Weill Institute for Neurosciences UCSF, USA*

*3 University of California, Berkeley-UCSF Grad. Program in Bioengineering, USA*

*4 Department. of Electrical Engr. and C.S., University of California, Berkeley, USA*

*5 Department of Neurology, UCSF, USA*

**Fast, Accurate, Unsupervised, and Time-Adaptive EEG-Based Auditory Attention Decoding For Neuro-Steered Hearing Devices**

Simon Geirnaert[1,2,3], Rob Zink[1,3], Tom Francart[2,3], Alexander Bertrand[1,3]

*1 STADIUS Center for Dynamical Systems, Signal Processing and Data Analytics, Department of Electrical Engineering (ESAT), KU Leuven, Belgium*

*2 ExpORL, Department of Neurosciences, KU Leuven, Belgium*

*3 Leuven.AI - KU Leuven institute for AI, Leuven, Belgium*

## Remediating Phonological Deficits in Dyslexia With Brain-Computer Interfaces

João Araújo[1], Benjamin D. Simons[2], Usha Goswami[1]

1 *Centre for Neuroscience in Education, Department of Psychology, University of Cambridge, Cambridge, United Kingdom*
2 *Department of Applied Mathematics and Theoretical Physics, University of Cambridge, Cambridge, United Kingdom*

## Brain-Body Interfaces To Assist and Restore Motor Functions In People With Paralysis

Elena Losanno[1], Marion Badi[2], Evgenia Roussinova[2], Andrew Bogaard[3], Maude Delacombaz[3], Solaiman Shokur[2], Silvestro Micera[1,2]

1 *The Biorobotics Institute and Department of Excellence in Robotics and AI, Scuola Superiore Sant'Anna, 56025 Pisa, Italy*
2 *Bertarelli Foundation Chair in Translational Neuroengineering, Center for Neuroprosthetics and Institute of Bioengineering, École Polytechnique Fédérale de Lausanne (EPFL), 1015 Lausanne, Switzerland*
3 *Department of Neuroscience and Movement Sciences, Platform of Translational Neurosciences, Section of Medicine, Faculty of Sciences and Medicine, University of Fribourg, 1700 Fribourg, Switzerland*

## Real-time Decoding of Leg Motor Function and Dysfunction From the Subthalamic Nucleus in Parkinson's Patients

Kyuhwa Lee[3], Yohann Thenaisie[1,2], Charlotte Moerman[1,2], Stefano Scafa[1,2,4], Andrea Gálvez[2,5], Elvira Pirondini[1,6,7], Morgane Burri[2,5], Jimmy Ravier[2,5], Alessandro Puiatti[4], Ettore Accolla[8], Benoit Wicki[9], André Zacharia[10,11,12], Mayte Castro Jiménez[11], Julien F. Bally[11], Grégoire Courtine[1,2,5,13], Jocelyne Bloch[1,2,5,13], Eduardo Martin Moraud[1,2]

1 *Department of Clinical Neurosciences, Lausanne University Hospital (CHUV) and University of Lausanne (UNIL), Lausanne CH-1011, Switzerland*
2 *NeuroRestore, Defitech Centre for Interventional Neurotherapies, CHUV, UNIL, and Ecole Polytechnique Fédérale de Lausanne (EPFL), Lausanne CH-1011, Switzerland*
3 *Wyss Center for Bio and Neuroengineering, Geneva CH-1202, Switzerland*
4 *Institute of Digital Technologies for Personalized Healthcare (MeDiTech), University of Southern Switzerland (SUPSI), Lugano-Viganello CH-6962 Switzerland*
5 *Faculty of Life Sciences, EPFL, NeuroX Institute, Lausanne CH-1015, Switzerland*
6 *Department of Physical Medicine and Rehabilitation, University of Pittsburgh, Pittsburgh 15213, PA, USA*
7 *Rehabilitation and Neural Engineering Labs, University of Pittsburgh, Pittsburgh 15213, PA, USA*
8 *Department of Neurology, Hôpital Fribourgeois, Fribourg University, Fribourg CH-1708, Switzerland*
9 *Department of Neurology, Hôpital du Valais, Sion CH-1951, Switzerland*

10 Clinique Bernoise, Crans-Montana CH-3963, Switzerland

11 Department of Neurology, Lausanne University Hospital (CHUV) and University of Lausanne, Lausanne CH-1011, Switzerland

12 Department of Medicine, University of Geneva, Geneva CH-1201, Switzerland

13 Department of Neurosurgery, Lausanne University Hospital (CHUV) and University of Lausanne, Lausanne CH-1011, Switzerland

**Real-Time Intraoperative Sensorimotor Cortex Localization and Consciousness Assessment With the Spatial and Spectral Profile Of the Median Nerve Somatosensory Evoked Potentials**

Priscella Asman[1], Giuseppe Pellizzer[2], Sujit Prabhu[3], Sudhakar Tummala[3], Shreyas Bhavsar[4], Israt Tasnim[1], Matthew J. Hall[1], Nuri F. Ince

1 Clinical Neural Engineering Lab, Biomedical Engineering Department, University of Houston, Houston, TX, USA

2 Research Service, Minneapolis VA Health Care System, Departments of Neurology and Neuroscience, University of Minnesota, Minnesota, MN, USA

3 Department of Neurosurgery, University of Texas MD Anderson Cancer Center, Houston, TX, USA

4 Department of Anesthesiology, University of Texas MD Anderson Cancer Center, Houston, TX, USA

**Closed-loop control of images based on electrocorticogram decoding in visual semantic space**

Ryohei Fukuma[1,2,3], Takufumi Yanagisawa[1,2,3,4], Shinji Nishimoto[5,6], Hidenori Sugano[7], Kentaro Tamura[8], Shota Yamamoto[1], Yasushi Iimura[7], Yuya Fujita[1], Satoru Oshino[1], Naoki Tani[1], Naoko Koide–Majima[5,6], Yukiyasu Kamitani[2,9], Haruhiko Kishima[1,4]

1 Department of Neurosurgery, Graduate School of Medicine, Osaka University, Suita, Japan

2 ATR Computational Neuroscience Laboratories, Seika-cho, Japan

3 Institute for Advanced Co-Creation Studies, Osaka University, Suita, Japan

4 Osaka University Hospital Epilepsy Center, Suita, Japan

5 Center for Information and Neural Networks (CiNet), National Institute of Information and Communications Technology (NICT), Suita, Japan

6 Graduate School of Frontier Biosciences, Osaka University, Suita, Japan

7 Department of Neurosurgery, Juntendo University, Tokyo, Japan

8 Department of Neurosurgery, Nara Medical University, Kashihara, Japan

9 Graduate School of Informatics, Kyoto University, Kyoto, Japan

**Designing Touch: Intracortical Neurohaptic Feedback in Virtual Reality**

Courtnie J. Paschall[1], Jason S. Hauptman[2], Rajesh P.N. Rao[3], Jeffrey G. Ojemann[2,4], Jeffrey Herron[4]

1 University of Washington, Dept. of Bioengineering, USA

2 Seattle Children's Hospital, Neurological Surgery, USA

*3 University of Washington, Paul G. Allen School of Computer Science, USA*
*4 University of Washington, Dept. of Neurological Surgery, USA*

**A Multimodal Brain-Computer Interface Approach Using Muscle Responses to Transcranial Magnetic Stimulation Of the Brain**
Kathy Ruddy, Colin Simon
*Trinity College Institute of Neuroscience, Dublin, Ireland*

**May the Force Be With You: Biomimetic Grasp Force Decoding For Brain Controlled Bionic Hands**
Elizaveta V. Okorokova[1], Anton R. Sobinov[2], John E. Downey[2], Qinpu He[1], Ashley van Driesche[2], David Satzer[4], Peter C. Warnke[3,4], Nicholas G. Hatsopoulos[1,2,3], Sliman J. Bensmaia[1,2,3]

*1 Committee on Computational Neuroscience, University of Chicago, Chicago, IL, USA*
*2 Department of Organismal Biology and Anatomy, University of Chicago, Chicago, IL, USA*
*3 Neuroscience Institute, University of Chicago, Chicago, IL, USA*
*4 Department of Neurological Surgery, University of Chicago, Chicago, IL, USA*

In addition, we posted videos from some of the nominated projects on the BCI Award website. Each video was developed by the team behind the project submission. Aside from learning more about the projects, you can also see and hear some of the people behind each project and get a sense of what different BCI research labs look like. Most videos last about 2 min and include:

• Clips of the BCI system in operation;
• Graphics, animations, and text to illustrate system components, procedures, and project results;
• Commentary from patients and project developers;
• Logos from the institutes where projects were executed; and/or
• Supporting references.

# 6   Summary

This book is about the 2022 Annual BCI Research Award. The next several chapters feature project descriptions based on the projects that were nominated for the BCI Research Award this year. Each chapter addresses how the system measures information from the brain, including different types of implanted and non-implanted approaches, such as EEG, ECoG, or MEG. Each project also describes the signal translation and outputs, such as a speller on a monitor, prosthetic limb, or exoskeleton. Most chapters report BCIs for patient applications, including BCI systems that could restore touch, movement, communication, or freedom from epilepsy. The concluding chapter presents the winners of the 2022 BCI Research Awards, shares

some information about next year's awards, and features some discussion. Next year's awards will feature some changes in sponsors and other minor details, along with the new jury. However, we will not change the submission procedure, award criteria, or number of nominees and winners in the 2023 BCI Research Award.

# References

1. Wolpaw JR, Birbaumer N, McFarland DJ, Pfurtscheller G, Vaughan TM (2002) Brain–computer interfaces for communication and control. Clin Neurophysiol 113(6):767–791
2. Abiri R, Borhani S, Sellers EW, Jiang Y, Zhao X (2019) A comprehensive review of EEG-based brain–computer interface paradigms. J Neural Eng 16(1):011001
3. Allison BZ, Kübler A, Jin J (2020) 30+ years of P300 brain-computer interfaces. Psychophysiology:e13569
4. Wolpaw JR, Wolpaw EW (2012) Brain-computer interfaces: something new under the sun. Brain-Comput Interfaces Principles Pract 14
5. Angrick M, Luo S, Rabbani Q, Candrea DN, Shah S, Milsap GW, ... Crone NE (2023) Online speech synthesis using a chronically implanted brain-computer interface in an individual with ALS. medRxiv, 2023-06
6. Metzger SL et al (2023) Highly generalizable spelling using a silent-speech BCI in a person with severe anarthria. In: Guger C, Allison B, Rutkowski TM, Korostenskaja M (eds) Brain-computer interface research. Springer, Heidelberg
7. Biasiucci A, Leeb R, Iturrate I, Perdikis S, Al-Khodairy A, Corbet T, Millán JDR (2018) Brainactuated functional electrical stimulation elicits lasting arm motor recovery after stroke. Nat Commun 9(1):1–13
8. Pichiorri F, Toppi J, de Seta V, Colamarino E, Masciullo M, Tamburella F et al (2023) Exploring high-density corticomuscular networks after stroke to enable a hybrid Brain-Computer Interface for hand motor rehabilitation. J NeuroEng Rehab 20(1):5
9. Sebastián-Romagosa M, Cho W, Ortner R, Murovec N, Von Oertzen T, Kamada K et al (2020) Brain computer interface treatment for motor rehabilitation of upper extremity of stroke patients—a feasibility study. Front Neurosci 14
10. Ruddy KL et al (2023) Keeping our eyes on the prize; Are we losing sight of the 'why' in BCI for neurorehabilitation? In: Guger C, Allison B, Rutkowski TM, Korostenskaja M (eds) Brain-computer interface research. Springer, Heidelberg

# Remediating Phonological Deficits in Dyslexia with Brain-Computer Interfaces

**João Araújo, Benjamin D. Simons, and Usha Goswami**

**Abstract** BCIs offer science-based interfaces for human enhancement, enabling people to improve cognitive skills that may be difficult for them to learn. Here, we design a non-invasive EEG-BCI relying on auditory inputs and visual feedback to optimise brain patterns related to phonology (speech-sound) and reading deficits in children with dyslexia. Drawing from a decade of dyslexia neuroscience research on perceptive 'temporal sampling' along with computational modelling of EEG collected from over 100 children, we engineered a decoder for online BCI control. We designed an engaging interface aimed at teaching children how to self-regulate neural oscillatory patterns related to phonological difficulties in dyslexia, using a range of ideas derived from competition-winning motor imagery paradigms to BCIs for aircraft control.

## 1 Introduction

Non-invasive BCIs—based on EEG—have seen their usage rise in the last decade with applications ranging from flight control of drones [1] to the control of robotic arm prosthetics [2], previously assumed to be achievable only by using invasive neuroimaging techniques. Non-invasive BCIs have also been used in the rehabilitation of stroke and traumatic brain injury patients, showing promising results in restoring cognitive skills. Non-invasive BCIs have, however, rarely been used in the context of neurodevelopmental disorders such as dyslexia. Developmental dyslexia effects between 3% and 7% of the population and is primarily characterised

J. Araújo (✉) · U. Goswami
Centre for Neuroscience in Education, Department of Psychology, University of Cambridge, Cambridge, UK
e-mail: ja683@cam.ac.uk

B. D. Simons
Department of Applied Mathematics and Theoretical Physics, University of Cambridge, Cambridge, UK

by difficulties in reading and spelling, related to phonological (speech-sound) difficulties present from birth [3]. Previous intervention studies [4] found that neurofeedback protocols aiming to increase channel coherence for the alpha band were successfully learned by dyslexic children and were linked to improvement of spelling. Other studies have used different band ratios and at least one clinical trial has been registered to tackle hemispheric imbalances seen in dyslexic children in certain frequency bands [5]. Neurofeedback paradigms and tools have also been proposed [6], tackling speech-brain entrainment—a neural mechanism atypical in dyslexia and related to phonological impairments.

While this growing body of work is certainly encouraging, there are some limitations in the literature that can make it difficult to assess how effective BCI-based interventions are in remediating the atypical cognitive profiles of dyslexia. These limitations include very low EEG channel counts (e.g., two channels), small sample size and heterogeneity of participant inclusion criteria across studies. In our view, greater success is likely if a theory- and data-driven decoder could be developed, utilising a simple paradigm that is easy to learn across multiple sessions. With this in mind, we designed a novel intervention that aims to leverage concepts from both auditory and phonological theories of dyslexia [3], as well as from the most recent advances in BCI research.

## 2    Operant Learning BCI for Dyslexia

### 2.1    Overview

If there is an association between oscillatory brain patterns and reading/phonology difficulties, being able to change the characteristics of these oscillations might ameliorate the typical cognitive symptoms in dyslexia. Therefore, we created a non-invasive BCI targeting the self-regulation of these oscillations. We drew inspiration from BCIs developed for prosthetic limb control, drone flight and silent speech decoding—creating a closed-loop operant learning BCI for dyslexia. For the decoder, we relied on a body of experimental and theoretical work based on the Temporal Sampling theory (see below). Figure 1 shows an illustration of the BCI setup.

For the participant, the goal is to learn the BCI control of a spaceship shown on the screen—making it ascend as far as possible on the gaming window in each session. Participants receive a stronger visual reinforcement (green glow) the higher they make the spaceship go. No reinforcement is given if the spaceship's position is below a threshold line located across the middle of the game window. Listening to the audio signal of a story as input, the participant is encouraged to use cognitive strategies focused on auditory processing to modulate their oscillatory patterns that will control the spaceship. The spaceship's position is estimated via real-time classification of time-series EEG data using a pre-trained signal processing and
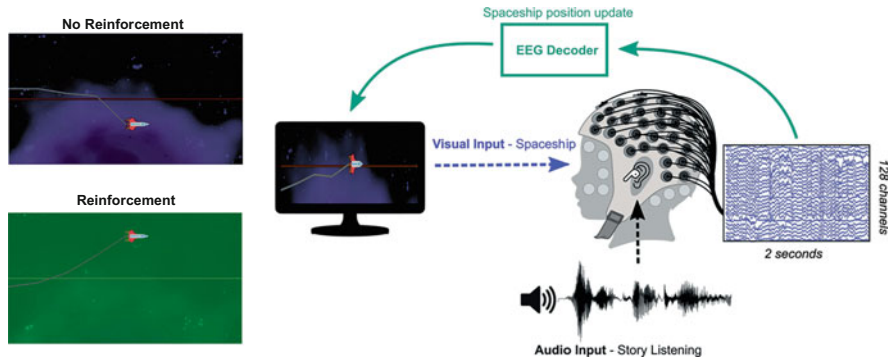
**Fig. 1** Illustration of the new Operant-Learning BCI setup for dyslexia: The participant controls a spaceship cursor with their oscillations. An audio stream of a story is presented throughout the session to allow for top-down cognitive strategies focused on auditory processing. A visual green glow is also shown as a reinforcement whenever the participant is able to "lift" the ship above a threshold line (bottom left)

machine learning model. This feedforward model shows minimal computational overhead, allowing for smooth online control of the BCI with minimal lags.

## 2.2 Decoder Design Based on the Temporal Sampling Theory

Dyslexia is primarily diagnosed on the basis of difficulties in reading and spelling once schooling begins. However, at-risk children show atypical processing of phonology (the sound structure of speech) from infancy. Across languages, children with dyslexia show impairments in processing the speech amplitude envelope (i.e., lower-frequency amplitude modulations) [7] and rise times (i.e., speech "edges"), with associated difficulties in processing speech rhythm [8]. It has been hypothesized that these difficulties are related to atypical neural oscillatory responses to the speech envelope for children: Temporal Sampling theory [9–11]. Subsequent EEG studies with dyslexic children have shown a relationship between accurate neural encoding of the speech envelope and prosodic awareness [12], as well as differences in neural entrainment (i.e., brain-stimulus synchronisation) to rhythmic audio-visual inputs [13]. Recent modelling of EEG collected during passive listening tasks from 113 British and Australian children found distinctive differences in dynamic cortical representations of speech input in children with dyslexia for the delta and theta frequency bands, using different speech perception tasks [14].

Here we use this previous body of research to create a biologically-relevant and theory-driven decoder for our BCI. To achieve this, we aimed to derive a single-trial metric that could effectively distinguish neurotypical and dyslexic EEG patterns and could be estimated in close-to real-time. Previous approaches to single-trial EEG classification of dyslexia have also drawn inspiration from temporal sampling

theory. These approaches try to model EEG features using auto-encoders for anomaly detection [15], CNNs [16] and SVMs [17], with different degrees of success (0.6–0.9 AUC). Some of these models show good accuracies and most of them would add a relatively small delay to a BCI system if they were doing real-time feedforward prediction of an EEG segment. The problem, however, is that most of these models work with features that can potentially take a long time to engineer (such as graph-based connectivity features) and/or are not straightforward to interpret, despite deriving originally from bandpass-filtered signals (like fractal-based features). While these models can work well for offline classification, it is not yet known whether a decoder based on these complex EEG features could be learned easily by a human participant. Accordingly, our decoder is based on a linear SVM applied to an EEG signal that is both spatially- and temporally-filtered—in accordance with the classifier we recently built [14], which showed 80% accuracy and 0.77 AUC. Specifically, we choose a bandpass filter to isolate the delta band (Butterworth filter of order 4, 1–4 Hz) and we estimate the best spatial weights of our channels using Common Spatial Patterns—CSP; a technique frequently used in the motor imagery literature (see [18] for an overview). Both the SVM weights and CSP filters used in our BCI are also previously estimated from [14], enabling us to leverage previously-collected EEG datasets featuring children with dyslexia to create the decoder. Since these model weights and features were estimated for a dataset where the participants were watching a cartoon, we kept the audiovisual nature of the task intact on our BCI design.

### 2.3 From Signal Classification to Feedback

Although our decoder is based on a classifier, its main output for this BCI should not be binary per se. Instead, we want to provide an easily-accessible quantitative feedback on how close participants are to the goal at each point in time to maximize the outcome of the BCI learning process. To achieve this goal, we created a controller that allows a spaceship to travel continuously on the screen (rather than in a binary way or in a stepwise fashion). To achieve this, we revised our original EEG single-trial CSP-SVM classifier:

$$\text{classification}(x) = sign\left[W^T var\left(S^T x\right) + b\right]$$

to the following:

$$\text{position}(x) = \sigma\left[W^T var\left(S^T x\right) + b\right]$$

$$\sigma(z) = 1/(1 + exp[-\lambda_1(z - \lambda_2)])$$

Here $x$ represents a bandpass-filtered window of EEG data at some timepoint $t$, $W$ and $b$ represent the pre-trained weights and bias units, respectively, of the linear

SVM model, and $S$ denotes the matrix of pre-trained spatial filters on which to project the EEG data. We apply a logistic activation function instead of *sign* to generate a continuous position on the screen, so that the spaceship would be placed at the bottom or top of the gaming window if the position is closer to 1 or 0 respectively. Conveniently, if at a certain timepoint our EEG classification lies close to the classification hyperplane (i.e., $W^T \, var \, (S^T x) + b \approx 0$), this results in a position estimation around the center of the screen (i.e., $\approx 0.5$). This means that the threshold line drawn in the middle of the gaming window is also a low-dimensional representation of the SVM classification hyperplane.

To implement the decoder, we further need to take into account the fact that different participants may show patterns with higher or lower positional variances around the classification hyperplane. Some of our participants might not be able to reach high-confidence non-dyslexic EEG patterns while others may find their brain patterns are always very confidently classified as non-dyslexic. To account for these potential issues, we add two corrective parameters: $\lambda_1$ changes the slope of the sigmoid function, which in practice defines how much the position will change on the screen given some change in the distance between the EEG window feature space and the classification hyperplane. This correction is particularly useful, as it does not change the classification (i.e., the sign of the classification is unaltered) and can be extremely helpful to improve the user experience for participants with very low or very high variances on their SVM output. The second parameter, $\lambda_2$, allows for a potential bias regarding the participant's ability to reach the different sides of the hyperplane, i.e., where they cannot reach either a "dyslexic" or "non-dyslexic" classification—to avoid ceiling/floor effects on the BCI. This parameter does require an obvious trade-off between the BCI experience and classification accuracy. However, in the case of a participant with a strong pattern of dyslexia classification, this parameter can be progressively set to a lower value as the participant gets better at the task. Figure 2 illustrates how these two $\lambda$ parameters change the spaceship position estimation.

Both corrective parameters are estimated on a participant-by-participant basis using their data from short baseline runs. The full signal processing pipeline is shown below on Fig. 3.

## 2.4   Pilot Data and Validation

Currently, the BCI software has already been coded and we are running some pilot usability tests with adult participants before testing children. These pilot studies will also help to optimize the final interface and to decide the best way to estimate the control parameters for the decoder. The eventual target participants are children aged 8–12 years old—children with dyslexia (experimental group) and without dyslexia (control group). Each pilot participant will perform 10 sessions of this protocol (1 session/day across 2 weeks, excluding weekends). To assess the cognitive effectiveness of this paradigm, we plan to compare phonology and reading metrics
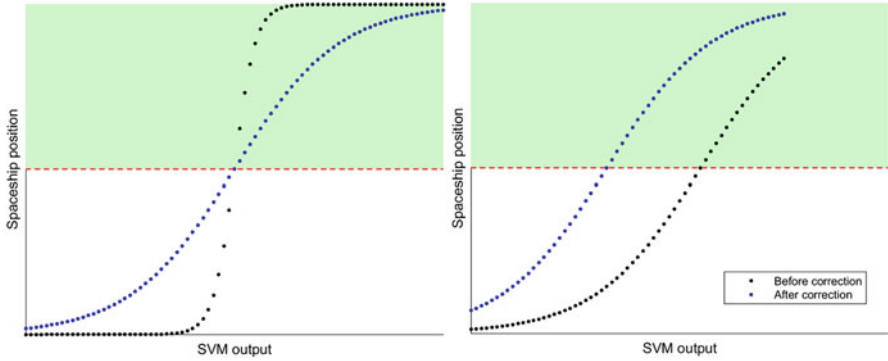
**Fig. 2** Influence of the $\lambda$ parameters on the spaceship position estimation: On the left, we have an example of a participant with a high variance of the SVM output (but no classification bias), leading most of its estimated spaceship positions to be very close to both the lower and upper corner of the screen (black dots). However, if we apply a positive $\lambda_1$ correction term to the classifier ($<1$ in the case of high variance and $>1$ in the case of low variance), we can control the slope of this position, leading to a better BCI experience. Similarly, when we have a participant who is consistently classified as dyslexic or control, we can apply the $\lambda_2$ correction term that allows for a more balanced distribution of the spaceship position. On both figures, the dashed red line refers to the threshold of the desirable (i.e., non dyslexic classification) spaceship position
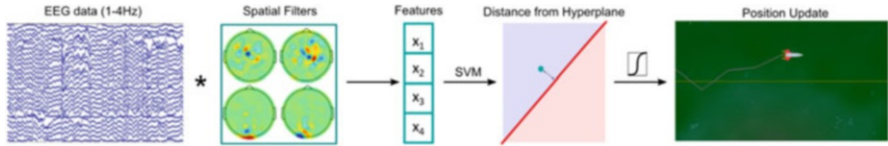


**Fig. 3** Signal processing pipeline to estimate the spaceship's position in real-time: The bandpass-filtered EEG signal is projected in a few pre-trained CSP spatial filters and its variance becomes the classifier's feature space. Once the pre-trained model is applied to these features, the distance from these projected features and the classification hyperplane is "squashed" into a sigmoid—defining the final position of the spaceship

taken before the first BCI session and after the last BCI session. As the cortical dynamics being targeted should only improve phonology and reading, we will also test arithmetic reasoning at the start and end of the protocol as a control. If the intervention is successful, a relationship between BCI performance and phonology/ reading performance is expected.

# References

1. Fricke T et al (2015) Brain control of horizontal airplane motion-a comparison of two approaches. In: AIAA atmospheric flight mechanics conference
2. Edelman BJ et al (2019) Noninvasive neuroimaging enhances continuous neural tracking for robotic device control. Sci Robot 4(31):eaaw6844

3. Goswami U (2022) Theories of developmental dyslexia. In: Skeide M (ed) The Cambridge handbook of dyslexia and dyscalculia. Cambridge University Press, pp 5–24
4. Breteler MH et al (2010) Improvements in spelling after QEEG-based neurofeedback in dyslexia: a randomized controlled treatment study. Appl Psychophysiol Biofeedback 35(1): 5–11
5. Vanutelli ME, Lucchiari C, Antonietti A (2021) Using neurofeedback to restore inter-hemispheric imbalance: a study protocol for adults with dyslexia. Front Psychol:5158
6. Carrera Arias FJ, Molinaro N, Lizarazu M (2021) Real-time EEG neurofeedback as a tool to improve neural entrainment to speech. bioRxiv:2021.04.19.440176
7. Di Liberto GM et al (2018) Atypical cortical entrainment to speech in the right hemisphere underpins phonemic deficits in dyslexia. Neuroimage 175:70–79
8. Goswami U et al (2002) Amplitude envelope onsets and developmental dyslexia: a new hypothesis. Proc Natl Acad Sci 99(16):10911–10916
9. Goswami U (2011) A temporal sampling framework for developmental dyslexia. Trends Cognitive Sci 15(1):3–10
10. Goswami U (2015) Sensory theories of developmental dyslexia: three challenges for research. Nat Rev Neurosci 16(1):43–54
11. Goswami U (2022) Language acquisition and speech rhythm patterns: an auditory neuroscience perspective. Royal Society Open Science
12. Power AJ et al (2016) Neural encoding of the speech envelope by children with developmental dyslexia. Brain Lang 160:1–10
13. Power AJ et al (2013) Neural entrainment to rhythmic speech in children with developmental dyslexia. Front Hum Neurosci 7:777
14. Araújo J et al (2022) Atypical cortical encoding of speech identifies children with Dyslexia versus Developmental Language Disorder. bioRxiv:2022.10.26.513864
15. Ortiz A et al (2020) Dyslexia diagnosis by eeg temporal and spectral descriptors: an anomaly detection approach. Int J Neural Syst 30(07):2050029
16. Ortiz A et al (2020) Dyslexia detection from EEG signals using SSA component correlation and convolutional neural networks. Springer International Publishing, Cham
17. Gallego-Molina NJ et al (2022) Complex network modelling of EEG band coupling in dyslexia: an exploratory analysis of auditory processing and diagnosis. Knowl Based Syst:108098
18. Blankertz B et al (2007) Optimizing spatial filters for robust EEG single-trial analysis. IEEE Signal Process Mag 25(1):41–56

# Highly Generalizable Spelling Using a Silent-Speech BCI in a Person with Severe Anarthria

**Sean L. Metzger, Jessie R. Liu, David A. Moses, Maximilian E. Dougherty, Margaret P. Seaton, Kaylo T. Littlejohn, Josh Chartier, Gopala K. Anumanchipalli, Adelyn Tu-Chan, Karunesh Ganguly, and Edward F. Chang**

**Abstract** Speech is one of the most natural and efficient ways to communicate and is a fundamental aspect of daily life. Assistive brain-computer interface (BCI)

Sean L. Metzger, Jessie R. Liu and David A. Moses contributed equally with all other contributors.

S. L. Metzger · J. R. Liu · E. F. Chang (✉)
Department of Neurological Surgery, University of California (UCSF), San Francisco, CA, USA

Weill Institute for Neurosciences UCSF, San Francisco, CA, USA

University of California, Berkeley-UCSF Graduate Program in Bioengineering, Berkeley, CA, USA
e-mail: edward.chang@ucsf.edu

D. A. Moses · J. Chartier
Department of Neurological Surgery, University of California (UCSF), San Francisco, CA, USA

Weill Institute for Neurosciences UCSF, San Francisco, CA, USA

M. E. Dougherty · M. P. Seaton
Department of Neurological Surgery, University of California (UCSF), San Francisco, CA, USA

K. T. Littlejohn · G. K. Anumanchipalli
Department of Neurological Surgery, University of California (UCSF), San Francisco, CA, USA

Weill Institute for Neurosciences UCSF, San Francisco, CA, USA

Department of Electrical Engineering and Computer Science, University of California, Berkeley, CA, USA

A. Tu-Chan
Department of Neurology, UCSF, San Francisco, CA, USA

K. Ganguly
Weill Institute for Neurosciences UCSF, San Francisco, CA, USA

Department of Neurology, UCSF, San Francisco, CA, USA

technology has the potential to restore communication to people who cannot speak or type due to paralysis. Recent advances have enabled users to communicate by attempting to speak, type, or handwrite intended messages. Another approach may be to spell out intended words and sentences with a BCI that is controlled by natural attempts to speak. As part of an ongoing clinical trial we recorded low- and high-frequency electrocorticography (ECoG) signals from a 128-channel high-density array implanted over the sensorimotor cortex of a brainstem-stroke survivor with severe anarthria (the inability to articulate speech) and quadriparesis while he silently attempted to spell out words and sentences using the NATO phonetic alphabet.

**Keywords** ECoG · BCI · Anarthria · Neuroprosthesis · Sensorimotor cortex

## 1   Introduction

Devastating neurological conditions such as amyotrophic lateral sclerosis (ALS) and stroke can lead to anarthria, the loss of ability to articulate speech [1]. Anarthria patients can have intact language skills and cognition, but paralysis may inhibit their ability to operate assistive communication devices, severely limiting communication with family, friends, and caregivers and lowering self-reported quality of life [2].

Brain-computer interfaces (BCIs) have the potential to restore communication to such patients by decoding neural activity into intended messages [3]. Existing BCIs for communication traditionally rely on decoding imagined arm and hand movements into letters to enable the user to spell out sentences [4, 5]. Although implementations of this approach have exhibited promising results, natural attempts to speak may offer faster and more natural control for a communication BCI.

To assess this, we recently developed a speech neuroprosthesis to directly decode full words in real time from the cortical activity of a person with anarthria and paralysis as he attempted to speak [6]. This approach exhibited promising decoding accuracy and speed, but as an initial study focused on a preliminary 50-word vocabulary. While direct word decoding with a limited vocabulary has immediate practical benefit, expanding access to a larger vocabulary of at least 1000 words would cover over 85% of the content in natural English sentences [7] and enable effective day-to-day use of assistive-communication technology [8]. Hence, a powerful complementary technology could expand current speech-decoding approaches to enable users to spell out intended messages from a large and generalizable vocabulary while still allowing fast, direct word decoding to express frequent and commonly used words. Separately, in this prior work the participant was controlling the neuroprosthesis by attempting to speak aloud, making it unclear if the approach would be viable for potential users who cannot produce any vocal output whatsoever.

Here, we demonstrate that real-time decoding of silent attempts to say 26 alphabetic code words from the NATO phonetic alphabet can enable highly accurate and rapid spelling in a clinical-trial participant (ClinicalTrials.gov; NCT03698149) with paralysis and anarthria.

## 2   Methods

We designed a sentence-spelling system to enable real-time BCI spelling using silent speech attempts (Fig. 1). We first trained models using data collected as the participant said individual NATO code words ("Alpha", "Bravo", etc.) in isolation. Then, during testing, when the participant was ready to begin spelling a sentence, he attempted to silently say an arbitrary word. A speech-detection model processed each time point of data to detect this initial silent-speech attempt (Fig. 1a–c). Once an attempt to speak was detected, a paced spelling procedure began, where every 2.5 s, the participant was visually cued to silently attempt to say the NATO code word associated with a letter (Fig. 1d, e). He would silently attempt to say the code word corresponding to each letter in the sentence he was trying to create, in order and in time with these cues. A deep-neural-network classifier processed each 2.5-s window of neural activity after each visual cue and was trained to predict the probability of each of the 26 alphabetic code words as well as a hand-motor command the participant used to turn off the system (Fig. 1f). In real time, we used a beam-search algorithm to process the predictions. The beam-search algorithm automatically inserted spaces and predicted the most likely sentence, which was continuously displayed to the participant. We found that restricting words within a 1152-word vocabulary and using a language model to prioritize linguistically probable sentences significantly improved decoding. Once the participant had attempted to spell out the entire sentence, he attempted to squeeze his right hand to turn off the spelling procedure (Fig. 1g, h). If the neural classifier predicted this motor movement with a probability of greater than 80%, the procedure was stopped and the most likely sentence was finalized (Fig. 1i).

We evaluated the performance of the system in real time as the participant attempted to spell out 150 sentences (two repetitions each of 75 unique sentences) during a copy-typing task. We measured performance using character and word error rates. For characters and words, the error rate is defined as the edit distance, which is the minimum number of character or word deletions, insertions, and substitutions required to convert the predicted sentence to the target sentence that was displayed to the participant, divided by the total number of characters or words in the target sentence, respectively. These metrics are commonly used to assess the decoding performance of automatic speech recognition and BCI systems. With a vocabulary of 1152 words, we observed a median character error rate (CER) of 6.13% and median word error rate (WER) of 10.53 across the real-time test blocks (Fig. 2a, b), with significant improvements attributed to enforcement of this vocabulary (removal of out-of-vocabulary words) and inclusion of a language model that prioritized
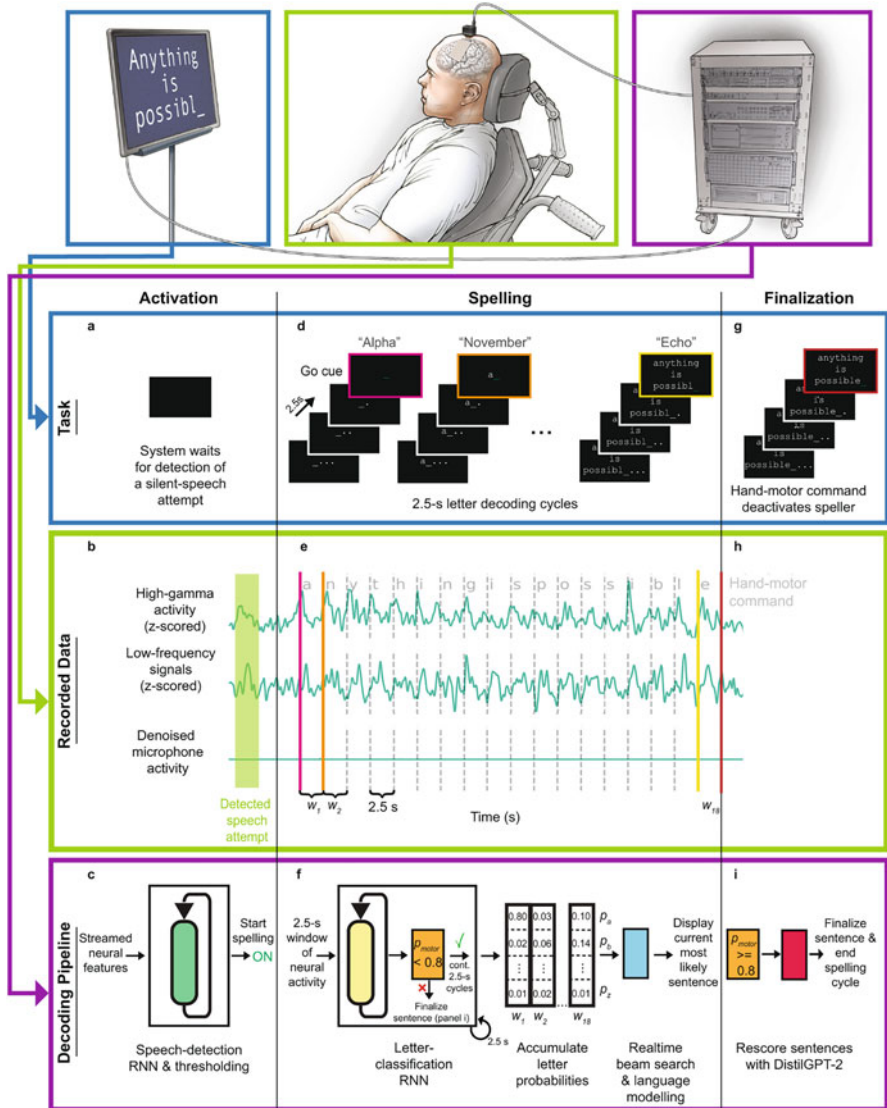
**Fig. 1** Overview of the real-time spelling system. (**a**) At the start of a sentence-spelling trial, the participant attempts to silently say a word to volitionally activate the speller. (**b**) Neural features (high-gamma activity and low-frequency signals) are extracted in real time from the recorded cortical data throughout the task. The features from a single electrode are depicted. For visualization, the traces were smoothed with a Gaussian kernel with a standard deviation of 150 ms. The microphone signal shows that there is no vocal output during the task. (**c**) The speech-detection model, consisting of a recurrent neural network (RNN) and thresholding operations, processes the neural features to detect a silent-speech attempt. Once an attempt is detected, the spelling procedure begins. (**d**) During the spelling procedure, the participant spells out the intended message throughout letter-decoding cycles that occur every 2.5 s. Each cycle, the participant is visually presented with a countdown and eventually a go cue. At the go cue, the participant attempts to silently say the code word representing the desired letter. (**e**) High-gamma activity and low-frequency signals are computed throughout the spelling procedure for all electrode channels and parceled into 2.5-s

linguistically probable sentences. 70% of sentences were decoded without error, and 92% of the unique sentences were decoded perfectly at least one of the two times they were attempted. We also observed median typing rates of 29.4 characters per minute (CPM) and 6.86 words per minute (WPM) across test blocks (Fig. 2c, d). These rates are higher than the median rates of 17.37 CPM and 4.16 WPM observed with the participant as he used his commercially available Tobii Dynavox assistive-typing device (as measured in our previous work [9]).

In offline experiments, we simulated the copy-typing spelling results using three larger vocabularies composed of 3303, 5249, and 9170 words that we selected based on their words' frequencies in large-scale English corpora. We observed that the
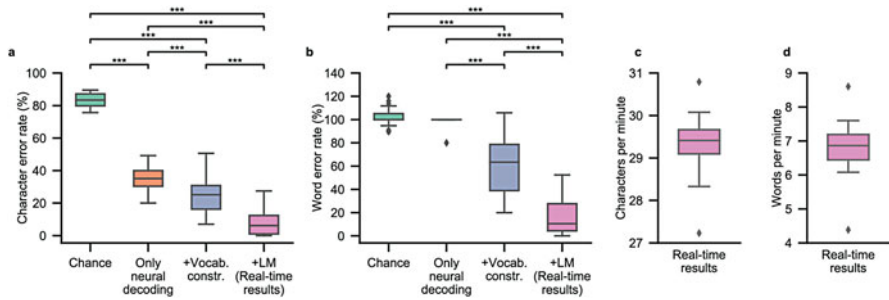


**Fig. 2** Character error rates (CERs) observed during real-time sentence spelling with a language model (LM), denoted as '+LM (Real-time results)', and offline simulations in which portions of the system were omitted. In the 'Chance' condition, sentences were created by replacing the outputs from the neural classifier with randomly generated letter probabilities without altering the remainder of the pipeline. In the 'Only neural decoding' condition, sentences were created by concatenating together the most likely character from each of the classifier's predictions during a sentence trial (no whitespace characters were included). In the '+Vocab. constraints' condition, the predicted letter probabilities from the neural classifier were used with a beam search that constrained the predicted character sequences to form words within the 1152-word vocabulary. The final condition '+ LM (Real-time results)' incorporates language modeling. (***$P < 0.0001$). (**b**) Word error rates (WERs) for real-time results and corresponding offline omission simulations from (**a**). (**c**) The decoded characters per minute during real-time testing. (**d**) The decoded words per minute during real-time testing. In (**a**)–(**d**), the distribution depicted in each boxplot was computed across $n = 34$ real-time blocks (in each block, the participant attempted to spell between two and five sentences)

---

**Fig. 1** (continued) non-overlapping time windows. (**f**) An RNN-based letter-classification model processes each of these neural time windows to predict the probability that the participant was attempting to silently say each of the 26 possible code words or attempting to perform a hand-motor command. Prediction of the hand-motor command with at least 80% probability ends the spelling procedure. (**i**) Otherwise, the predicted letter probabilities are processed by a beam-search algorithm in real time and the most likely sentence is displayed to the participant. (**g**) After the participant spells out his intended message, he attempts to squeeze his right hand to end the spelling procedure and finalize the sentence. (**h**) The neural time window associated with the hand-motor command is passed to the classification model. (**i**) If the classifier confirms that the participant attempted the hand-motor command, a neural network-based language model (DistilGPT-2) rescores valid sentences. The most likely sentence after rescoring is used as the final prediction
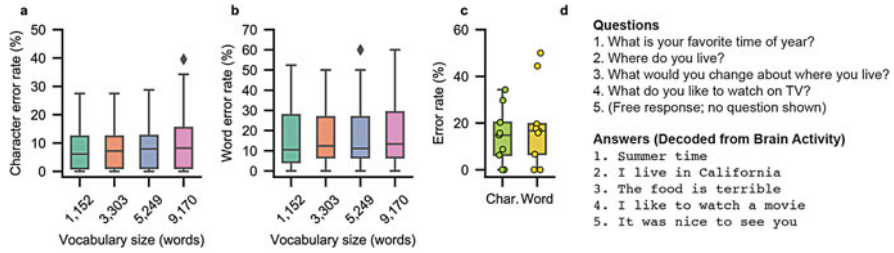
**Fig. 3** (**a**) Simulated character error rates from the copy-typing task (from Fig. 1) with different vocabularies, including the original vocabulary used during real-time decoding. (**b**) Word error rates from the corresponding simulations in (**a**). (**c**) CERs and WERs across the volitionally chosen responses and messages decoded in real time during the conversational task condition. Each boxplot corresponds to $n = 9$ blocks (in each of these blocks, the participant attempted to spell between two and four conversational responses). (**d**) Examples of presented questions from trials of the conversational task condition (left) along with corresponding responses decoded from the participant's brain activity (right). In the final example, the participant spelled out his intended message without being prompted with a question

system was able to readily generalize to using these larger vocabularies without a significant increase in error rates, with a median CER of 8.23% and median WER of 13.3% (Fig. 3a, b) across test trials using the 9170 word vocabulary.

Finally, the participant attempted to use the system to freely respond to questions and volitionally produce sentences, resulting in a median CER of 14.8% and WER of 16.7% across 28 real-time trials (Fig. 3c, d). These results demonstrate that our spelling approach can enable a user to generate freeform responses to questions as well as unprompted, volitionally chosen messages.

## 3 Discussion

Here, we demonstrated that a paralyzed clinical-trial participant (ClinicalTrials.gov; NCT03698149) with anarthria could control a neuroprosthesis to spell out intended messages in real time using attempts to silently speak. With phonetically rich code words to represent individual letters and an attempted hand movement to indicate an end-of-sentence command, we used deep-learning and language-modeling techniques to decode sentences from electrocorticographic (ECoG) signals. These results significantly expand our previous word-decoding findings with the same participant by facilitating large-vocabulary sentence decoding through spelling.

Previous implementations of spelling brain-computer interfaces (BCIs) have demonstrated that users can type out intended messages by visually attending to letters on a screen [10, 11], by using motor imagery to control a two-dimensional computer cursor [4, 12], or by attempting to handwrite letters [5]. BCI performance using penetrating microelectrode arrays in hand-motor cortex has steadily improved over the past 20 years, recently achieving spelling rates as high as 90 characters per

minute with a single participant, although this participant was able to speak normally [5]. Our results extend the list of immediately practical and clinically viable control modalities for spelling-BCI applications to include silently attempted speech with an implanted ECoG array, which may be preferred for daily use by some patients due to the relative naturalness of speech and may be more chronically robust across patients through the use of less invasive, non-penetrating electrode arrays with broader cortical coverage.

Overall, these results further validate silently attempted speech as an effective alternative behavioral strategy to imagined speech and expand findings from our previous work involving the decoding of overt-speech attempts with the same participant [9], indicating that the production of residual vocalizations during speech attempts is not necessary to control a speech neuroprosthesis. These findings illustrate the viability of attempted-speech control for individuals with complete vocal-tract paralysis (such as those with locked-in syndrome), although future studies with these individuals are required to further our understanding of the neural differences between overt-speech attempts, silent-speech attempts, and purely imagined speech as well as how specific medical conditions might affect these differences. In future communication neuroprostheses, it may be possible to use a combined approach that enables rapid decoding of full words or phrases from a limited, frequently used vocabulary as well as slower, generalizable spelling for out-of-vocabulary items.

**Author note**  Words and figures in this chapter draw from our recent article on these results in *Nature Communications* [13]. The article contains further analyses that may be of interest to the reader.

# References

1. Beukelman DR, Fager S, Ball L, Dietz A (2007) AAC for adults with acquired neurological conditions: a review. Augment Altern Commun 23:230–242
2. Felgoise SH, Zaccheo V, Duff J, Simmons Z (2016) Verbal communication impacts quality of life in patients with amyotrophic lateral sclerosis. Amyotroph Lateral Scler Front Degener 17: 179–183
3. Brumberg JS, Pitt KM, Mantie-Kozlowski A, Burnison JD (2018) Brain–computer interfaces for augmentative and alternative communication: a tutorial. Am J Speech Lang Pathol 27:1–12
4. Pandarinath C et al (2017) High performance communication by people with paralysis using an intracortical brain-computer interface. elife 6:1–27
5. Willett FR, Avansino DT, Hochberg LR, Henderson JM, Shenoy KV (2021) High-performance brain-to-text communication via handwriting. Nature 593:249–254
6. Moses DA, Leonard MK, Makin JG, Chang EF (2019) Real-time decoding of question-and-answer speech dialogue using human cortical activity. Nat Commun 10:3096
7. Adolphs S, Schmitt. (2003) Lexical coverage of spoken discourse. Appl Linguis 24:425–438
8. van Tilborg A, Deckers SRJM (2016) Vocabulary selection in AAC: application of core vocabulary in atypical populations. Perspect ASHA Spec Interest Groups 1:125–138
9. Moses DA et al (2021) Neuroprosthesis for decoding speech in a paralyzed person with anarthria. N Engl J Med 385:217–227
10. Rezeika A et al (2018) Brain–computer interface spellers: a review. Brain Sci 8:57

11. Sellers EW, Ryan DB, Hauser CK (2014) Noninvasive brain-computer interface enables communication after brainstem stroke. Sci Transl Med 6:257re7
12. Vansteensel MJ et al (2016) Fully implanted brain–computer interface in a locked-in patient with ALS. N Engl J Med 375:2060–2066
13. Metzger SL et al (2022) Generalizable spelling using a speech neuroprosthesis in an individual with severe limb and vocal paralysis. Nat Commun 13:6510

# Fast, Accurate, Unsupervised, and Time-Adaptive EEG-Based Auditory Attention Decoding for Neuro-steered Hearing Devices

**Simon Geirnaert, Rob Zink, Tom Francart, and Alexander Bertrand**

**Abstract**  More than 5% of the world's population suffers from disabling hearing loss. Hearing aids and cochlear implants are crucial for improving their quality of life. However, current hearing technology does not work well in cocktail party scenarios, where several people talk simultaneously. This is mainly because the hearing device does not know which speaker the user is attending to, and so which speaker should be amplified relative to the background noise. In this project, we have developed novel signal processing algorithms for electroencephalography (EEG)-based auditory attention decoding to steer the hearing device towards the attended speaker based on the user's attention. We propose algorithms that are fast, accurate, and able to adapt automatically to (changes in) the EEG data of individual users. These are crucial ingredients towards the realization of practically viable neuro-steered hearing devices.

S. Geirnaert (✉)
STADIUS Center for Dynamical Systems, Signal Processing, and Data Analytics, Department of Electrical Engineering (ESAT), KU Leuven, Heverlee, Belgium

ExpORL, Department of Neurosciences, KU Leuven, Leuven, Belgium

Leuven.AI – KU Leuven Institute for AI, Leuven, Belgium
e-mail: simon.geirnaert@esat.kuleuven.be; simon.geirnaert@kuleuven.be

R. Zink
STADIUS Center for Dynamical Systems, Signal Processing, and Data Analytics, Department of Electrical Engineering (ESAT), KU Leuven, Heverlee, Belgium

T. Francart
ExpORL, Department of Neurosciences, KU Leuven, Leuven, Belgium

Leuven.AI – KU Leuven Institute for AI, Leuven, Belgium
e-mail: tom.francart@kuleuven.be

A. Bertrand
STADIUS Center for Dynamical Systems, Signal Processing, and Data Analytics, Department of Electrical Engineering (ESAT), KU Leuven, Heverlee, Belgium

Leuven.AI – KU Leuven Institute for AI, Leuven, Belgium
e-mail: alexander.bertrand@kuleuven.be

# 1   Introduction

## 1.1   The Auditory Attention Decoding Problem

The World Health Organization estimates that more than 5% of the world's population, or 430 million people, suffers from disabling hearing loss and requires rehabilitation. This group is expected to grow to more than 7% by 2050 [1]. As hearing loss tremendously impacts society both on an economic and individual level (e.g., social isolation, loneliness), effective assistive hearing devices such as hearing aids and cochlear implants are required to restore communication by improving speech intelligibility.

While newly developed hearing devices more and more contain advanced speech enhancement and noise suppression algorithms, they still underperform in so-called 'cocktail party' scenarios, where multiple persons are talking simultaneously. In these situations, hearing devices lack a fundamental piece of knowledge: They do not know which speaker the hearing device user *wants* to attend to. Correspondingly, they have no information about which speech signal to enhance (i.e., the attended speaker) and which others to consider as noise and thus suppress (i.e., the unattended speaker(s)). We refer to this problem as the *auditory attention decoding* (AAD) problem.

While the AAD problem can be tackled using heuristics such as eye gaze direction or by simply selecting the loudest speaker, they fail in several practical scenarios, for example, when listening to a public address system, eavesdropping, or when driving a car. Selecting and thereby amplifying the wrong (unattended) speaker can be avoided by pursuing a more ideal strategy: decoding the auditory attention from where it originates, i.e., the brain. As shown by Mesgarani and Chang [2], certain characteristics (such as the speech envelope) of the attended speech signal are better encoded in the brain than those of the unattended speech signal(s), which, in turn, opens the possibility to develop algorithms to decode the auditory attention from brain signals. Incorporating such AAD algorithms in a hearing device could then lead to a new type of brain-computer interface (BCI) technology to assist hearing-impaired people: a *neuro-steered hearing device* (Fig. 1). There exist other use cases of AAD in BCIs as well, such as in consumer earphones and other hearables [4].

## 1.2   Neuro-steered Hearing Devices

Figure 1 shows a conceptual overview of a neuro-steered hearing device with its main ingredients: a speaker separation and enhancement block, an AAD block to determine the attended speaker based on the brain signals of the listener, and a
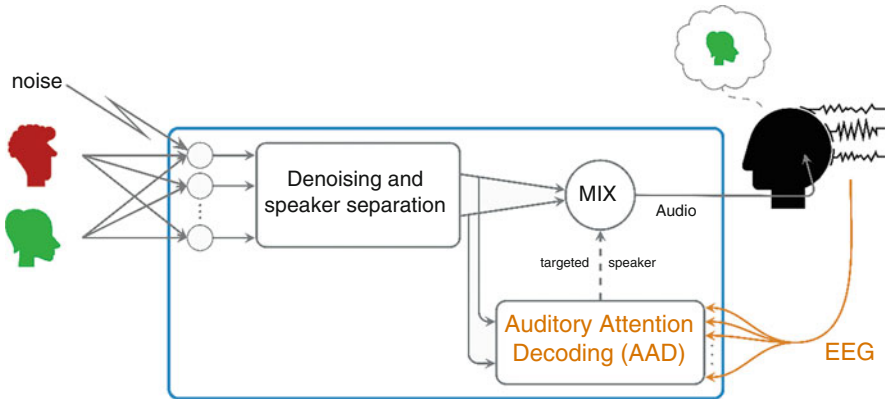
**Fig. 1** In a neuro-steered hearing device, the AAD algorithm informs the hearing device about which speaker needs to be amplified based on the EEG signals. Based on Figure 1 in [3]

mixing block that mixes the separated speech signals based on the retrieved information about the attended speaker.

We use electroencephalography (EEG) as a neurorecording modality because it is non-invasive, wearable, and relatively cheap. These are all crucial features for the widespread usage of neuro-steered hearing devices during daily-life activities. Furthermore, EEG has an excellent temporal resolution, which is critical for tracking fast modulations in speech and for low-latency processing in BCIs in general.

One of the most common paradigms for AAD—*stimulus reconstruction* (SR)—is based on the principle of neural tracking of speech signals, i.e., the auditory cortex tracks time-varying characteristics of the attended speech stimulus [5]. Correspondingly, it has been shown that in a cocktail party scenario with two competing speakers, it is possible to reconstruct from the neural signals a spectrogram [2] or envelope [6] that better reflects the spectrogram or speech envelope of the attended speech signal than the unattended one. The SR algorithm then exploits this stronger neural tracking of the attended speech signal for AAD by reconstructing an envelope from the EEG signals of the listener using a neural decoder and correlating this reconstructed envelope with the individual speech envelopes of the competing speakers [7]. The speech envelope of the speaker that exhibits the highest correlation is then identified as the attended speaker (Fig. 2a). This neural decoder can be modeled and trained in various ways. In [3], we provide an extensive review of the different ways to train the neural decoder, as well as other AAD algorithms beyond SR.

**a**



**b**
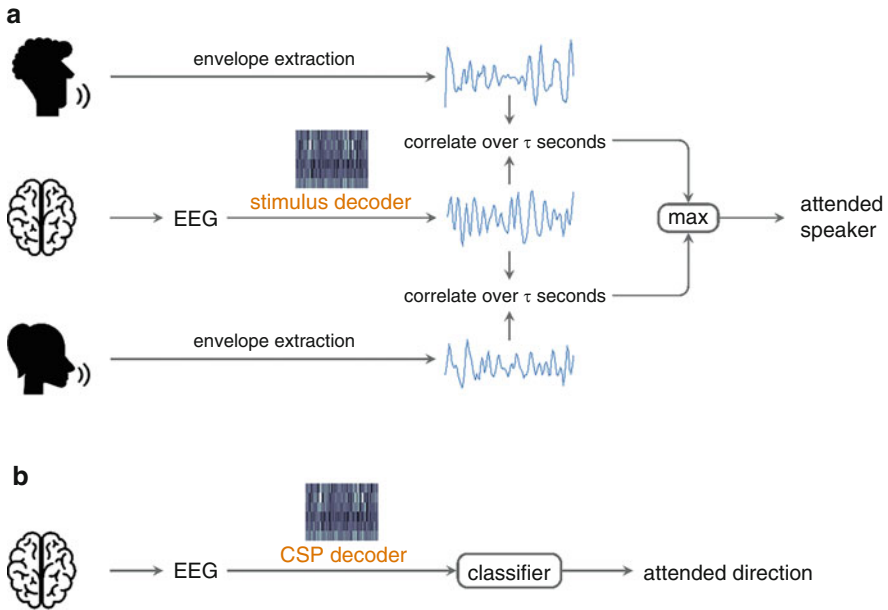


**Fig. 2** (**a**) In the SR algorithm, a neural stimulus decoder is applied on the EEG to reconstruct the attended speech envelope. Based on Figure 3a in [3]. (**b**) In the CSP algorithm, the attended spatial direction is directly decoded from the EEG lateralization patterns

## 1.3 Two Fundamental Problems with Stimulus Reconstruction

The SR algorithm suffers from two critical limitations that are dealt with in this chapter:

1. The neural stimulus decoder is traditionally trained in a *supervised* manner and remains *fixed over time* [7]. To be able to train this neural decoder to reconstruct the attended speech envelope from the EEG in a data-driven way, the attended speaker needs to be known at training time. The necessity for attention labels during training requires a cumbersome calibration session for each new user, in which the user is instructed to attend to a particular speaker. Furthermore, this also prevents adapting the neural decoder to changes in the EEG signal characteristics, making it suboptimal.

2. The SR algorithm suffers from quickly decreasing accuracy when reducing the number of EEG/speech envelope samples to make a decision (the decision window length) (see Fig. 4a). This is an effect of the notoriously low signal-to-noise ratio of the stimulus-following neural response in the EEG, making the estimation of the correlation coefficients highly susceptible to interference from other neural processes when reducing the decision window length [3]. As a result, the SR algorithm is too slow in detecting switches in auditory attention, resulting
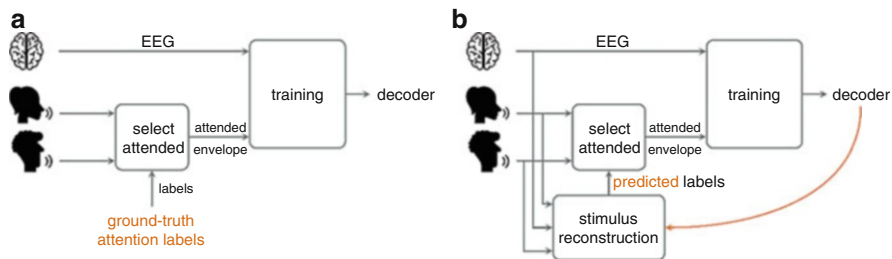
**Fig. 3** (**a**) The neural stimulus decoder is traditionally trained in a supervised manner, i.e., the ground-truth attention labels are required to select the attended speech envelope. (**b**) In [8], we propose an unsupervised training procedure where the ground-truth attention labels are replaced by the predicted labels when applying the learned decoder

in too large delays in changing the relative gain between the competing speakers in the hearing device [10].

Therefore, we have developed novel AAD signal processing algorithms to overcome both challenges, i.e., by designing an unsupervised and time-adaptive SR algorithm (Sect. 2) and exploiting an alternative AAD paradigm: decoding the spatial focus of auditory attention (Sect. 3).

## 2 Unsupervised and Time-Adaptive Stimulus Reconstruction

### 2.1 Supervised Training of the Neural Stimulus Decoder

Traditionally, the neural stimulus decoder in the SR algorithm (Fig. 2a) is a linear spatio-temporal filter, integrating EEG channels and post-stimulus time lags to reconstruct a sample of the attended speech envelope [7, 10]. Given a training set of EEG data and speech envelopes of the competing speakers, the filter weights of this neural decoder can be found by minimizing the mean squared error (MMSE) between the reconstructed envelope from the EEG and the attended speech envelope.[1] This training procedure is conceptually summarized in Fig. 3a. A crucial feature of this training procedure is that it is *supervised*, i.e., it requires the ground-truth attention labels to select the correct speech envelope as the target during training.

Depending on the training data used in this supervised training procedure, two versions of the neural stimulus decoder exist: a user-specific or user-independent decoder [7, 8]. The former is trained with data from the end user, while the latter is trained with data from other users. As expected, the user-specific decoder leads to

---

[1] An extensive mathematical explanation can be found in, e.g., [8].
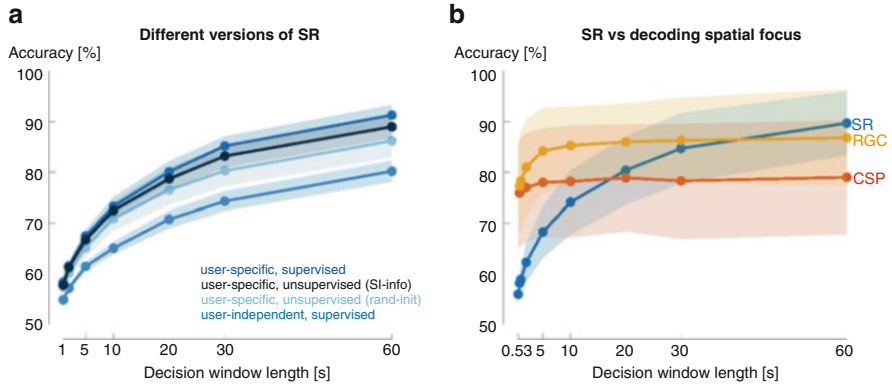
**Fig. 4** (**a**) Different versions of the linear SR algorithm, all showing a degrading accuracy for short decision window lengths. Based on Figure 5a from [8]. (**b**) Decoding the spatial focus of auditory attention with CSPs or RGCs gives a substantial improvement for the shorter decision window lengths. Based on Figure 1 from [9]

higher AAD performances (see Fig. 4a), as it is tailored towards the brain of the specific end user [7, 8]. However, it lacks the plug-and-play characteristic of the user-independent decoder that can be pre-implemented on a hearing device, whereas the user-specific decoder requires a cumbersome training session for each new end user [8]. In this training session, the user then needs to be instructed to listen to one of multiple competing speech signals to be able to generate the required ground-truth labels.

In [8], we proposed an *unsupervised but user-specific* stimulus decoder to combine the best of both worlds. As it is unsupervised, i.e., it does not require ground-truth attention labels, it retains part of the plug-and-play characteristic of the user-independent decoder, while it can achieve higher performances because it still uses user-specific data. In Sect. 2.2, we explain how this unsupervised training procedure works using a batch of EEG/speech envelope training data but *without* ground-truth attention labels, while its extension to a time-adaptive updating procedure is explained in Sect. 2.3.

## 2.2 Unsupervised Training of the Neural Stimulus Decoder

Again assume the availability of a batch of EEG/speech envelope training data, however, now *without* knowing which of the two competing speakers corresponds to the attended speaker at each point in time. Correspondingly, the training scheme as proposed in Fig. 3a has become unfeasible due to the unavailability of the ground-truth attention labels. Therefore, in [8], we proposed an alternative unsupervised training scheme that replaces the ground-truth attention labels with the predicted labels on the training data using a previously trained decoder, as conceptually shown

in Fig. 3b. The key idea is that this creates a closed-loop, iterative predict-and-update procedure, where

1. the trained decoder is used to (re)predict attention labels on the training data using SR,
2. the (re)predicted attention labels are used to (re)select the attended speech envelope such that the neural stimulus decoder can be retrained. Step 1 can then be repeated.

When using an MMSE-based linear spatio-temporal filter as stimulus decoder, we have shown that this procedure converges after a few iterations (under some mild conditions) and that it can be interpreted as a fixed-point iteration algorithm. This interpretation explains the self-leveraging effect in the iterative updating procedure, i.e., it leverages its own predicted labels to converge to a better decoder, even when starting from a random decoder. Furthermore, in the spirit of transfer learning, we have developed a version that allows incorporating labeled data from users other than the end user (as in the user-independent decoder) in the updating procedure.

Figure 4a shows the AAD accuracy (number of correct decisions) versus the decision window length (number of time samples used to make a decision) for the supervised user-specific decoder, the supervised user-independent decoder, the unsupervised user-specific decoder when starting from a random decoder, and the unsupervised user-specific decoder with user-independent side-information.[2] The unsupervised but user-specific decoder substantially outperforms the user-independent decoder while retaining the 'plug-and-play' characteristic, not requiring ground-truth attention labels. Adding labeled user-independent side information in the unsupervised updating procedure even enables accuracies close to the optimal supervised user-specific decoder.

This unsupervised training procedure opens the possibility for a fully automatically updating decoder over time, as explained in the following section.

## 2.3 Time-Adaptive Unsupervised Updating of the Neural Stimulus Decoder

While the unsupervised training procedure for the neural stimulus decoder in Sect. 2.2 removes the necessity of having access to ground-truth attention labels during training, it still assumes the availability of a batch of EEG/speech envelope data. Furthermore, it results in a decoder that remains fixed during operation, not adapting to the long-term signal changes that are characteristic of EEG. These non-stationarities in the EEG originate, for example, from the inherent non-stationarity of neural signals, changing electrode-skin contact impedances, and shifting or loosening electrodes. Modifying the unsupervised training algorithm

---

[2]All details about the data and experiments can be found in [8].
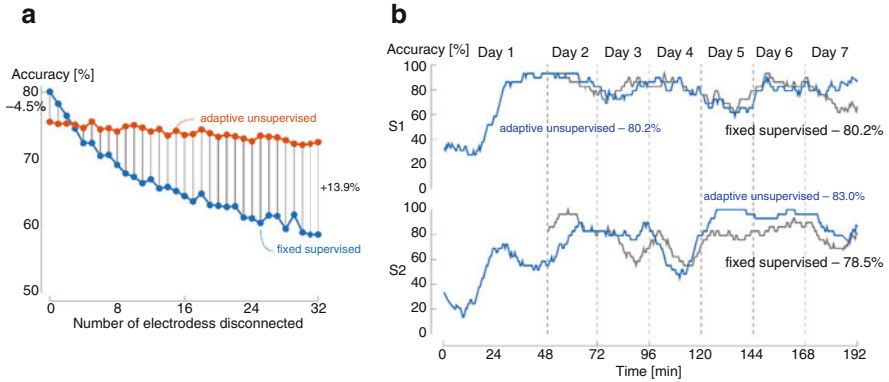
**Fig. 5** (**a**) When electrodes are disconnected from a 64-channel BioSemi EEG system during an AAD experiment, the pre-trained fixed supervised decoder shows degrading performances, while the time-adaptive unsupervised decoder can find alternative ways of reconstructing the attended speech envelope that are as effective. (**b**) The time-adaptive unsupervised decoder performs at least as well as the fixed supervised decoder in an AAD experiment across multiple recording days (two participants). Based on Figure 7a and 8b in [11]

from Sect. 2.2 to be time-adaptive is therefore crucial to adapt to these non-stationarities to obtain higher performances. Furthermore, it also alleviates the need for a dedicated training session for each new end user, fully realizing the plug-and-play potential of the unsupervised decoder.

Consider now the practical use case where EEG data and speech envelopes of the competing speakers are continuously being recorded. In [11], we proposed a single-shot predict-and-update scheme based on a recursive implementation of the linear neural stimulus decoder. The key idea is to predict the attention label using the previous decoder on the new incoming data window and to use this predicted label to update the parameters of the decoder using exponential weighting. This exponential weighting hyperparameter then determines the tradeoff between the speed of adaptation to non-stationarities and the accuracy of the resulting decoder. From our experiments, a good choice for this hyperparameter led to an adaptation time of 20 min to adapt the decoder to a new end user, starting from a random decoder.

Figure 5a compares the pretrained fixed supervised decoder with the proposed time-adaptive unsupervised decoder when simulating disconnecting EEG electrodes during an AAD experiment (on a 64-channel BioSemi EEG system).[3] After disconnecting EEG electrodes, the time-adaptive unsupervised decoder finds alternative ways of reconstructing the attended speech envelope that are clearly as effective as before. The pretrained fixed supervised decoder cannot take these disconnections into account and, therefore, shows decreasing performance. From the moment that more than three electrodes are disconnected, it is outperformed by the time-adaptive decoder, which requires no pretraining and updates fully

---

[3] All details about the data and experiments can be found in [11].

automatically. Furthermore, as shown in Fig. 5b, the time-adaptive unsupervised decoder performs at least as well as the fixed supervised decoder in an AAD experiment that reflects the practical use-case of a neuro-steered hearing device in which data is collected across multiple recording days. The time-adaptive decoder then adapts to the changes in, for example, EEG setup, electrode impedances, conditions, and state of mind of the user, *without* any external intervention or supervision.

These various results show the added value of the developed time-adaptive unsupervised SR algorithm that allows adaptation to the EEG signal changes and to a specific end-user. As such, it is a crucial enabler towards the online application of AAD in practical neuro-steered hearing devices.

## 3    Decoding the Spatial Focus of Auditory Attention

While the availability of a time-adaptive unsupervised SR algorithm represents an essential step towards practical AAD, it is still based on the SR algorithm that is too slow to adequately detect switches in auditory attention (see Sect. 1.3 and [10]). Therefore, there has been an increasing interest in decoding auditory attention by tapping into other characteristics of the neural activity, i.e., other than neural tracking of the speech envelope. One of these characteristics is based on the hypothesis that the neural signals change depending on the direction of spatial attention to the attended speaker. For example, it has been shown that there exist alpha-power lateralization patterns depending on the attended spatial location in a competing-stimuli experiment [12, 13]. Bednar and Lalor [14] tried reconstructing the attended sound source trajectory from the EEG in a moving competing speaker scenario. Specifically for AAD, Vandecappelle et al. [15] proposed to use a convolutional neural network to discriminate between left and right attended solely based on the EEG. Using such an AAD algorithm also impacts the conceptual overview of a neuro-steered hearing device (Fig. 1), as it does not require the individual speech signals anymore for AAD itself. Furthermore, the attended spatial direction is a different piece of information that now comes out of the AAD block, which can be used, for example, to steer a beamformer towards the correct location.

In [16], we proposed an alternative algorithm to decode the spatial focus of auditory attention based on the popular common spatial patterns (CSP) filtering algorithm in BCI literature [17]. The idea is to apply a neural CSP decoder on the EEG signals to perform a smart dimensionality reduction that amplifies the discriminative patterns between, for example, left/right attended. The attended direction can be classified by computing features based on the energy of the output signals in a particular decision window (Fig. 2b). Figure 4b shows that exploiting this alternative paradigm with the CSP algorithm substantially improves accuracy on the very short decision windows, which is paramount to detecting switches in auditory attention. Furthermore, we have shown that this also works in a three-class scenario with multiple directions of attention and background babble noise, with a reduced number

of EEG channels around the ear, and in a user-independent context [16]. Lastly, in [18], we employed a nonlinear extension based on Riemannian geometry-based classification (RGC) [9] to obtain even higher performances (Fig. 4b), especially in the multi-class scenario [19].

The high AAD accuracy at short decision windows of these algorithms that decode the spatial focus of auditory attention makes them excellent candidates as fast and accurate decision-making AAD algorithms. However, these algorithms do not seem to work well in every scenario, and it is currently unclear what boundary conditions are required to make them work. Furthermore, there seems to be a considerable time dependency in the CSP decoding, in the sense that decoding performance drops or sometimes completely fails for test segments that are recorded (much) later in time than the segments used to train the decoder [19]. Further research towards these boundary conditions, the underlying neural processes that drive the CSP decoding, and the time dependency is required to realize the potential that these algorithms hold.

## 4    Conclusion and Future Challenges

In this project, we have contributed several key components towards the practical application of AAD in neuro-steered hearing devices. The time-adaptive unsupervised AAD algorithm is a crucial enabler towards the online application of AAD, being able to automatically adapt to the end-user and the non-stationarities in the EEG data. Furthermore, a faster and more accurate AAD algorithm could be obtained by exploiting the varying EEG lateralization patterns based on the attended spatial direction. These innovations lead to several follow-up challenges, such as evaluating the CSP and RGC algorithms in various listening scenarios to identify their boundary conditions, resolving the time-dependency that exists in the CSP algorithm between training and testing data, and building a time-adaptive unsupervised CSP/RGC algorithm, for example, by combining it with the time-adaptive unsupervised SR algorithm.

More generally, the main signal processing-related challenges to realize practical neuro-steered hearing devices are mainly situated in integrating all the different building blocks (see Fig. 1). Firstly, while several papers investigate the combination of speech enhancement algorithms with SR [20–23], a similar integration between beamforming algorithms and algorithms that decode the spatial focus of attention would be interesting to research. An exciting alternative approach is combining speech enhancement and AAD in an all-in-one algorithm [24, 25]. Secondly, an adaptive gain control system should be installed based on the AAD decisions that takes the tradeoff between speed and accuracy [10] and subjective listening parameters into account. Thirdly, a practical neuro-steered hearing device requires a wearable and concealable EEG recording system using miniaturized EEG sensors, such as in-ear [26] or around-the-ear [27] EEG. While AAD has been tested with channel selection algorithms [28] and wearable EEG systems [29], there is not yet a

practically viable solution. Finally, the human in the loop needs to be considered as well. It is therefore paramount to investigate neurofeedback effects on AAD in a closed-loop system in real-life scenarios [30]. Using the time-adaptive SR algorithm, such a closed-loop system could tap into the concept of co-adaptive learning, in which both the human and algorithm learn over time, hopefully resulting in improved performance.

# References

1. World Health Organization (2021) World report on hearing. Technical Report
2. Mesgarani N, Chang EF (2012) Selective cortical representation of attended speaker in multi-talke speech perception. Nature 485:233–236
3. Geirnaert S, Vandecappelle S, Alickovic E, de Cheveigné A, Lalor EC, Meyer BT, Miran S, Francart T, Bertrand A (2021) Electroencephalography-based auditory attention decoding: toward neurosteered hearing devices. IEEE Signal Process Mag 38(4):89–102
4. Belo J, Clerc M, Schön D (2021) EEG-based auditory attention detection and its possible future application for passive BCI. Front Comp Sci 3(661178)
5. Aiken SJ, Picton TW (2008) Human cortical responses to the speech envelope. Ear Hear 29(2): 135–157
6. Ding N, Simon JZ (2012) Emergence of neural encoding of auditory objects while listening to competing speakers. Proc Natl Acad Sci U S A 109(29):11854–11859
7. O'Sullivan JA, Power AJ, Mesgarani N, Rajaram S, Foxe JJ, Shinn-Cunningham BG, Slaney M, Shamma SA, Lalor EC (2014) Attentional selection in a cocktail party environment can be decoded from single-trial EEG. Cereb Cortex 25(7):1697–1706
8. Geirnaert S, Francart T, Bertrand A (2021) Unsupervised self-adaptive auditory attention decoding. IEEE J Biomed Health Inf 25(10):3955–3966
9. Geirnaert S, Francart T, Bertrand A (2021) Riemannian geometry-based decoding of the directional focus of auditory attention using EEG. In: Proceedings of the 2021 IEEE International Conference on Acoustics, Speech and Signal Processing (ICASSP), pp 1115–1119
10. Geirnaert S, Francart T, Bertrand A (2020) An interpretable performance metric for auditory attention decoding algorithms in a context of neuro-steered gain control. IEEE Trans Neural Syst Rehabil Eng 28(1):307–317
11. Geirnaert S, Francart T, Bertrand A (2022) Time-adaptive unsupervised auditory attention decoding using EEG-based stimulus reconstruction. IEEE J Biomed Health Inf 26(8): 3767–3778
12. Kerlin JR, Shahin AJ, Miller LM (2010) Attentional gain control of ongoing cortical speech representations in a "cocktail party". J Neurosci 20(2):620–628
13. Wöstmann M, Herrmann B, Maess B, Obleser J (2016) Spatiotemporal dynamics of auditory attention synchronize with speech. Proc Natl Acad Sci U S A 113(14):3873–3878
14. Bednar A, Lalor EC (2020) Where is the cocktail party? Decoding locations of attended and unattended moving sound sources using EEG. NeuroImage 205(116283)

15. Vandecappelle S, Deckers L, Das N, Ansari AH, Bertrand A, Francart T (2021) EEG-based detection of the locus of auditory attention with convolutional neural networks. eLife 10:e56481
16. Geirnaert S, Francart T, Bertrand A (2021) Fast EEG-based decoding of the directional focus of auditory attention using common spatial patterns. IEEE Trans Biomed Eng 68(5):1557–1568
17. Blankertz B, Tomioka R, Lemm S, Kawanabe M, Müller K-R (2007) Optimizing spatial filters for robust EEG single-trial analysis. IEEE Signal Process Mag 25(1):41–56
18. Barachant A, Bonnet S, Congedo M, Jutten C (2012) Multiclass brain-computer interface classification by riemannian geometry. IEEE Trans Biomed Eng 59(4):920–928
19. Geirnaert S (2022) Signal processing algorithms for EEG-based auditory attention decoding. PhD thesis, Department of Electrical Engineering, KU Leuven, Leuven, Belgium. https://theses.eurasip.org/theses/921/signal-processing-algorithms-for-eeg-based/
20. Van Eyndhoven S, Francart T, Bertrand A (2017) EEG-informed attended speaker extraction from recorded speech mixtures with application in neuro-steered hearing prostheses. IEEE Trans Biomed Eng 64(5):1045–1056
21. Han C, O'Sullivan JA, Luo Y, Herrero J, Mehta AD, Mesgarani N (2019) Speaker-independent auditory attention decoding without access to clean speech sources. Sci Adv 5(eaav6134)
22. Aroudi A, Doclo S (2020) Cognitive-driven binaural beamforming using EEG-based auditory attention decoding. IEEE/ACM Trans Audio Speech Lang Process 28:862–875
23. Das N, Zegers J, Van Hamme H, Francart T, Bertrand A (2020) Linear versus deep learning methods for noisy speech separation for EEG-informed attention decoding. J Neural Eng 17(4): 046039
24. Hosseini M, Celotti L, Plourde É (2022) End-to-end brain-driven speech enhancement in multi-talker conditions. IEEE/ACM Trans Audio Speech Lang Process 30:1718–1733
25. Ceolini E, Hjortkjær J, Wong DD, O'Sullivan JA, Raghavan VS, Herrero J, Mehta AD, Liu SC, Mesgarani N (2020) Brain-informed speech separation (BISS) for enhancement of target speaker in multitalker speech perception. NeuroImage 223(117282)
26. Kappel SL, Rank ML, Toft HO, Andersen M, Kidmose P (2019) Dry-contact electrode ear-EEG. IEEE Trans Biomed Eng 66(1):150–158
27. Debener S, Emkes R, De Vos M, Bleichner MG (2015) Unobtrusive ambulatory EEG using a smartphone and flexible printed electrodes around the ear. Scientific Rep 5(16743)
28. Mundanad Narayanan A, Bertrand A (2020) Analysis of miniaturization effects and channel selection strategies for EEG sensor networks with application to auditory attention detection. IEEE Trans Biomed Eng 67(1):234–244
29. Mirkovic B, Bleichner MG, De Vos M, Debener S (2016) Target speaker detection with concealed EEG around the ear. Front Neurosci 10(349)
30. Zink R, Proesmans S, Bertrand A, Van Huffel S, De Vos M (2017) Online detection of auditory attention with mobile EEG: closing the loop with neurofeedback. bioRxiv 218727

# Closed-Loop Control of Images Based on Electrocorticogram Decoding in Visual Semantic Space

**Ryohei Fukuma, Takufumi Yanagisawa, Shinji Nishimoto, Hidenori Sugano, Kentaro Tamura, Shota Yamamoto, Yasushi Iimura, Yuya Fujita, Satoru Oshino, Naoki Tani, Naoko Koide-Majima, Yukiyasu Kamitani, and Haruhiko Kishima**

R. Fukuma (✉)
Department of Neurosurgery, Graduate School of Medicine, Osaka University, Suita, Japan

ATR Computational Neuroscience Laboratories, Seika-cho, Japan

Institute for Advanced Co-Creation Studies, Osaka University, Suita, Japan

T. Yanagisawa
Department of Neurosurgery, Graduate School of Medicine, Osaka University, Suita, Japan

ATR Computational Neuroscience Laboratories, Seika-cho, Japan

Institute for Advanced Co-Creation Studies, Osaka University, Suita, Japan

Osaka University Hospital Epilepsy Center, Suita, Japan
e-mail: tyanagisawa@nsurg.med.osaka-u.ac.jp

S. Nishimoto · N. Koide-Majima
Center for Information and Neural Networks (CiNet), National Institute of Information and Communications Technology (NICT), Suita, Japan

Graduate School of Frontier Biosciences, Osaka University, Suita, Japan

H. Sugano · Y. Iimura
Department of Neurosurgery, Juntendo University, Tokyo, Japan

K. Tamura
Department of Neurosurgery, Nara Medical University, Kashihara, Japan

S. Yamamoto · Y. Fujita · S. Oshino · N. Tani
Department of Neurosurgery, Graduate School of Medicine, Osaka University, Suita, Japan

Y. Kamitani
ATR Computational Neuroscience Laboratories, Seika-cho, Japan

Graduate School of Informatics, Kyoto University, Kyoto, Japan

H. Kishima
Department of Neurosurgery, Graduate School of Medicine, Osaka University, Suita, Japan

Osaka University Hospital Epilepsy Center, Suita, Japan

**Abstract** Neural representations of visual perception are intentionally modulated by mental imagery and attention. In the present study, we hypothesized that visual images decoded from electrocorticograms (ECoGs) could be controlled to represent intentional meaning in a closed-loop condition. ECoGs were recorded while subjects watched videos containing natural scenes, while the annotations of the scenes in the videos were converted into vectors in the visual semantic space using a word-embedding model; decoders were trained to infer the semantic vector from the ECoG. By presenting images based on the inferred vectors in real time, four subjects successfully controlled the images to show an orally instructed meaning. Closed-loop control of inferred images revealed a novel interaction between visual perception and imagery.

**Keywords** Electrocorticogram · Visual imagery · Brain-computer interface · Neurofeedback

## 1   Introduction

Neural activities in the visual cortex are not only evoked by externally driven "bottom-up" sensory information but also modulated by internally generated "top-down" signals such as mental imagery [1, 2] and attention [3]. Neural representation of the visual cortex has been investigated by using neural decoding; prior studies using functional magnetic resonance imaging (fMRI) have demonstrated that perceived images can be inferred as semantic attributes of images [4, 5] or reconstructed images [6–8]. Interestingly, recent studies have shown that a trained decoder with neural activities during visual perception successfully inferred mental image content [7, 9], revealing common neural representations between visual perception and imagery in the visual cortex [7, 9–11]. Furthermore, the neural representation of visual perception was shown to be modulated by attention in searching for an object of an instructed category [12]. Therefore, both externally provided bottom-up sensory information and internally generated top-down signals of mental imagery and attention affect neural representation in the visual cortex.

Although brain activities can be modulated intentionally by attention and mental imagery, it is unknown whether people can intentionally control the various images decoded from their brain activity. A previous study demonstrated that people can intentionally control the superposition of two images of familiar individuals based on hippocampal signals in a closed-loop condition [13]. Image selection might be controlled by mental imagery, thoughts, and attention. In addition, some recent studies using fMRI demonstrated that people can control the output of a decoder that infers some visual perception features (e.g., orientation and colour) based on cortical activity in the visual cortex in a closed-loop condition, although the subjects were not aware of the decoded visual feature during the control [14]. People might be able to intentionally control the images of various semantic attributes decoded from the visual cortex in a closed-loop condition.

The high temporal resolution and wide cortical area coverage of electrocorticograms (ECoGs) [15] make them suitable for evaluating visual information that is sparsely represented in the visual cortex [4]. Furthermore, it has been shown that ECoGs can not only infer several semantic categories of perceived images [16, 17] but also some novel objects that were not included in the training dataset by decoding in a semantic space [18]. Hence, ECoG can be decoded to precisely infer the semantic information of natural visual stimuli in real time, which is important for closed-loop control. Here, we hypothesize that subjects can control images decoded from ECoGs of the visual cortex by intending to show images with specific semantic attributes.

## 2 Materials and Methods

### 2.1 Subjects

Four subjects with drug-resistant epilepsy (# of males: 3; age: $28.0 \pm 11.2$, mean $\pm$ standard deviation [SD]) who were implanted with subdural electrodes around the visual cortex were included in this study. The study adhered to the Declaration of Helsinki and was performed in accordance with the experimental protocol approved by the ethics committee of each hospital (Osaka University Medical Hospital: Approval No. 14353, UMIN000017900; Juntendo University Hospital: Approval No. 18-164; Nara Medical University Hospital: Approval No. 2098).

### 2.2 ECoG Recordings

The experiment was carried out with subjects either seated on their bed or seated on chairs. During the experiment, ECoGs were recorded at 10 kHz by EEG-1200 (Nihon Koden, Tokyo, Japan). Visual stimuli (video stimuli, or real-time feedback image) were presented to the subjects on a computer screen placed in front of them; the timing of the visual stimuli was monitored by DATAPixx3 (VPixx Technologies, Quebec, Canada) to record simultaneously with ECoGs.

### 2.3 Experimental Procedures

In the video stimuli task, six 10-min videos were presented to the subjects. The six videos were constructed by sequentially concatenating short scenes from trailers or behind-the-scenes features of cinema and animation downloaded from Vimeo. The videos contained objects with various types of semantic meanings, such as humans, animals, landscapes, and words. There were no duplicated scenes in the videos. To

**Fig. 1** Experimental setting during the real-time feedback task: The subjects were instructed to control the feedback image by visual imagery so that the feedback images kept showing the instructed meaning ("word", "landscape", or "human face")
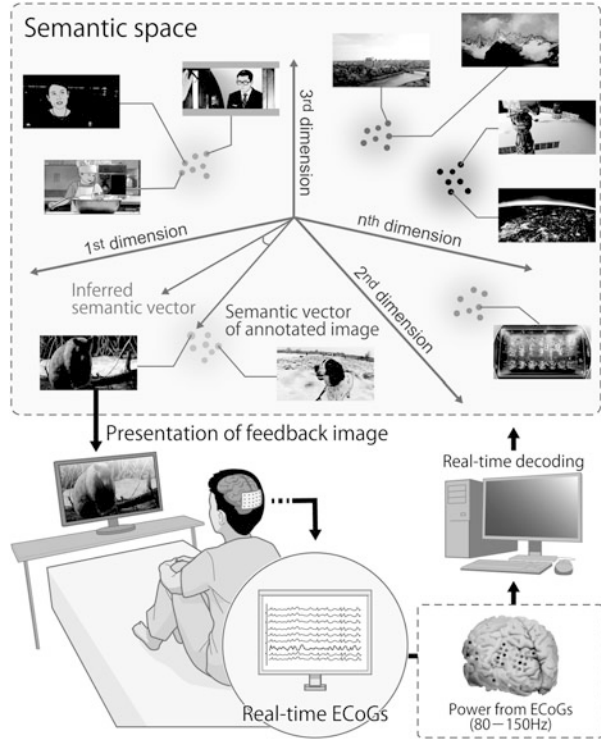


minimize subject fatigue, there were intervals between the presentations of the six videos, resulting in the entire video stimuli task being completed in 1–3 days.

Following the video stimuli task, the subjects participated in a real-time feedback task; in the task, the subjects were shown feedback images in the closed-loop condition (Fig. 1). The feedback images were determined by a decoder trained with ECoGs recorded during the video stimuli task. Each trial of the real-time feedback task started with a 4.5-s blank screen, during which one of the three instructions ("word", "landscape", or "human face") was given orally; following the blank screen, 32 frames of feedback images were presented sequentially with an interval of 250 ms. The subjects were instructed to control the feedback images by visual imagery so that the feedback images kept showing the instructed semantic meaning. The feedback images were selected based on the highest Pearson's correlation coefficient between the semantic vector (see Sect. 2.4) decoded in real time from the latest 1-s ECoGs and the semantic vectors of the candidate scenes from the annotated images of the video stimuli. The trials were repeated 120 times (40 trials for each instruction) with a randomized instruction order.

## 2.4 Construction of the Semantic Vector

From the stimuli videos, 1000-dimensional semantic vectors representing the semantic information of each scene were created. A still image was cropped from the videos every second for annotation by five annotators; from the annotations, nouns, verbs, and adjectives were extracted, lemmatized, and converted to 1000-dimensional vectors using a skip-gram model [19] trained with a Japanese Wikipedia dump. The vectors were averaged within each image to form a semantic vector of the corresponding 1-s scene.

## 2.5 Decoder for the Real-Time Feedback Task

The decoder used in the real-time feedback task was a ridge regression model trained from the 1000-dimensional semantic vectors of the video stimuli and high-$\gamma$ power (80–150 Hz) of the corresponding 1-s ECoGs. To train the decoder, cross-validation was used to determine the best $\lambda$.

## 2.6 Evaluation for the Real-Time Feedback Task

For each feedback frame of the trials in the real-time feedback task, control accuracy was evaluated in a three-choice classification manner. First, the semantic vector inferred to select the feedback image for a frame was calculated for its Pearson's correlation coefficients against three semantic vectors each corresponding to the three instructions ("word", "landscape", or "human face"); when the correlation coefficient with the given instruction for the trial was the highest among the three correlation coefficients, the prediction was considered correct. In a similar three-choice manner, success or failure of control for each trial was evaluated using three correlation coefficients against the three instructions averaged among the 32 frames.

## 3 Results

Representative feedback images of a trial with "landscape" instruction are shown in Fig. 2a; during this trial, Subject E01 could successfully control the feedback images closer to the meaning of "landscape" (shown with red underline). Among the 120 trials of the real-time feedback task, the three-choice classification accuracy peaked in the middle of the trial with an accuracy of 52.5% (Fig. 2b). The overall three-choice classification accuracy for the same subject was 45.83%, which was significantly higher than chance level ($P = 0.0021$, one-sided permutation test). The
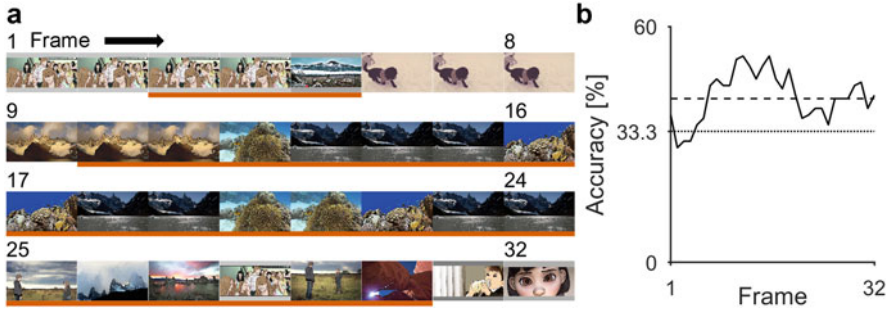
**Fig. 2** Performance for real-time control of the feedback image by E01: (**a**) Representative feedback images during the real-time feedback task of E01 are shown for one trial with "landscape" instruction. Images underlined in red are the correct decoding, considered as a three-choice classification in each frame. (**b**) For each frame of the feedback image, the three-choice accuracy of Subject E01 is shown. The dotted line denotes the chance level, whereas the dashed line denotes the significance level of FDR-corrected $P = 0.05$ estimated by a one-sided permutation test

other three subjects also showed significant accuracies (E02: 50.00%, $P < 0.0001$; E03: 41.67%, $P = 0.031$; E04: 41.67%, $P = 0.0065$). Therefore, all four subjects who participated in the real-time feedback task succeeded in controlling the feedback image towards the instructed semantic meaning.

## 4   Discussion

Our results demonstrate that ECoGs can be used to infer the semantic vectors of natural scenes represented in the visual semantic space. By combining decoding in visual semantic space with real-time visual feedback, all subjects successfully controlled the inferred vector to be closer to one of the three instructed meanings. In other words, the feedback was controlled by the interaction between the intention to control the feedback and the visual feedback decoded in a representational space; here, we call this intentional control of the feedback representational brain-computer interaction (rBCI).

There are several possible strategies for controlling feedback images in real-time feedback tasks. Neural activity in the visual cortex is affected by various top-down factors, such as imagery [1, 2] and attention [3]. According to interviews after the real-time feedback task, some subjects reported that they focused on part of the feedback image that had closer meaning to the instruction (e.g., subtitles in the image during trials with "word" instruction), even though they were instructed to control the feedback image by visual imagery. However, it is difficult to explain the successful control of the feedback images only by attention. In the candidate images of the feedback, many images contained "human face" attributes, and 98.8% of the images had a higher correlation coefficient between the semantic vector of the image and the "human face" vector than between the semantic vector and the "landscape"

or "word" vector; nonetheless, it was difficult to show images containing "human face" attributes during the "human face" trials. Therefore, it is suggested that the feedback images were at least controlled by top-down signals of both mental imagery and attention. Because the rBCI is a novel experience for humans, in which the external stimuli causing bottom-up information are directly affected by top-down signals, it will reveal the novel properties of the relationship between them [20]. Further studies are necessary to reveal how the bottom-up information represented by cortical activities is modulated by top-down signals.

# References

1. Winlove CIP et al (2018) The neural correlates of visual imagery: a co-ordinate-based meta-analysis. Cortex 105:4–25. https://doi.org/10.1016/j.cortex.2017.12.014
2. Pearson J (2019) The human imagination: the cognitive neuroscience of visual mental imagery. Nat Rev Neurosci 20:624–634. https://doi.org/10.1038/s41583-019-0202-9
3. Kastner S, De Weerd P, Desimone R, Ungerleider LG (1998) Mechanisms of directed attention in the human extrastriate cortex as revealed by functional MRI. Science 282:108–111. https://doi.org/10.1126/science.282.5386.108
4. Nishida S, Nishimoto S (2018) Decoding naturalistic experiences from human brain activity via distributed representations of words. NeuroImage 180:232–242. https://doi.org/10.1016/j.neuroimage.2017.08.017
5. Nishimoto S et al (2011) Reconstructing visual experiences from brain activity evoked by natural movies. Curr Biol 21:1641–1646. https://doi.org/10.1016/j.cub.2011.08.031
6. Miyawaki Y et al (2008) Visual image reconstruction from human brain activity using a combination of multiscale local image decoders. Neuron 60:915–929. https://doi.org/10.1016/j.neuron.2008.11.004
7. Shen G, Horikawa T, Majima K, Kamitani Y (2019) Deep image reconstruction from human brain activity. PLoS Comput Biol 15:e1006633. https://doi.org/10.1371/journal.pcbi.1006633
8. Naselaris T, Prenger RJ, Kay KN, Oliver M, Gallant JL (2009) Bayesian reconstruction of natural images from human brain activity. Neuron 63:902–915. https://doi.org/10.1016/j.neuron.2009.09.006
9. Naselaris T, Olman CA, Stansbury DE, Ugurbil K, Gallant JL (2015) A voxel-wise encoding model for early visual areas decodes mental images of remembered scenes. NeuroImage 105:215–228. https://doi.org/10.1016/j.neuroimage.2014.10.018
10. Horikawa T, Kamitani Y (2017) Generic decoding of seen and imagined objects using hierarchical visual features. Nat Commun 8:15037. https://doi.org/10.1038/ncomms15037
11. Breedlove JL, St-Yves G, Olman CA, Naselaris T (2020) Generative feedback explains distinct brain activity codes for seen and mental images. Curr Biol 30:2211–2224 e2216. https://doi.org/10.1016/j.cub.2020.04.014

12. Cukur T, Nishimoto S, Huth AG, Gallant JL (2013) Attention during natural vision warps semantic representation across the human brain. Nat Neurosci 16:763–770. https://doi.org/10.1038/nn.3381
13. Cerf M et al (2010) On-line, voluntary control of human temporal lobe neurons. Nature 467:1104–1108. https://doi.org/10.1038/nature09510
14. Watanabe T, Sasaki Y, Shibata K, Kawato M (2017) Advances in fMRI real-time neurofeedback. Trends Cogn Sci 21:997–1010. https://doi.org/10.1016/j.tics.2017.09.010
15. Yanagisawa T et al (2012) Electrocorticographic control of a prosthetic arm in paralyzed patients. Ann Neurol 71:353–361. https://doi.org/10.1002/ana.22613
16. Liu H, Agam Y, Madsen JR, Kreiman G (2009) Timing, timing, timing: fast decoding of object information from intracranial field potentials in human visual cortex. Neuron 62:281–290. https://doi.org/10.1016/j.neuron.2009.02.025
17. Wang W, Degenhart AD, Sudre GP, Pomerleau DA, Tyler-Kabara EC (2011) Decoding semantic information from human electrocorticographic (ECoG) signals. Conf Proc IEEE Eng Med Biol Soc 2011:6294–6298. https://doi.org/10.1109/IEMBS.2011.6091553
18. Rupp K et al (2017) Semantic attributes are encoded in human electrocorticographic signals during visual object recognition. NeuroImage 148:318–329. https://doi.org/10.1016/j.neuroimage.2016.12.074
19. Mikolov T, Sutskever I, Chen K, Corrado G, Dean J (2013) Distributed representations of words and phrases and their compositionality. Proceedings of the 26th International Conference on Neural Information Processing Systems 2:3111–3119
20. Heeger DJ (2017) Theory of cortical function. Proc Natl Acad Sci U S A 114:1773–1782. https://doi.org/10.1073/pnas.1619788114

# Digital Bridge to Restore Voluntary Control of Leg Movements After Paralysis

**Andrea Galvez, Guillaume Charvet, Jocelyne Bloch, Grégoire Courtine, and Henri Lorach**

**Abstract** Spinal cord injury disrupts the connection between the brain and the regions of the spinal cord located below the lesion. This disruption impairs or even suppresses voluntary control of muscles, leading to permanent paralysis. Yet, the motor cortex remains able to generate meaningful neuronal activity during attempts to move the paralyzed limbs. This activity can be detected as electrical potential recorded at the surface of the brain. Similarly, the regions of the spinal cord involved in the control of leg muscles are generally intact, and can be reactivated using epidural electrical stimulation. Here, we designed a digital bridge between the motor cortex and the regions of the spinal cord involved in the control of leg movements, with the aim to restore voluntary control of leg muscles in a participant with paralysis due to a chronic spinal cord injury. We built this implantable digital bridge by linking an epidural electrocorticographic recording system to an implanted epidural spinal cord stimulation system. We initiated a clinical study to test the safety and efficacy of this Brain Spine Interface (BSI) in restoring voluntary control of leg muscles to stand and walk after spinal cord injury.

**Keywords** ECoG · Spinal cord injury · Brain-spine interface (BSI) · Epidural electrical stimulation · Motor cortex

A. Galvez · J. Bloch · G. Courtine · H. Lorach (✉)
NeuroX Institute, School of Life Sciences, Ecole Polytechnique Fédérale de Lausanne (EPFL), Geneva, Switzerland

Department of Clinical Neuroscience, Lausanne University Hospital (CHUV) and University of Lausanne (UNIL), Lausanne, Switzerland

NeuroRestore, Defitech Center for Interventional Neurotherapies, EPFL/CHUV/UNIL, Lausanne, Switzerland
e-mail: henri.lorach@epfl.ch

G. Charvet
University Grenoble Alpes, CEA, LETI, Clinatec, Grenoble, France

# 1   Introduction

The brain sends commands to neurons located in the lumbosacral spinal cord to control standing and walking. The vast majority of spinal cord injuries do not alter these neurons directly. However, the interruption of the information flow from the brain deprives these neurons of essential sources of excitation and control, resulting in permanent paralysis.

Our group and others have investigated the mechanisms by which epidural electrical stimulation of the spinal cord can reactivate those neurons [1–6]. It was found that the stimulation modulates the activity of specific neuronal populations including motoneurons by targeting the large diameter afferents where they enter the spinal cord through the dorsal root entry zones. Preprogrammed stimulation sequences targeting the individual dorsal root entry zones enabled standing and basic walking in people with paralysis due to a spinal cord injury. These sequences must be synchronized with the intended leg movements. For this purpose, the participants wore motion sensors that enabled the detection of residual movements in order to trigger the pre-programmed stimulation sequences. This strategy provided some degree of voluntary control over leg movements, but this control was limited and relied on compensatory strategies. Consequently, the control of walking was not perceived as natural and the patients showed limited ability to adapt leg movements to changing terrains and volitional demands, which are critical features for daily life activities.

In parallel, brain-computer interface (BCI) technologies were developed to predict motor intentions from cortical activity. In particular, during walking, pronounced modulations in the beta and gamma frequency bands are correlated to gait phases [7–10] and could be used as inputs to drive a prosthetic approach. Clinical evidence using electroencephalography (EEG) to control functional electrical stimulation (FES) showed the potential benefits of brain-controlled stimulation in stroke participants [11–13] as well as in paraplegic patients [14]. However, the cumbersomeness and sensitivity to motion artefacts make this method unrealistic for a widespread mobile and home-use application. On the other side of the spectrum, highly invasive intracortical recording electrodes are used in participants with tetraplegia to operate robotic arms [15], restore communication [16] or control FES of the upper limb [17]. Such intracortical arrays require a transcutaneous connector and a computational platform that is not suited to mobile applications. An intermediate modality between EEG and intracortical recordings captures the local field potentials at the surface of the brain or the dura mater using electrocorticography (ECoG). This modality provides robust signals with limited amount of noise and high stability over time while being fully implantable [18–22].

## 2  Design of the Fully Implantable Brain Spine Interface

Following a proof of concept in a nonhuman primate model of spinal cord injury [23], we designed a digital bridge between the brain and spinal cord to restore volitional control of muscle activity in humans. This design aimed at restoring a more natural and adaptive control of walking in humans with paralysis due to a spinal cord injury [24]. To establish this digital bridge, we integrated two fully-implanted systems that enable **recording** of cortical activity and **stimulation** of the lumbosacral spinal cord wirelessly and in real-time (Fig. 1). We leveraged the *WIMAGINE®* technology consisting of an 8-by-8 grid of 64 electrodes (4 mm × 4.5 mm pitch in antero-posterior and medio-lateral axes respectively) and recording electronics that are embedded within a 50-mm diameter circular-shaped titanium case presenting the same thickness as the skull (C. S. [18, 25]). ECoG signals are sampled at 586 Hz and streamed wirelessly through an ultrahigh frequency antenna (UHF, 402–405 MHz).

The ECoG signals are transferred to a portable decoding environment that extracts temporal, spectral and spatial features in real time and correlates those features to the intention to move the leg. More specifically, the features are fed into a decoding algorithm that predicts the attempts to move the lower limbs based
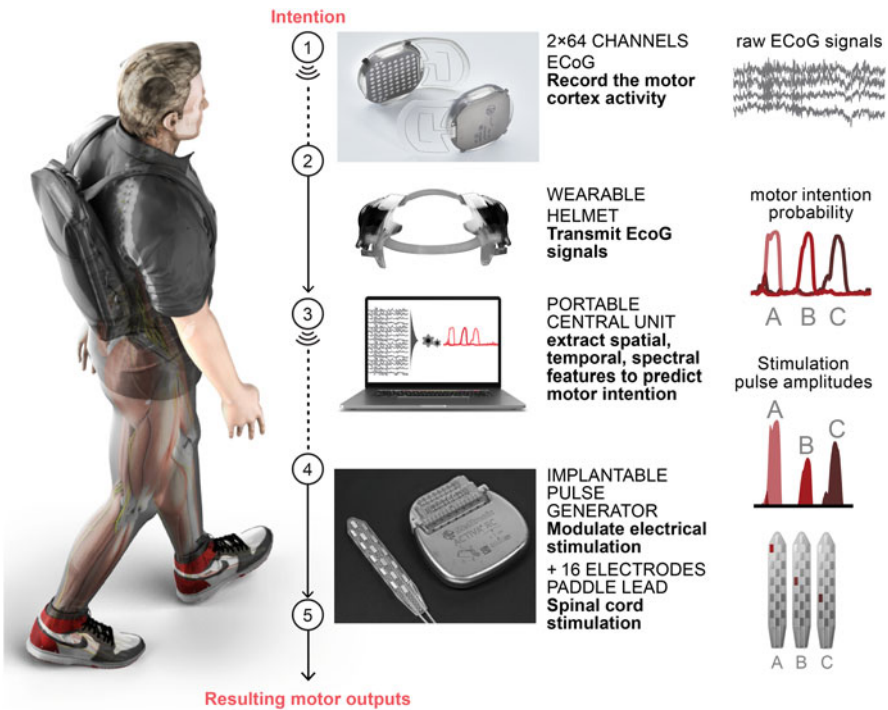


**Fig. 1**  Design of the brain spine interface (Photos: ©Jimmy Ravier)

on a recursive exponentially weighted Markov-switching multi-linear model algorithm [26]. This algorithm is a mixture of multilinear experts' algorithms integrating a Hidden Markov Model (HMM) classifier, called ***gating***, and a set of independent regression models, called ***experts***. The ***gating*** classifier predicts which joint is intended to be mobilized, while each ***expert*** is dedicated to predicting the direction and relative amplitude of the intended movement. The outputs of the model are encoded into continuous modulations of joint-specific stimulation programs within pre-established functional ranges of amplitudes. The algorithm can be recalibrated iteratively, which supports online calibration within a few minutes. Concretely, the participant receives visual and/or auditory cues to perform specific movements (e.g. "Right Hip Flexion", "Rest"). The data are labelled by the cue and the requested amplitude of movement. Every 15 s, the algorithm updates the coefficients of the model and provides updated stimulation commands.

These commands are continuously relayed to the spinal cord through an implantable pulse generator (*ACTIVA RC®*, Medtronic). We modified the firmware of the generator, which is commonly used for deep brain stimulation, to enable real-time control over stimulation parameters with a latency as low as 100 ms. Electrical pulses are delivered using an implantable paddle lead (*Specify 5-6-5®*, Medtronic) positioned over the epidural space to target the dorsal root entry zones of the lumbosacral spinal segments. Each stimulation configuration modulates specific ensembles of motor pools through the recruitment of the dorsal root entry zones projecting to the spinal cord regions wherein these motor pools reside [5, 27]. This physiological principle enables the regulation of extension and flexion movements from each joint. We leveraged this principle to configure a library of targeted epidural electrical stimulation programs that mobilized the hip, knee and ankle joints from both sides. Practically, we can configure combinations of anodes and cathodes, stimulation frequencies and amplitudes to steer electrical currents in order to achieve gradual control over the activity of the targeted muscle groups.

This integrated chain of hardware and software establishes a wireless digital bridge between the brain and spinal cord–a *digital bridge* that converts cortical activity into the analog modulation of epidural electrical stimulation programs to tune leg muscle activation, and thus regain standing and walking after paralysis due to a spinal cord injury.

## 3   Design of Stimo-BSI Clinical Trial (NCT04632290)

We designed the clinical study to test the safety and preliminary efficacy of this *BSI* to restore voluntary motor control of the lower limbs and promote neurological recovery. In order to assess the specific contribution of brain inputs to drive the stimulation compared to preprogrammed stimulation patterns, we opened the study to three participants who completed the main phase of the STIMO clinical trial (NCT02936453). This previous study involved a 5-month neurorehabilitation program supported by targeted epidural electrical stimulation of the spinal cord
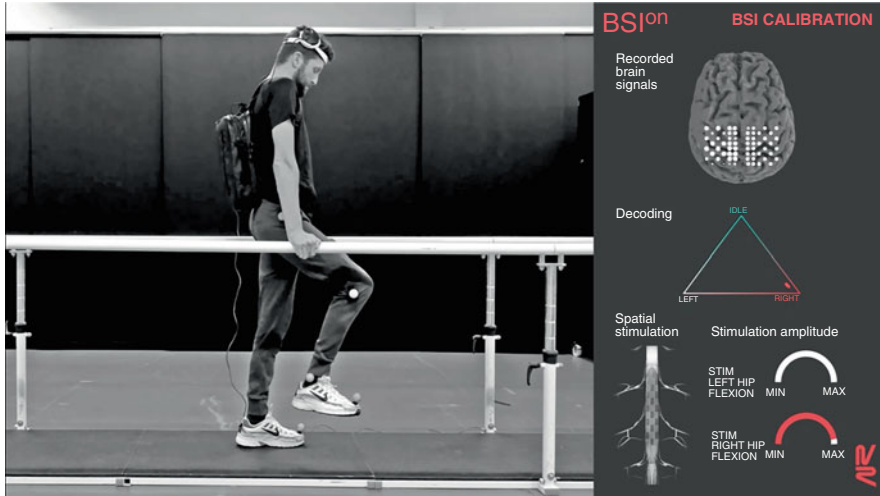
**Fig. 2** Restoration of voluntary hip flexion using the BSI (Photos: ©Jimmy Ravier)

[5, 6]. The STIMO-BSI follow-up trial involves the implantation of the two cortical *WIMAGINE®* recording systems, followed by a 1-month period of calibration and a 50-session rehabilitation phase. Pre-implantation, post-implantation and post-rehabilitation measures are performed including neurological evaluations (ASIA score) and functional evaluations (10-m walking test, 6-min walking test, Time Up and Go, Berg Balance Scale, quantitative gait analysis).

Pre-operativelly, we use anatomical and functional mapping to locate the optimal placements for the cortical and spinal implants. In particular, magnetoencephalography during lower limb motor attempts is used to validate the capacity of the participant to elicit detectable cortical signals in the leg sensorimotor area [28]. Implantation of the stimulation lead over the dorsal epidural space of the spinal cord is performed using high resolution MRI to locate the trajectory of the roots and predict the optimal location to cover most efficiently the lower limb motor pools [5].

After surgical implantation of the system, the digital bridge is calibrated for single joint movements before combining different movements together. The system is designed to control up to six independent muscle groups simultaneously with a latency close to 1 s. The same paradigm can be then used in a mobile environment to trigger leg movements associated with standing and walking (Fig. 2).

In this context, we implanted a 38-year-old male who had sustained an incomplete cervical (C5/C6) spinal cord injury during a biking accident 10 years prior to his enrollment. The STIMO program had allowed him to regain the ability to step with the help of a front-wheel walker. Despite continued use of the stimulation at home for approximately 3 years, he had reached a neurological recovery plateau that motivated him to enroll in STIMO-BSI. This study was approved by the Swiss authorities (EUDAMED CIV-20-07-034126) and was conducted in accordance with the Declaration of Helsinki.

For this participant, the digital bridge restored continuous, intuitive and robust control of walking with a front-wheel walker as well as with crutches. When the digital bridge was turned off, the participant instantly lost the ability to perform any step despite detected attempts to walk from the modulation of cortical activity. Walking could resume as soon as the digital bridge was turned back on. The participant reported experiencing a natural and precise control over his movements, allowing him to adapt and walk through different terrains. In contrast, walking with external sensors and preprogrammed stimulation sequences required compensatory strategies. When standing or walking with the digital bridge the control "feels more natural" and gives him a "freedom that [he] didn't have before".

The participant completed the rehabilitation phase that involved walking with the digital bridge, performing single-joint movements with the digital bridge, balance with the digital bridge, and standard physiotherapy. This neurorehabilitation program mediated pronounced neurological and functional improvements. In particular, this recovery correlated with gains in motor scores, and enhanced standing and walking capacities that were captured in an increase in WISCI II scores. Specifically, the participant exhibited improvements in all the conventional clinical assessments such as the 6-min walk test, weight-bearing capacities, timed up and go, Berg Balance Scale, and walking quality.

Finally, we designed a system that could be operated by the participant without any assistance. This system includes a front-wheel walker equipped with an integrated case that embeds all the components of the digital bridge. A tactile-based interface allows the participant to interact with the tailored software in order to launch an activity, verify the placement of the headset, and adjust the minimum and maximum amplitudes of stimulation programs. The configuration of the hardware and software is completed with minimal user inputs within less than 5 min, after which the participant can leverage the digital bridge for neurorehabilitation or to support activities of daily living.

## 4   Discussion

Our technological and clinical design establishes the first-in-human proof of concept of a continuous link between the brain and the region of the spinal cord that controls muscle activity. This digital bridge restores voluntary control over previously paralyzed muscles in a natural and intuitive way in a participant with spinal cord injury. We are continuously improving the capacity of the system in terms of usability, latency and degrees of freedom. Miniaturization of the acquisition and computing system into an embedded platform will further increase patient acceptability and prepare the dissemination of this therapy. Finally, while we found that decoders could remain stable over several weeks, recent advances in self-supervised learning could enable automatic recalibration of the system without need of explicit labelling of the data. These developments require time and resources, but we do not anticipate technical hurdles to realize this transition.

Expanding the concept of a digital bridge to the cervical spinal cord may also support the restoration of arm and hand movements after spinal cord injury or stroke, auguring a new era in the treatment of motor deficits due to neurological disorders.

# References

1. Angeli CA, Boakye M, Morton RA, Vogt J, Benton K, Chen Y, Ferreira CK, Harkema SJ (2018) Recovery of over-ground walking after chronic motor complete spinal cord injury. N Engl J Med 379(13):1244–1250. https://doi.org/10.1056/NEJMoa1803588

2. Schirmer CM, Shils JL, Arle JE, Rees Cosgrove G, Dempsey PK, Tarlov E, Kim S et al (2011) Heuristic map of myotomal innervation in humans using direct intraoperative nerve root stimulation. J Neurosurg Spine SPI 15(1):64–70. https://doi.org/10.3171/2011.2.SPINE1068

3. Gill ML, Grahn PJ, Calvert JS, Linde MB, Lavrov IA, Strommen JA, Beck LA et al (2018) Neuromodulation of lumbosacral spinal networks enables independent stepping after complete paraplegia. Nat Med 24(11):1677–1682. https://doi.org/10.1038/s41591-018-0175-7

4. Mesbah S, Herrity A, Ugiliweneza B, Angeli C, Gerasimenko Y, Boakye M, Harkema S (2023) Neuroanatomical mapping of the lumbosacral spinal cord in individuals with chronic spinal cord injury. Brain Commun 5(1):fcac330. https://doi.org/10.1093/braincomms/fcac330

5. Rowald A, Komi S, Demesmaeker R, Baaklini E, Hernandez-Charpak SD, Paoles E, Montanaro H et al (2022) Activity-dependent spinal cord neuromodulation rapidly restores trunk and leg motor functions after complete paralysis. Nat Med 28(2):260–271. https://doi.org/10.1038/s41591-021-01663-5

6. Wagner FB, Mignardot J-B, Le Goff-Mignardot CG, Demesmaeker R, Komi S, Capogrosso M, Rowald A et al (2018) Targeted neurotechnology restores walking in humans with spinal cord injury. Nature 563(7729):65–71. https://doi.org/10.1038/s41586-018-0649-2

7. McCrimmon CM, Wang PT, Heydari P, Nguyen A, Shaw SJ, Gong H, Chui LA, Liu CY, Nenadic Z, Do AH (2017) Electrocorticographic encoding of human gait in the leg primary motor cortex. Cereb Cortex 28(8):2752–2762. https://doi.org/10.1093/cercor/bhx155

8. Seeber M, Scherer R, Wagner J, Solis-Escalante T, Müller-Putz GR (2014) EEG beta suppression and low gamma modulation are different elements of human upright walking. Front Hum Neurosci 8(July):485–485. https://doi.org/10.3389/fnhum.2014.00485

9. Seeber M, Scherer R, Wagner J, Solis-Escalante T, Müller-Putz GR (2015) High and low gamma EEG oscillations in central sensorimotor areas are conversely modulated during the human gait cycle. NeuroImage 112(May):318–326. https://doi.org/10.1016/j.neuroimage.2015.03.045

10. Wagner J, Solis-Escalante T, Grieshofer P, Neuper C, Müller-Putz G, Scherer R (2012) Level of participation in robotic-assisted treadmill walking modulates midline sensorimotor EEG

rhythms in able-bodied subjects. NeuroImage 63(3):1203–1211. https://doi.org/10.1016/j.neuroimage.2012.08.019

11. Biasiucci A, Leeb R, Iturrate I, Perdikis S, Al-Khodairy A, Corbet T, Schnider A et al (2018) Brain-actuated functional electrical stimulation elicits lasting arm motor recovery after stroke. Nat Commun 9(1):2421. https://doi.org/10.1038/s41467-018-04673-z

12. Jovanovic LI, Kapadia N, Lo L, Zivanovic V, Popovic MR, Marquez-Chin C (2019) Restoration of upper-limb function after chronic severe hemiplegia: a case report on the feasibility of a brain-computer interface controlled functional electrical stimulation therapy. Am J Phys Med Rehabil. Publish Ahead of Print. https://journals.lww.com/ajpmr/Fulltext/publishahead/Restoration_of_upper_limb_function_after_chronic.98294.aspx

13. McCrimmon CM, King CE, Wang PT, Cramer SC, Nenadic Z, An HD (2014) Brain-controlled functional electrical stimulation for lower-limb motor recovery in stroke survivors. Annu Int Conf IEEE Eng Med Biol Soc 2014:1247–1250. https://doi.org/10.1109/EMBC.2014.6943823

14. Selfslagh A, Shokur S, Campos DSF, Donati ARC, Almeida S, Yamauti SY, Coelho DB, Bouri M, Nicolelis MAL (2019) Non-invasive, brain-controlled functional electrical stimulation for locomotion rehabilitation in individuals with paraplegia. Sci Rep 9(1):6782. https://doi.org/10.1038/s41598-019-43041-9

15. Hochberg LR, Bacher D, Jarosiewicz B, Masse NY, Simeral JD, Vogel J, Haddadin S et al (2012) Reach and grasp by people with tetraplegia using a neurally controlled robotic arm. Nature 485(May):372

16. Willett FR, Avansino DT, Hochberg LR, Henderson JM, Shenoy KV (2021) High-performance brain-to-text communication via handwriting. Nature 593(7858):249–254. https://doi.org/10.1038/s41586-021-03506-2

17. Ajiboye AB, Willett FR, Young DR, Memberg WD, Murphy BA, Miller JP, Walter BL et al (2017) Restoration of reaching and grasping movements through brain-controlled muscle stimulation in a person with tetraplegia: a proof-of-concept demonstration. Lancet 389(10081):1821–1830. https://doi.org/10.1016/S0140-6736(17)30601-3

18. Benabid AL, Costecalde T, Eliseyev A, Charvet G, Verney A, Karakas S, Foerster M et al (2019) An exoskeleton controlled by an epidural wireless brain–machine interface in a tetraplegic patient: a proof-of-concept demonstration. Lancet Neurol. https://doi.org/10.1016/S1474-4422(19)30321-7

19. Larzabal C, Bonnet S, Costecalde T, Auboiroux V, Charvet G, Chabardes S, Aksenova T, Sauter-Starace F (2021) Long-term stability of the chronic epidural wireless recorder WIMAGINE in tetraplegic patients. J Neural Eng 18(5):056026. https://doi.org/10.1088/1741-2552/ac2003

20. Moses DA, Metzger SL, Liu JR, Anumanchipalli GK, Makin JG, Sun PF, Chartier J et al (2021) Neuroprosthesis for decoding speech in a paralyzed person with anarthria. N Engl J Med 385(3):217–227. https://doi.org/10.1056/NEJMoa2027540

21. Pels EGM, Aarnoutse EJ, Leinders S, Freudenburg ZV, Branco MP, van der Vijgh BH, Snijders TJ, Denison T, Vansteensel MJ, Ramsey NF (2019) Stability of a chronic implanted brain-computer interface in late-stage amyotrophic lateral sclerosis. Clin Neurophysiol 130(10):1798–1803. https://doi.org/10.1016/j.clinph.2019.07.020

22. Vansteensel MJ, Pels EGM, Bleichner MG, Branco MP, Denison T, Freudenburg ZV, Gosselaar P et al (2016) Fully implanted brain–computer interface in a locked-in patient with ALS. N Engl J Med 375(21):2060–2066. https://doi.org/10.1056/NEJMoa1608085

23. Capogrosso M, Milekovic T, Borton D, Wagner F, Moraud EM, Mignardot J-B, Buse N et al (2016) A brain–spine interface alleviating gait deficits after spinal cord injury in primates. Nature 539(November):284

24. Lorach H, Charvet G, Bloch J, Courtine G (2022) Brain-spine interfaces to reverse paralysis. Natl Sci Rev January:nwac009. https://doi.org/10.1093/nsr/nwac009

25. Mestais CS, Charvet G, Sauter-Starace F, Foerster M, Ratel D, Benabid AL (2015) WIMAGINE: Wireless 64-channel ECoG recording implant for long term clinical applications.

IEEE Trans Neural Syst Rehabil Eng 23(1):10–21. https://doi.org/10.1109/TNSRE.2014.2333541

26. Moly A, Costecalde T, Martel F, Martin M, Larzabal C, Karakas S, Verney A et al (2022) An adaptive closed-loop ECoG decoder for long-term and stable bimanual control of an exoskeleton by a tetraplegic. J Neural Eng 19(2):026021. https://doi.org/10.1088/1741-2552/ac59a0

27. Capogrosso M, Wenger N, Raspopovic S, Musienko P, Beauparlant J, Luciani LB, Courtine G, Micera S (2013) A computational model for epidural electrical stimulation of spinal sensorimotor circuits. J Neurosci 33(49):19326–19340. https://doi.org/10.1523/JNEUROSCI.1688-13.2013

28. Auboiroux V, Larzabal C, Langar L, Rohu V, Mishchenko A, Arizumi N, Labyt E, Benabid A-L, Aksenova T (2020) Space–time–frequency multi-sensor analysis for motor cortex localization using magnetoencephalography. Sensors 20(9). https://doi.org/10.3390/s20092706

# Brain-Body Interfaces to Assist and Restore Motor Functions in People with Paralysis

**Elena Losanno, Marion Badi, Evgenia Roussinova, Andrew Bogaard, Maude Delacombaz, Solaiman Shokur, and Silvestro Micera**

**Abstract** Brain-Body Interfaces (BBIs) restore the connection between brain motor commands and body movements actuated via electrical stimulation. BBIs have emerged as a solution to achieve two complementary rehabilitation objectives in people with motor deficits: induce long-lasting neurological recovery and assist motor functions during daily activities. Here, we describe representative promising implementations for both applications and future steps toward their diffusion into clinical practice. We also present our assistive BBI approach to restore hand functions based on intrafascicular stimulation of arm nerves and decoding of neural manifold dynamics in the primary motor cortex. Preclinical tests demonstrate that our solution is promising for providing motor dexterity and decoding stability.

Solaiman Shokur and Silvestro Micera contributed equally with all other contributors.

E. Losanno
The Biorobotics Institute and Department of Excellence in Robotics and AI, Scuola Superiore Sant'Anna, Pisa, Italy

M. Badi · E. Roussinova · S. Shokur
Bertarelli Foundation Chair in Translational Neuroengineering, Center for Neuroprosthetics and Institute of Bioengineering, École Polytechnique Fédérale de Lausanne (EPFL), Lausanne, Switzerland

A. Bogaard · M. Delacombaz
Department of Neuroscience and Movement Sciences, Platform of Translational Neurosciences, Section of Medicine, Faculty of Sciences and Medicine, University of Fribourg, Fribourg, Switzerland

S. Micera (✉)
The Biorobotics Institute and Department of Excellence in Robotics and AI, Scuola Superiore Sant'Anna, Pisa, Italy

Bertarelli Foundation Chair in Translational Neuroengineering, Center for Neuroprosthetics and Institute of Bioengineering, École Polytechnique Fédérale de Lausanne (EPFL), Lausanne, Switzerland
e-mail: silvestro.micera@epfl.ch; silvestro.micera@santannapisa.it

## 1  Introduction

Far from being yet one more 'Brain-X-interface' in a field that already has considerable nomenclature, Brain-Body Interfaces (BBIs) describe neuroprostheses that allow users to voluntarily control the movement of their bodies. Brain activity recorded from cortical sensorimotor areas using invasive or non-invasive interfaces is translated into motion commands to actuate limbs via electrical stimulation of neuromuscular structures. This requires tackling two neurotechnological modules—one for motor decoding and one for movement restoration—and their interaction [1]. The BBI concept is very interesting for at least two reasons. First, the control of the 'own' body—as opposed to an external actuator—might be the preferred assistive solution for patients with motor deficits [2]. Second, BBIs allow the contingent link between brain activity and body mobilization, creating the conditions for Hebbian-like plasticity close to the injured tissue [3]. Building on this hypothesis, studies have shown that BBIs can promote neurological recovery, particularly in stroke survivors and patients with motor-complete spinal cord injury (SCI), as we will describe here.

In this section, we will show representative studies of both aspects, but instead of a detailed list of implementations, we will concentrate on two examples of applications that have, in our view, great potential to evolve in the future into clinical practice: (1) fully non-invasive and minimally invasive BBIs aiming to induce long-lasting neurological recovery; and (2) BBIs based on implantable components to assist motor functions.

## 2  BBI for Neurological Recovery

Until recently, the chances of achieving significant long-lasting neurological and functional recovery in individuals with the most severe cases of sensory-motor deficiencies due to SCI or stroke were considered negligible. While a considerable amount of spontaneous neurological recovery is observed at the acute phase for both SCI [4, 5] and stroke patients [6], it is absent during the chronic phase. During the early stage, the recovery is a combination of restitution (spontaneous restoring of the functionality of damaged neural tissue), substitution (reorganization of partly-spared neural pathways to relearn lost functions), and compensatory mechanisms [6].

At the chronic phase, the neurorehabilitation for stroke patients aims to promote adaptive plasticity of structure and function in the undamaged brain toward

**Fig. 1** Examples of therapeutic BBIs. (**a**) EEG activity is used to trigger the wrist flexion/extension via sFES as part of a neurorehabilitation protocol for stroke patients (www.recoverix.at/). (**b**) A BBI based on EEG decoding and lower-limb sFES was used in a 5-month long intervention in two patients with chronic SCI, leading to a marked motor recovery in one of the two patients [15]

recovery, driven by motor training. Protocols such as constraint-induced motor therapy, where the subject is forced to use the paralyzed limb [7], have shown significant results in stroke patients who have residual motor functions at the onset of the protocol. For stroke survivors with severe motor loss, BBIs to actuate the paretic limb based on the decoded motor intention have been proposed as an alternative to induce activity-based plasticity [8]. These strategies were successfully tested for both upper-limb [9–12] and lower-limb motor neurorehabilitation [13, 14], leading to substantial motor improvements and brain plasticity. In these protocols, patients' motor intentions are generally recorded via electroencephalography (EEG) and decoded in real-time to control surface functional electrical stimulation (sFES) to trigger muscle contractions in the subject's paretic limb (Fig. 1a). A central role for neural recovery is played by the simultaneous engagement of descending and ascending neural pathways, which induces Hebbian-like plasticity [3].

Recent studies have also shown that BBIs could induce some neural recovery in people with SCI [15, 16]. The integration of EEG-based decoding and lower-limb sFES in a 5-month long protocol showed a marked motor recovery below the lesion in one out of the two patients who followed the training [15] (Fig. 1b). The hypothesis for such partial recovery comes from the observation that the majority of patients diagnosed as motor-complete SCI using the ASIA scale have preserved fibers at the lesion level [17, 18]. In other words, by involving the SCI subject in training that targets both cortical and spinal plasticity, it is possible to engage the remaining fibers to recover functions below the lesion. This hypothesis was confirmed in the rat SCI model. A study with motor-complete rats showed that training integrating commands via intracortical signals and epidural spinal cord stimulation (SCS) enhanced neurological recovery compared to epidural SCS training alone [16].

## 2.1  Future Perspectives

The key element in BBIs for neurological recovery is the synchronization between the efferent and afferent signals [3] rather than very precise multi-DoF decoding. Also, the intervention is temporary and the optimal recording/stimulation sites may change over time following recovery. For all of these reasons, most of the implementations are based on non-invasive or minimally invasive motor decoding and movement restoration modules. In the following, we will describe some of the directions in which the two modules are currently evolving and highlight the importance of including somatosensory feedback.

### 2.1.1  Motor Decoding

As mentioned earlier, in therapeutic BBIs, motor decoding is generally based on EEG. EEG is the most widely used brain signal acquisition method because it is non-invasive thus practical, and offers a high temporal resolution. However, EEG has some limitations that can affect the efficacy of the intervention: it requires skill and time to place and calibrate the system, has a low spatial resolution, and is susceptible to external noise. These limitations can lead to low decoding accuracy, in particular when classifying fine movements, and make the therapy unreliable or suboptimal. To increase spatial resolution and thus control performance in a wider range of tasks, some groups are exploring high-density EEG systems [19, 20]. Usually these systems include between 160 and 256 electrodes, but denser layouts with up to 1024 electrodes also exist. A recent study demonstrated the possibility of decoding individual finger movements with ultra-high-density EEG with quite good accuracy [21], paving the way for targeted interventions for hand rehabilitation.

Other groups are working to improve the decoding accuracy of BBIs for post-stroke upper-limb rehabilitation using hybrid control solutions based on the combination of EEG and EMG signals [22–24]. Another advantage of integrating the central with the peripheral motor intention in stroke survivors is that the cortical compensation (i.e., the increased motor control by the disinhibited contralesional hemisphere) can be better suppressed, thereby reinforcing the desired projection of motor commands to target muscles and the efficacy of the intervention [23]. Hybrid control strategies make use of features expressing the cortico-muscular coupling, i.e., the synchrony between EEG and EMG activity, for movement classification.

Alternatives to EEG are also being investigated. While invasive technologies such as electrocorticography (ECoG) or intracortical electrodes may not provide a large enough benefit-risk ratio for a therapeutic system at their current stage, electrode grids implanted in the subgaleal space (i.e., the intermediate space between the skin on the scalp and the skull) offer a minimally invasive option to avoid repeated placement of the electrodes and improve signal quality compared to EEG [25, 26]. Studies on motor decoding based on subgaleal signals are currently missing. However, it has been promisingly shown that meaningful high gamma

activity (which is thought to concur with the activity of single neurons [27] and is informative for motor decoding) can be recorded using subgaleal electrodes similarly to ECoG [28].

### 2.1.2  Movement Restoration

sFES is the most commonly used technique for neurorehabilitation. In the field of therapeutic sFES, there has been recent increased interest in multi-pad electrodes (see [29] for a review) and textile-based devices [30]. Multi-pad electrodes can more flexibly shape the electric field, thus increasing selectivity, and temporally distribute stimuli over different muscle areas, thus delaying the onset of fatigue. In this way, more targeted and effective interventions can be developed. Another advantage of multi-pad electrodes for rehabilitative use is their flexibility in personalizing the intervention. With multiple independent stimulation channels the stimulation paradigm can not only be tailored to each patient's anatomy and clinical condition, but also optimized over time based on the patient's response to treatment. On the other hand, textile-based systems improve comfort and wearability which are particularly important for extension to home treatment.

Besides sFES, epidural SCS has shown remarkable therapeutic effect in the SCI population, likely because residual supraspinal commands spatiotemporally converge with the activation of spinal circuits with this technique, favoring functional neuroplasticity [31–33]. But non-invasive alternatives to epidural SCS are also being tested and show promising results [34–36]. An 18 week intervention combining administration of monoaminergic solution and transcutaneous SCS at the lumbosacral segments with five motor-complete SCI patients showed the generation of stepping-like movement in a gravity-neutral position [34]. Importantly, following the training, the patients were able to generate lower-limb movements even in the absence of stimulation. Further analysis provided electrophysiological evidence of the reestablishment of functional connectivity between the brain and the spinal cord.

### 2.1.3  Sensory Feedback

Most people who suffer a SCI or stroke end up having not only motor, but also sensory deficits. Because sensation plays a crucial role in motor control, providing somatosensory input congruent with the evoked movement may facilitate neural plasticity and increase the effectiveness of therapeutic interventions in these patients. A recent study has shown that a sFES approach that simultaneously provides muscular and cutaneous activation leads to greater sensorimotor improvements than motor-only treatments in chronic stroke patients [37].

## 3   BBIs for Assistance

Assistive BBIs should provide the user with good dexterity and guarantee stability, allowing patients to recover a certain degree of independence. Thus, we identify the following key technical challenges to overcome: the motor decoding strategy should ideally be easy to learn, accurate, and stable over time; the movement restoration module should provide good selectivity and not be prone to rapid fatigue.

Early examples of assistive BBIs include intracortical control of hand functions via sFES or implanted muscle stimulation (also known as implanted FES) in monkeys [38–40]. In the past 5 years, there have been also demonstrations of assistive BBIs for hand control in people with tetraplegia [41–43]. One of the first studies was performed at Case Western University [42]. The participant was implanted with an intracortical array in the primary motor cortex (M1) and stimulating electrodes in forearm muscles (Fig. 2a). Intended hand movements were decoded from intracortical signals based on a linear decoder and used to drive implanted FES for grasping and an arm support for reaching. Using the BBI, the participant could perform simple, functional tasks such as drinking and self-feeding. The same group is now conducting a clinical trial to test a BBI based on epineural stimulation integrating sensory feedback in patients with high tetraplegia [46]. Nerve cuff electrodes called C-FINEs are implanted around nerve branches of the upper limb to reactivate shoulder, arm, and hand movements based on the subject's motor intention, as decoded from M1 recordings. Motor control is coupled with stimulation of the somatosensory cortex to restore sensation.

Recently, we have validated an assistive BBI solution for grasping in a monkey based on decoding of neural manifold (i.e., low-dimensional space in which neural population activity is constrained [45]) dynamics and intrafascicular stimulation (Fig. 2b) [44]. Brain signals were recorded via an intracortical array in the hand area of M1, while hand opening and closing were evoked by electrical stimuli delivered via intrafascicular electrodes called TIMEs implanted in the animal's radial and median nerves. Neural manifold dynamics were linearly mapped to both the amplitude of intrafascicular stimulation and the position of a cursor to provide visual feedback and instructions to the animal. We instructed the monkey to move the cursor towards vertical and horizontal targets by modulating her cortical activity, thereby enabling the voluntary control of smooth hand opening and closing.

### 3.1   Future Perspectives

As emerged from the examples described above, research groups working on assistive BBIs went towards the use of systems with implantable components. Besides proving higher dexterity and thus independence in a wider range of activities, implantable devices increase comfort for daily use, reducing time and need for assistance in the setting up process and improving aesthetics. Some clinical
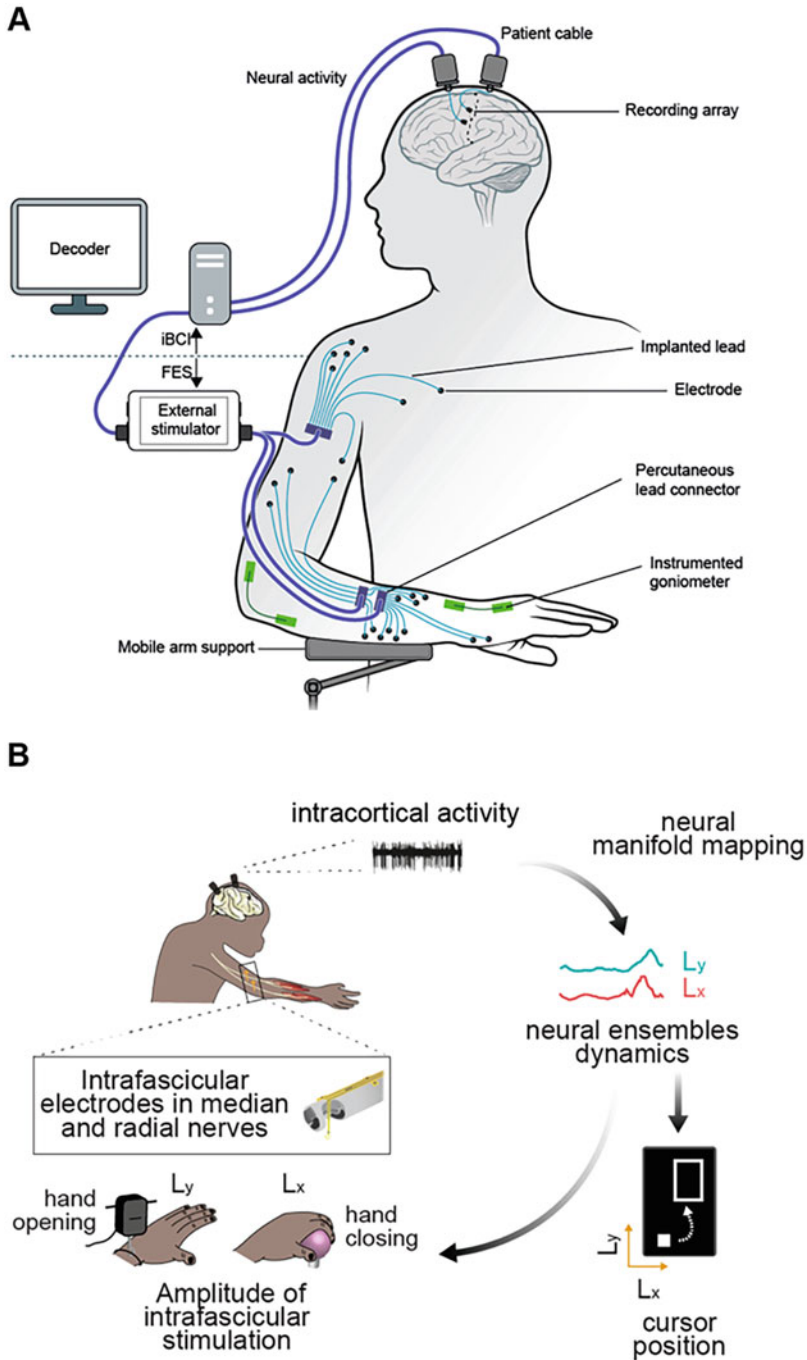
**Fig. 2** Examples of assistive BBIs. (**a**) An invasive BBI to restore reaching and grasping was tested in a patient with high cervical SCI [42]: neural activity was recorded with intracortical electrodes and used to drive implanted FES for grasping and an arm support for reaching, based on a linear

demonstrations of these implantable technologies have been performed, but different scientific and technological challenges remain to be addressed for their effective translation to clinical practice. In the following, we will describe some features that could promote the clinical use of assistive BBIs.

### 3.1.1 Motor Decoding

Most of the animal studies on assistive BBIs have used intracortical electrodes, and in particular Utah arrays [47], to record brain signals. In the last 5 years, Utah arrays have been also employed in human BBI studies. Intracortical interfaces have the highest recording resolution and thus give the highest control accuracy and dimensionality. For example, they have been used for continuous 10-DoF prosthetic arm control [48] and to decode kinematics of multiple finger groups online [49]. However, intracortical electrodes cause considerable scarring in their proximity [50, 51] leading to low stability of the signal and affecting decoding performance over time. This is a crucial issue for clinical applications. To preserve performance of standard decoding algorithms without frequently collecting calibration data, efforts have been made to implement automatic, unsupervised recalibration methods [52, 53].

Another promising solution to get stable performance is represented by decoders that exploit neural plasticity to compensate for recording instabilities [54]. In this framework, we have shown that a monkey could intuitively learn to modulate these dynamics and adapt modulation to long-term recording changes using a motor decoding strategy based on the direct mapping between intrinsic neural ensemble dynamics and output variables [44]. In more detail, we computed a neural manifold [45] associated with a hand motor task once, then used neural dynamics along the manifold axes to drive the position of a cursor in real-time. We tested this paradigm in a point-to-point cursor control task over a 16-week incremental training protocol: the monkey showed rapid learning of new tasks and a stable success rate of ~90% until the end of the protocol, without recalibration of the control space. Further studies in animals and patients with paralysis are necessary to validate the use of manifold-based direct control as an easy-to-learn and stable motor decoding strategy for future BBIs.

At the same time, several groups are working to increase stability of intracortical implants by improving electronics. Examples include development of subcellular electrodes that induce little foreign body response [55, 56], or "neural dust", i.e., miniaturized electronic implants covering large cortical areas that wirelessly transmit neural data [57, 58].

---

**Fig. 2** (continued) decoder. (**b**) Our BBI solution to restore grasping was tested in a chronically implanted monkey [44]: intracortical activity projected along the axes of a motor neural manifold [45] was used to drive both intrafascicular stimulation of the median and radial nerves and the position of a cursor to give visual feedback and instructions to the animal

ECoG represents a less invasive alternative to intracortical interfaces that is thought to be less susceptible to long-term instabilities [59]. After the first offline demonstrations of motor decoding using ECoG activity recorded in epileptic patients [60–64], ECoG systems have become popular for online control of exoskeletons [65] or robotic limbs [66, 67] in people with paralysis. Moreover, wireless portable ECoG systems are now under preclinical [68] or clinical [65, 69] testing. It is however yet unknown if the ECoG recording resolution will be sufficient for decoding fine movements, such as those of the hand.

### 3.1.2 Movement Restoration

To promote clinical usage of assistive BBIs, the movement restoration module should be designed to approach the true dexterity of the limb to reanimate while minimizing complexity of the surgery and its associated risks. Thus, the level of the neuromuscular system to target with stimulation should be chosen depending on the application. For example, epidural SCS, whose surgery is well-established, has been demonstrated as an effective approach to restore coarse movements, such as walking [33, 70] and reaching [71]. However, more selectivity and thus a more distal stimulation target is necessary to restore fine movements, such as those of the hand. Implanted FES has been traditionally used to evoke hand functions [72], but it relies on the implantation of multiple distributed electrodes, making the surgical intervention long and extensive. Targeting the motor fibers of the peripheral nervous system via intrafascicular electrodes offers an option to provide similar dexterity to implanted FES with a lower number of implants. A study with monkeys done by our group [73] showed that intrafascicular stimulation via TIMEs can evoke multiple selective grasps and hand extension movements with only two implants in the median and radial nerves. Moreover, it was possible to produce functional levels of force that could be sustained over prolonged periods of time with limited muscle fatigue. While the validation in patients with paralysis is currently missing, intrafascicular stimulation seems a very promising solution for clinical BBIs to restore fine movements.

Another challenge in developing effective clinical BBIs is that motor responses to electrical stimulation can change due to the emergence of fatigue or perturbations such as spinal reflexes in SCI patients. A robust and reliable movement restoration module should automatically compensate for these changes. A possibility for that would be to use closed-loop controllers that modify the stimulation parameters in real-time to maintain a target motor response [74]. Some demonstrations of closed-loop neuroprostheses have been performed in which the amplitude or frequency of stimulation was modulated by feedback controllers to maintain a target grasp force or step height [75–77], leading to accurate motor outputs.

More generally, we believe that the efficacy and safety of assistive BBIs is improved if the movement restoration module has some level of autonomy and shares control with the motor decoding module [78]. Shared control could be implemented by providing information about the body interaction with objects to

the stimulation controller, which would consequently perform low-level actions, such as obstacle avoidance or "economic" object securing (i.e., securing an object with the minimum force that does not cause slippage to avoid undue muscle fatigue). This would reduce the burden of user input, optimize neuroprosthesis use, and increase safety. Interaction with objects could be detected using electronic skins (see [79] for a review) or recordings from the body's own sensory stream [80], such as sensory nerves [81] or the somatosensory cortex [82].

### 3.1.3 Sensory Feedback

The integration of sensory feedback would also add great value to assistive BBIs in terms of performance and safety. In a recent study, a BBI for grasping was combined with an arm vibrotactile array to provide touch information, leading to greater functionality than a pure motor BBI [82]. This approach is an example of sensory substitution, where sensation is provided by the electrical or mechanical stimulation of a substitutive district [83]. Alternatively, sensation could be restored using biomimetic sensory feedback by electrically stimulating an intact region of the natural sensory pathway [83]. An example region is the somatosensory cortex targeted by the group of Case Western University for their current clinical trial [46].

## 4   Conclusion

In summary, we foresee the development of BBIs in two complementary directions: non-invasive or minimally-invasive BBIs for temporary neurorehabilitation and implantable BBIs for long-term assistive use. For an assistive BBI to restore hand movements, a particularly interesting solution to have a good trade-off between dexterity and number of implants might be the use of intrafascicular stimulation of the peripheral nerves. Decoding stability could be instead provided by the manifold-based direct control strategy.

Eventually, when the burden of surgical and technological costs is lower, one could imagine that the two approaches of therapeutic and assistive BBIs converge to one. Hybrid systems based on an invasive motor decoding module and a non-invasive movement restoration module (e.g., ECoG-based control of a multi-pad sFES system) could also be viable solutions in the short term.

## References

1. Shokur S, Mazzoni A, Schiavone G, Weber DJ, Micera S (2021) A modular strategy for next-generation upper-limb sensory-motor neuroprostheses. Med 2(8):912–937. https://doi.org/10.1016/j.medj.2021.05.002

2. Collinger JL, Boninger ML, Bruns TM, Curley K, Wang W, Weber DJ (2013) Functional priorities, assistive technology, and brain-computer interfaces after spinal cord injury. J Rehabil Res Dev 50(2):145–160. https://doi.org/10.1682/jrrd.2011.11.0213

3. Ethier C, Gallego J, Miller L (2015) Brain-controlled neuromuscular stimulation to drive neural plasticity and functional recovery. Curr Opin Neurobiol 33:95–102. https://doi.org/10.1016/j.conb.2015.03.007

4. Steeves JD et al (2007) Guidelines for the conduct of clinical trials for spinal cord injury (SCI) as developed by the ICCP panel: clinical trial outcome measures. Spinal Cord 45(3):206–221. https://doi.org/10.1038/sj.sc.3102008

5. Harrop JS et al (2011) Neurologic improvement after thoracic, thoracolumbar, and lumbar spinal cord (conus medullaris) injuries. Spine (Phila Pa 1976) 36(1):21–25. https://doi.org/10.1097/BRS.0b013e3181fd6b36

6. Langhorne P, Bernhardt J, Kwakkel G (2011) Stroke rehabilitation. Lancet 377(9778): 1693–1702. https://doi.org/10.1016/S0140-6736(11)60325-5

7. Taub E, Uswatte G, Pidikiti R (1999) Constraint-Induced Movement Therapy: a new family of techniques with broad application to physical rehabilitation – a clinical review. J Rehabil Res Dev 36(3):237–251

8. Soekadar SR, Birbaumer N, Slutzky MW, Cohen LG (2015) Brain–machine interfaces in neurorehabilitation of stroke. Neurobiol Dis 83:172–179. https://doi.org/10.1016/j.nbd.2014.11.025

9. Daly JJ, Cheng R, Rogers J, Litinas K, Hrovat K, Dohring M (2009) Feasibility of a new application of noninvasive Brain Computer Interface (BCI): a case study of training for recovery of volitional motor control after stroke. J Neurol Phys Ther 33(4):203–211. https://doi.org/10.1097/NPT.0b013e3181c1fc0b

10. Young BM et al (2014) Changes in functional brain organization and behavioral correlations after rehabilitative therapy using a brain-computer interface. Front Neuroeng 7. https://www.frontiersin.org/articles/10.3389/fneng.2014.00026. Accessed 22 Dec 2022. [Online]

11. Biasiucci A et al (2018) Brain-actuated functional electrical stimulation elicits lasting arm motor recovery after stroke. Nat Commun:1–13. https://doi.org/10.1038/s41467-018-04673-z

12. Jovanovic LI, Kapadia N, Lo L, Zivanovic V, Popovic MR, Marquez-Chin C (2020) Restoration of upper limb function after chronic severe hemiplegia: a case report on the feasibility of a brain-computer interface-triggered functional electrical stimulation therapy. Am J Phys Med Rehabil 99(3):e35–e40. https://doi.org/10.1097/PHM.0000000000001163

13. Takahashi M et al (2012) Event related desynchronization-modulated functional electrical stimulation system for stroke rehabilitation: a feasibility study. J NeuroEng Rehabil 9(1):56. https://doi.org/10.1186/1743-0003-9-56

14. Chung E, Park S-I, Jang Y-Y, Lee B-H (2015) Effects of brain-computer interface-based functional electrical stimulation on balance and gait function in patients with stroke: preliminary results. J Phys Ther Sci 27(2):513–516. https://doi.org/10.1589/jpts.27.513

15. Selfslagh A et al (2019) Non-invasive, brain-controlled functional electrical stimulation for locomotion rehabilitation in individuals with paraplegia. Sci Rep 9(1):1. https://doi.org/10.1038/s41598-019-43041-9

16. Bonizzato M et al (2018) Brain-controlled modulation of spinal circuits improves recovery from spinal cord injury. Nat Commun 9(1):3015. https://doi.org/10.1038/s41467-018-05282-6

17. Sherwood AM, Dimitrijevic MR, Barry McKay W (1992) Evidence of subclinical brain influence in clinically complete spinal cord injury: discomplete SCI. J Neurol Sci 110(1–2): 90–98. https://doi.org/10.1016/0022-510X(92)90014-C

18. Dimitrijevic MR, Gerasimenko Y, Pinter MM (1998) Evidence for a spinal central pattern generator in humans. Ann N Y Acad Sci:1–18

19. Gwin JT, Ferris D (2011) High-density EEG and independent component analysis mixture models distinguish knee contractions from ankle contractions. In: 2011 Annual International Conference of the IEEE Engineering in Medicine and Biology Society, pp 4195–4198. https://doi.org/10.1109/IEMBS.2011.6091041

20. Höller Y et al (2018) HD-EEG based classification of motor-imagery related activity in patients with spinal cord injury. Front Neurol 9. https://www.frontiersin.org/articles/10.3389/fneur.2018.00955. Accessed 22 Dec 2022. [Online]
21. Lee HS et al (2022) Individual finger movement decoding using a novel ultra-high-density electroencephalography-based brain-computer interface system. Front Neurosci 16:1009878. https://doi.org/10.3389/fnins.2022.1009878
22. Chowdhury A, Raza H, Meena YK, Dutta A, Prasad G (2019) An EEG-EMG correlation-based brain-computer interface for hand orthosis supported neuro-rehabilitation. J Neurosci Methods 312:1–11. https://doi.org/10.1016/j.jneumeth.2018.11.010
23. Guo Z et al (2022) Corticomuscular integrated representation of voluntary motor effort in robotic control for wrist-hand rehabilitation after stroke. J Neural Eng 19(2). https://doi.org/10.1088/1741-2552/ac5757
24. de Seta V et al (2022) Cortico-muscular coupling to control a hybrid brain-computer interface for upper limb motor rehabilitation: a pseudo-online study on stroke patients. Front Hum Neurosci 16. https://www.frontiersin.org/articles/10.3389/fnhum.2022.1016862. Accessed 22 Dec 2022. [Online]
25. Serruya MD, Rosenwasser RH (2021) An artificial nervous system to treat chronic stroke. Artif Organs 45(8):804–812. https://doi.org/10.1111/aor.13998
26. Yu KJ et al (2016) Bioresorbable silicon electronics for transient spatiotemporal mapping of electrical activity from the cerebral cortex. Nat Mater 15(7):782–791. https://doi.org/10.1038/nmat4624
27. Buzsáki G, Wang X-J (2012) Mechanisms of gamma oscillations. Annu Rev Neurosci 35:203–225. https://doi.org/10.1146/annurev-neuro-062111-150444
28. Olson JD et al (2016) Comparison of subdural and subgaleal recordings of cortical high-gamma activity in humans. Clin Neurophysiol 127(1):277–284. https://doi.org/10.1016/j.clinph.2015.03.014
29. Koutsou AD, Moreno JC, Del Ama AJ, Rocon E, Pons JL (2016) Advances in selective activation of muscles for non-invasive motor neuroprostheses. J Neuroeng Rehabil 13(1):56. https://doi.org/10.1186/s12984-016-0165-2
30. Marquez-Chin C, Popovic MR (2020) Functional electrical stimulation therapy for restoration of motor function after spinal cord injury and stroke: a review. Biomed Eng Online 19:34. https://doi.org/10.1186/s12938-020-00773-4
31. van den Brand R et al (2012) Restoring voluntary control of locomotion after paralyzing spinal cord injury. Science 336(6085):1182–1185. https://doi.org/10.1126/science.1217416
32. Asboth L et al (2018) Cortico-reticulo-spinal circuit reorganization enables functional recovery after severe spinal cord contusion. Nat Neurosci 21(4):576–588. https://doi.org/10.1038/s41593-018-0093-5
33. Wagner FB et al (2018) Targeted neurotechnology restores walking in humans with spinal cord injury. Nature 563(7729):65–71. https://doi.org/10.1038/s41586-018-0649-2
34. Gerasimenko YP et al (2015) Noninvasive reactivation of motor descending control after paralysis. J Neurotrauma 32(24):1968–1980. https://doi.org/10.1089/neu.2015.4008
35. Zhang F et al (2020) Cervical spinal cord transcutaneous stimulation improves upper extremity and hand function in people with complete tetraplegia: a case study. IEEE Trans Neural Syst Rehabil Eng 28(12):3167–3174. https://doi.org/10.1109/TNSRE.2020.3048592
36. Inanici F, Brighton LN, Samejima S, Hofstetter CP, Moritz CT (2021) Transcutaneous spinal cord stimulation restores hand and arm function after spinal cord injury. IEEE Trans Neural Syst Rehabil Eng 29:310–319. https://doi.org/10.1109/TNSRE.2021.3049133
37. Crema A et al (2022) Neuromuscular electrical stimulation restores upper limb sensory-motor functions and body representations in chronic stroke survivors. Med 3(1):58–74.e10. https://doi.org/10.1016/j.medj.2021.12.001
38. Moritz CT, Perlmutter SI, Fetz EE (2008) Direct control of paralysed muscles by cortical neurons. Nature 456(7222):7222. https://doi.org/10.1038/nature07418

39. Pohlmeyer EA et al (2009) Toward the restoration of hand use to a paralyzed monkey: brain-controlled functional electrical stimulation of forearm muscles. PLoS One 4(6):e5924. https://doi.org/10.1371/journal.pone.0005924

40. Ethier C, Oby ER, Bauman MJ, Miller LE (2012) Restoration of grasp following paralysis through brain-controlled stimulation of muscles. Nature 485(7398):7398. https://doi.org/10.1038/nature10987

41. Bouton CE et al (2016) Restoring cortical control of functional movement in a human with quadriplegia. Nature 533(7602):247–250. https://doi.org/10.1038/nature17435

42. Ajiboye AB et al (2017) Restoration of reaching and grasping in a person with tetraplegia through brain-controlled muscle stimulation: a proof-of-concept demonstration. Lancet 389(10081):1821–1830. https://doi.org/10.1016/S0140-6736(17)30601-3

43. Colachis SCI et al (2018) Dexterous control of seven functional hand movements using cortically-controlled transcutaneous muscle stimulation in a person with tetraplegia. Front Neurosci 12. https://doi.org/10.3389/fnins.2018.00208

44. Losanno E et al (2022) Validation of manifold-based direct control for a brain-to-body neural bypass. bioRxiv. https://doi.org/10.1101/2022.07.25.501351

45. Gallego JA, Perich MG, Miller LE, Solla SA (2017) Neural manifolds for the control of movement. Neuron 94(5):978–984. https://doi.org/10.1016/j.neuron.2017.05.025

46. Motor recruitment properties of multi-contact composite flat interface nerve electrodes (C-FINEs) in the human upper extremity. https://www.abstractsonline.com/pp8/?utm_campaign=Neuroscience%202022&utm_medium=email&_hsmi=227773073&_hsenc=p2ANqtz%2D%2Dr5rDoc9HylP7i3GROBr3cgl4qYOCpGEDrPYSlzZh5zgJ5C4c_ozc9j3pDXYJp3M_VHOoXgHQHYen8xvm5We15EqjquHG5dCsUfsxlYKYAMuh22cc&utm_content=227773073&utm_source=hs_email#!/10619/presentation/77361. Accessed 11 Jan 2023

47. Normann RA, Fernandez E (2016) Clinical applications of penetrating neural interfaces and Utah Electrode Array technologies. J Neural Eng 13(6):061003. https://doi.org/10.1088/1741-2560/13/6/061003

48. Wodlinger B, Downey JE, Tyler-Kabara EC, Schwartz AB, Boninger ML, Collinger JL (2014) Ten-dimensional anthropomorphic arm control in a human brain-machine interface: difficulties, solutions, and limitations. J Neural Eng 12(1):016011. https://doi.org/10.1088/1741-2560/12/1/016011

49. Nason SR et al (2021) Real-time linear prediction of simultaneous and independent movements of two finger groups using an intracortical brain-machine interface. Neuron 109(19): 3164–3177.e8. https://doi.org/10.1016/j.neuron.2021.08.009

50. Welle CG et al (2020) Longitudinal neural and vascular structural dynamics produced by chronic microelectrode implantation. Biomaterials 238:119831. https://doi.org/10.1016/j.biomaterials.2020.119831

51. Szymanski LJ et al (2021) Neuropathological effects of chronically implanted, intracortical microelectrodes in a tetraplegic patient. J Neural Eng 18(4):0460b9. https://doi.org/10.1088/1741-2552/ac127e

52. Bishop W et al (2014) Self-recalibrating classifiers for intracortical brain-computer interfaces. J Neural Eng 11(2):026001. https://doi.org/10.1088/1741-2560/11/2/026001

53. Jarosiewicz B et al (2015) Virtual typing by people with tetraplegia using a self-calibrating intracortical brain-computer interface. Sci Transl Med 7(313):313ra179. https://doi.org/10.1126/scitranslmed.aac7328

54. Orsborn AL, Moorman HG, Overduin SA, Shanechi MM, Dimitrov DF, Carmena JM (2014) Closed-loop decoder adaptation shapes neural plasticity for skillful neuroprosthetic control. Neuron 82(6):1380–1393. https://doi.org/10.1016/j.neuron.2014.04.048

55. Kozai TDY et al (2012) Ultrasmall implantable composite microelectrodes with bioactive surfaces for chronic neural interfaces. Nat Mater 11(12):1065–1073. https://doi.org/10.1038/nmat3468

56. Musk E, Neuralink (2019) An integrated brain-machine interface platform with thousands of channels. J Med Internet Res 21(10):e16194. https://doi.org/10.2196/16194

57. Seo D et al (2016) Wireless recording in the peripheral nervous system with ultrasonic neural dust. Neuron 91(3):529–539. https://doi.org/10.1016/j.neuron.2016.06.034
58. Lee J et al (2021) Neural recording and stimulation using wireless networks of microimplants. Nat Electron 4:1–11. https://doi.org/10.1038/s41928-021-00631-8
59. Schalk G, Leuthardt EC (2011) Brain-computer interfaces using electrocorticographic signals. IEEE Rev Biomed Eng 4:140–154. https://doi.org/10.1109/RBME.2011.2172408
60. Bundy DT, Pahwa M, Szrama N, Leuthardt EC (2016) Decoding three-dimensional reaching movements using electrocorticographic signals in humans. J Neural Eng 13(2):026021. https://doi.org/10.1088/1741-2560/13/2/026021
61. Hotson G et al (2014) Coarse electrocorticographic decoding of ipsilateral reach in patients with brain lesions. PLoS One 9(12):e115236. https://doi.org/10.1371/journal.pone.0115236
62. Pistohl T, Ball T, Schulze-Bonhage A, Aertsen A, Mehring C (2008) Prediction of arm movement trajectories from ECoG-recordings in humans. J Neurosci Methods 167(1): 105–114. https://doi.org/10.1016/j.jneumeth.2007.10.001
63. Pistohl T, Schulze-Bonhage A, Aertsen A, Mehring C, Ball T (2012) Decoding natural grasp types from human ECoG. NeuroImage 59(1):248–260. https://doi.org/10.1016/j.neuroimage.2011.06.084
64. Chestek CA et al (2013) Hand posture classification using electrocorticography signals in the gamma band over human sensorimotor brain areas. J Neural Eng 10(2):026002. https://doi.org/10.1088/1741-2560/10/2/026002
65. Benabid AL et al (2019) An exoskeleton controlled by an epidural wireless brain–machine interface in a tetraplegic patient: a proof-of-concept demonstration. Lancet Neurol 18(12): 1112–1122. https://doi.org/10.1016/S1474-4422(19)30321-7
66. Yanagisawa T et al (2011) Real-time control of a prosthetic hand using human electrocorticography signals. J Neurosurg 114(6):1715–1722. https://doi.org/10.3171/2011.1.JNS101421
67. Hotson G et al (2016) Individual finger control of a modular prosthetic limb using high-density electrocorticography in a human subject. J Neural Eng 13(2):026017–026017. https://doi.org/10.1088/1741-2560/13/2/026017
68. Wyss Center W (2022) ABILITY. Wyss Center. https://wysscenter.ch/advances/ability
69. Larzabal C et al (2021) Long-term stability of the chronic epidural wireless recorder WIMAGINE in tetraplegic patients. J Neural Eng 18(5):056026. https://doi.org/10.1088/1741-2552/ac2003
70. Rowald A et al (2022) Activity-dependent spinal cord neuromodulation rapidly restores trunk and leg motor functions after complete paralysis. Nat Med 28(2):260–271. https://doi.org/10.1038/s41591-021-01663-5
71. Powell MP et al (2022) Epidural stimulation of the cervical spinal cord improves voluntary motor control in post-stroke upper limb paresis. medRxiv. https://doi.org/10.1101/2022.04.11.22273635
72. Kilgore KL, Hoyen HA, Bryden AM, Hart RL, Keith MW, Peckham PH (2008) An implanted upper-extremity neuroprosthesis using myoelectric control. J Hand Surg 33(4):539–550. https://doi.org/10.1016/j.jhsa.2008.01.007
73. Badi M et al (2021) Intrafascicular peripheral nerve stimulation produces fine functional hand movements in primates. Sci Transl Med. https://doi.org/10.1126/scitranslmed.abg6463
74. C. Lynch and M. R. Popovic, "Closed-loop control for FES: past work and future directions." 2005.
75. C. Freschi, F. Vecchi, S. Micera, A. M. Sabatini, and P. Dario, Force control during grasp using FES techniques: preliminary results. 2000.
76. Ciancibello J et al (2019) Closed-loop neuromuscular electrical stimulation using feedforward-feedback control and textile electrodes to regulate grasp force in quadriplegia. Bioelectron Med 5:19. https://doi.org/10.1186/s42234-019-0034-y

77. Wenger N et al (2014) Closed-loop neuromodulation of spinal sensorimotor circuits controls refined locomotion after complete spinal cord injury. Sci Transl Med 6(255):255ra133. https://doi.org/10.1126/scitranslmed.3008325

78. Lebedev MA et al (2011) Future developments in brain-machine interface research. Clinics 66:25–32. https://doi.org/10.1590/S1807-59322011001300004

79. Chen H, Dejace L, Lacour SP (2021) Electronic skins for healthcare monitoring and smart prostheses. Annu Rev Control Robot Auton Syst 4(1):629–650. https://doi.org/10.1146/annurev-control-071320-101023

80. Haugland M, Sinkjaer T (1999) Interfacing the body's own sensing receptors into neural prosthesis devices. Technol Health Care 7(6):393–399

81. Haugland M, Lickel A, Haase J, Sinkjaer T (1999) Control of FES thumb force using slip information obtained from the cutaneous electroneurogram in quadriplegic man. IEEE Trans Rehabil Eng 7(2):215–227. https://doi.org/10.1109/86.769412

82. Ganzer PD et al (2020) Restoring the sense of touch using a sensorimotor demultiplexing neural interface. Cell 181(4):763–773.e12. https://doi.org/10.1016/j.cell.2020.03.054

83. Bensmaia SJ, Tyler DJ, Micera S (2020) Restoration of sensory information via bionic hands. Nat Biomed Eng. https://doi.org/10.1038/s41551-020-00630-8

# Keeping Our Eyes on the Prize; Are We Losing Sight of the 'Why' in BCI for Neurorehabilitation?

**Colin Simon and Kathy Ruddy**

*Technology is the answer. But what was the question?*
*Cedric Price (1966)*

**Abstract**  Studies using BCIs based upon non-invasive, scalp recorded electroencephalography (EEG) have consistently demonstrated utility, both as scientific tools for neuromodulation and for clinical neurorehabilitation purposes. They are particularly appealing in clinical contexts where physical movement is impaired, for instance following stroke. The intrinsic advantage of Brain-Computer Interfaces (BCIs) over alternate rehabilitation strategies is that they work even when output at the behavioural level is non-existent. Patients exhibiting minimal or no residual limb movement after a stroke cannot partake in gold standard physiotherapy, but might still demonstrate brain activity patterns when attempting to move the impaired limb. These patterns can be targeted to enhance recovery. However, the role of BCI should evolve once behavioural output is available. We must not be seduced by the allure of cutting-edge technology at the expense of targeting the specific neurophysiological features that are most likely to drive recovery. At the most basic mechanistic level, the majority of BCIs are driven by neural signals generated by imagination of movement. We need to revisit the question—could motor imagery alone could achieve the same outcomes, or what is the added clinical benefit of the BCI? Accordingly, what is the minimum required intervention using BCI (in terms of time and hardware) to establish a habit of good quality motor imagery that could then sustain rehabilitation without the technology? Motor imagery is free,

C. Simon (✉)
Trinity College Institute of Neuroscience and School of Psychology, Trinity College, Dublin, Ireland

K. Ruddy
Trinity College Institute of Neuroscience and School of Psychology, Trinity College, Dublin, Ireland

School of Psychology, Queen's University Belfast, Belfast, Northern Ireland
e-mail: RUDDYKL@tcd.ie

available to every person and at any time. Using technology to harness its virtues while not compromising its simplicity is the ultimate challenge for the field.

**Keywords** EEG · BCI · Transcranial Magnetic Stimulation (TMS) · Motor Evoked Potentials (MEP) · Stroke

Studies using BCIs based upon non-invasive, scalp recorded electroencephalography (EEG) have consistently demonstrated utility, both as scientific tools for neuromodulation and for clinical neurorehabilitation purposes. They are particularly appealing in clinical contexts where physical movement is impaired, for instance following stroke. Using a BCI where on-screen avatars are driven by neural activation in motor regions encourages the patient to engage in imagined or attempted movements. By providing tangible visual feedback and rewarding desirable neural features, activity in motor pathways is maintained. This may promote use-dependent plasticity and rewiring for recovery of function. However, clinical adoption of the approach has been limited. This is due mainly to difficulties with implementation in non-research settings, as training to achieve neural control of the BCI requires lengthy sessions over multiple days or weeks [1]. Human participants typically use imagined movements or scenarios to achieve BCI control that are associated with distinct scalp-detectable patterns of neural activity. The lack of spatial sensitivity of EEG to distinguish between different imagined (or even executed) movements from different muscles makes decoding and classifying the neural activity challenging, especially in the early days of training.

TMS-NF is a novel approach to provide richer, more muscle-specific feedback in a BCI [2]. In this closed loop system, the size of Motor Evoked Potentials (MEPs) in response to Transcranial Magnetic Stimulation (TMS) are incorporated into the NF signal, such that users can learn how to facilitate or inhibit their brain-muscle pathways by engaging mental strategies to make the MEP larger or smaller (Fig. 1). This typically results in a much faster (i.e. within one training session) grasp of how to execute distinct mental strategies in order to control the game, compared to those reported for EEG BCI. This also produces more spatially distinct and temporally stable neural signatures when the same mental strategies are later executed during simultaneous EEG recording [3]. TMS-NF would not be a practical long-term approach for neurorehabilitation due to the expense and size of the required apparatus, but if it could be used in the early phase of training while still in hospital, the learned strategies may transfer well to an EEG BCI that could be used by patients in their own homes (e.g. see Simon and Ruddy [4], and Fig. 1).

Stroke is one of the leading causes of death and disability worldwide, and incidence is rising at an alarming rate [5]. There have been substantial improvements to emergency stroke care, with advances in thrombolytic therapy leading to a 25% reduction in stroke related deaths. While this is undoubtedly a positive advance, the more worrying implication is that there is now an increasing number of survivors left with significant disabilities as a result of the brain damage, preventing them from leading independent lives. A major unsolved problem is getting the paralysed upper limb functional again. This is one of the key obstacles preventing independence in
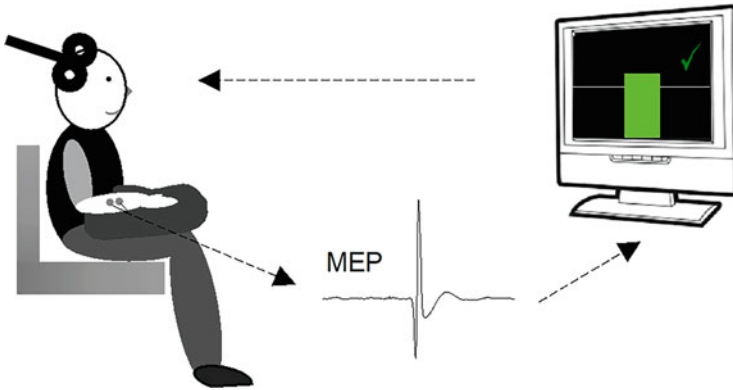
**Fig. 1** TMS Neurofeedback protocol used in Ruddy et al. [2]. The peak-peak amplitude of the motor evoked potential (MEP) following TMS is calculated in real-time and displayed to the participant. The height of the rectangle on the screen represents the amplitude of the participant's MEP. In UP training, participants are rewarded for exceeding their baseline amplitude (white horizontal line). In DOWN trials, they are rewarded for keeping amplitudes small, below the baseline. In a successful trial, when the baseline is exceeded, the bar turns green and a positive soundbite is played. In an unsuccessful trial, the bar turns red and a discouraging soundbite is played

stroke survivors, as without the use of one limb, they are unable to perform the most basic activities of daily living, such as dressing, preparing food, and personal care. As the brain-muscle pathways that previously controlled the upper limb are permanently damaged, recovery of function may only occur due to growth and development of new neural connections. In this field of research, novel, theory driven, innovative methods to promote this re-wiring of neural pathways are urgently needed.

BCIs take a wide range of different formats, providing user feedback from a variety of different neural signals. Some constitute assistive technology, circumventing the damaged nervous system to translate an intention to move into remote control of an external device. Others work upon harnessing the power of motor imagery to activate brain circuits involved in movement in order to promote an optimal neurochemical environment for neuroplastic processes to occur, and prevent further deterioration of unused pathways. The aforementioned are two very different approaches—one with a focus on compensation, finding a new way to achieve the desired task, and the other with a focus on restitution—regaining the capacity for the brain to control the appropriate muscles by reliance on rewiring and forming new neural connections to take on the function of the damaged neurons. Here we aim to more specifically demarcate the clinical instances in which the benefits of BCI are likely to supersede those of other approaches, with a view towards equipping researchers (and ultimately clinicians) with tools to choose the right BCI approach at the right time for the right patients.

First and foremost, we need to develop a clearer understanding of the underlying mechanisms—the neural elements that are being altered by the BCI—in order to provide clear medical justification, and a more standardised, scalable application of

brain-based physiotherapy. There is a wide heterogeneity in BCI design, slowing its clinical deployment [6]. Yet, a more pressing challenge is our limited understanding of the mechanisms that drive BCI control and BCI initiated recovery processes [1].

The myriad of proteins, cells, synapses, structural and functional networks that make up the brain, and the way they interact to produce measurable signals at the scalp, are yet to be consolidated into a comprehensive framework of brain health [7–9]. Instead of resorting to increasingly complex and expensive technology [10], it is crucial to devise innovative but minimalist ways to interact with the injured brain.

## 1 Identification of Appropriate Target Neural Signal

Any form of brain signal, ranging from protein-level fluctuations to network activities and oscillations, can be utilized for BCI. It is also valuable to consider the potential applications where brain-derived signals, such as motor evoked potentials from electromyography [2, 3], can be leveraged as inputs to inform a BCI [11, 12]. Here, we will focus predominantly on Electroencephalography (EEG) BCI, as the majority of BCIs capture brain activity through EEG [13].

For a BCI with a goal involving neurorehabilitation, the primary objective is to restore functional movement in the user. This distinguishes it from efforts to achieve the best possible control over the avatars/actuators in the BCI, which is often the focus from a bioengineering perspective. Rehabilitative BCI can target at least three separate dimensions for brain signal analysis: The signal will originate from a specific location, it will exhibit a distinct temporal development, and it will propagate itself spatiotemporally with an oscillation [14]. Researchers have successfully targeted all three dimensions for controlling BCI [10, 13, 15, 16]. In the spatial dimension, post-stroke BCI for rehabilitation may bring about functional change by enhancing activity dependant plasticity in motor regions [17, 18]. In the temporal dimension, the aim may be to augment conduction speed between the brain's motor areas [19, 20]. From a neural oscillations perspective, a target mechanism may be to bias neural oscillatory behaviour towards more 'normal' patterns than those typically detected from the post-stroke brain [21].

Rehabilitation contexts introduce issues that do not exist when testing with healthy controls: Firstly, signals recorded from the injured brain are often complex and idiosyncratic, and secondly, the chosen brain signal can be anticipated to evolve as the patient recovers. To deal with these complexities, we suggest a multi-phase BCI approach. Akin to physiotherapy, a multi-phase BCI may start targeting a specific brain signal during the acute phase of a brain injury, and progressively address patient needs until another BCI phase begins that may target another brain signal during the chronic phase of a brain injury. Ultimately, the best method to accomplish this depends on the specific rehabilitative objectives pursued.

## 2 Identifying Therapeutic Goals

The intrinsic advantage of Brain-Computer Interfaces (BCIs) over alternate rehabilitation strategies is that they work even when output at the behavioral level is non-existent. Patients exhibiting minimal or no residual limb movement after a stroke cannot partake in gold standard physiotherapy [22], but might still demonstrate brain activity patterns when attempting to move the impaired limb. These patterns can be targeted to enhance recovery [1]. However, the role of BCIs should evolve once behavioral output is available. Uncertainty about how BCI can engage neural recovery mechanisms in the brain means that standalone BCI therapy is unlikely to produce better results than conventional physiotherapy in cases where behavioural output is available. In this context, the role of the BCI may transition from being the primary feedback and training mechanism for a patient to take on a more complementary role in the recovery process.

## 3 Identifying the Most Appropriate Technology to Improve Function

In BCI research for neurorehabilitation, the primary objective is to facilitate neural recovery. Achieving accurate BCI control is secondary. As such, rehabilitative BCI is not so much a competition to employ the most cutting-edge methods for the best possible BCI control, but rather a race to identify the most clinically relevant aspects of healthy or injured brains.

So-called black box machine learning methods, where the result is uninterpretable to humans, are not recommended as BCI components [23]. While they may have advantages over more traditional methods, many require large datasets, which are generally unsustainable in both the academic and medical fields. Furthermore, since researchers or clinicians are not able to oversee the results, these methods carry risks such as overfitting and negative adaptation, rendering them ethically questionable as well as impractical [24, 25]. As a result, theory-led methods are preferable.

In situations where there are few or no constraints imposed on the data by the chosen brain signal or the rehabilitative objective, unbiased data processing methods can provide benefits. Unbiased methods take all available data and determine for themselves what is important and what is not, without referring to predetermined goals. They can offer greater flexibility in identifying optimal solutions for BCI control, including adaptations to signal changes over time, adaptations to patient idiosyncrasies, and the exploration of potential solutions not previously considered by researchers. However, unbiased processes may lack the necessary methodological power to validate BCI mechanisms and are potentially more susceptible to noise.

Based on the qualities of the brain signal and the requirements dictated by the rehabilitative objective, most BCI designs will gravitate towards a specific technological solution. If these qualities or the rehabilitation objective change during the

rehabilitation process, the technology employed should adapt correspondingly. While this multimodal approach may initially appear more complex, it is likely to yield superior results and more standardized protocols.

## 4  Thinking Outside the (Black) Box

The presented steps are intended to help BCI design by encouraging innovative solutions. For example, multimodal and multiphasic BCIs may also incorporate phases or modes where the brain is not the signal generator but rather a signal processor. The brain could be the receiver of a stimulus such as transcranial magnetic stimulation or a sensory stimulus. This could enhance the specificity of the generated brain signal along various dimensions, making it easier to design a rehabilitative objective around it.

For this purpose, we have developed a multimodal and multiphasic BCI using a TMS-BCI in the initial phase and an EEG-BCI in the subsequent phase. Preliminary results suggest that the multimodal approach was successful in facilitating BCI control compared to a unimodal, single-phase group (2-Phase BCI).

Alternatively, the brain signal could be augmented with additional behavioural data. For example, wearable devices could provide a BCI with an additional signal dimension, enabling the BCI to make more complex decisions. Such multimodal and multiphasic approaches may allow for the targeting of different aspects of rehabilitation during the same treatment or the application of different BCI strengths simultaneously.

A multiphasic approach to rehabilitative BCI could also contribute to its success. To achieve success, BCIs must not only be mechanistically sound and effective but also scalable on a grand scale, ideally allowing patients to use them with minimal clinical supervision. This has yet to be fully realized as researchers continue to strive to find simple and effective solutions. However, a multiphasic approach may help BCIs have a short, intensive acute care phase, followed by a long-term easy solution for at-home use.

In an experiment we designed [4], we developed a clinically relevant but minimal BCI setup. This setup was dispatched to participants' homes, and they were instructed to set it up and train using online guidance. The results affirmed the feasibility of this approach.

## 5  Conclusion

Brain-Computer Interfaces (BCIs) continue to gain momentum as an appealing method for restoring motor function in a neurorehabilitation context. However, we must not be seduced by the allure of cutting edge technology at the expense of targeting the specific neurophysiological features that are most likely to drive

recovery. At the most basic mechanistic level, the majority of BCIs are driven by neural signals generated by imagination of movement. We need to revisit the question—could motor imagery alone could achieve the same outcomes, or what is the added clinical benefit of the BCI? Accordingly, what is the minimum required intervention using BCI (in terms of time and hardware) to establish a habit of good quality motor imagery that could then sustain rehabilitation without the technology? Motor imagery is free, available to every person and at any time. Using technology to harness its virtues while not compromising its simplicity is the ultimate challenge for the field.

# References

1. Simon C, Bolton DAE, Kennedy NC, Soekadar SR, Ruddy KL (2021) Challenges and opportunities for the future of brain-computer interface in neurorehabilitation. Front Neurosci 15:814. https://doi.org/10.3389/fnins.2021.699428
2. Ruddy K, Balsters J, Mantini D, Liu Q, Kassraian-Fard P, Enz N, Mihelj E, Subhash Chander B, Soekadar SR, Wenderoth N (2018) Neural activity related to volitional regulation of cortical excitability. elife 7:e40843. https://doi.org/10.7554/eLife.40843
3. Mihelj E, Bächinger M, Kikkert S, Ruddy K, Wenderoth N (2021) Mental individuation of imagined finger movements can be achieved using TMS-based neurofeedback. NeuroImage 242:118463. https://doi.org/10.1016/j.neuroimage.2021.118463
4. Simon C, Ruddy KL (2022) A wireless, wearable Brain-Computer Interface for neurorehabilitation at home; A feasibility study. In: 2022 10th International Winter Conference on Brain-Computer Interface (BCI), pp 1–6. https://doi.org/10.1109/BCI53720.2022.9734849
5. McElwaine P, McCormack J, Harbinson J, National Stroke Programme (2016) Irish Heart Foundation/HSE National Stroke Audit Rehabilitation Units 2016
6. Baniqued PDE, Stanyer EC, Awais M, Alazmani A, Jackson AE, Mon-Williams MA, Mushtaq F, Holt RJ (2021) Brain–computer interface robotics for hand rehabilitation after stroke: a systematic review. J NeuroEng Rehabil 18(1):Article 1. https://doi.org/10.1186/s12984-021-00820-8
7. Bassetti CLA, Endres M, Sander A, Crean M, Subramaniam S, Carvalho V, Di Liberto G, Franco OH, Pijnenburg Y, Leonardi M, Boon P (2022) The European Academy of Neurology Brain Health Strategy: one brain, one life, one approach. Eur J Neurol 29(9):2559–2566. https://doi.org/10.1111/ene.15391
8. Cattaneo G, Bartrés-Faz D, Morris TP, Sánchez JS, Macià D, Tarrero C, Tormos JM, Pascual-Leone A (2018) The Barcelona brain health initiative: a cohort study to define and promote determinants of brain Health. Front Aging Neurosci 10. https://www.frontiersin.org/articles/10.3389/fnagi.2018.00321
9. Chen Y, Demnitz N, Yamamoto S, Yaffe K, Lawlor B, Leroi I (2022) Defining brain health: a concept analysis. Int J Geriat Psychiatry 37(1). https://doi.org/10.1002/gps.5564
10. Saibene A, Caglioni M, Corchs S, Gasparini F (2023) EEG-based BCIs on motor imagery paradigm using wearable technologies: a systematic review. Sensors 23(5):Article 5. https://doi.org/10.3390/s23052798
11. Cruz A, Pires G, Lopes AC, Nunes UJ (2019) Detection of stressful situations using GSR while driving a BCI-controlled wheelchair. In: 2019 41st Annual International Conference of the IEEE Engineering in Medicine and Biology Society (EMBC), pp 1651–1656. https://doi.org/10.1109/EMBC.2019.8857748
12. Zimmermann R, Marchal-Crespo L, Lambercy O, Fluet M-C, Riener R, Wolf M, Gassert R (2011) Towards a BCI for sensorimotor training: initial results from simultaneous fNIRS and

biosignal recordings. In: 2011 Annual International Conference of the IEEE Engineering in Medicine and Biology Society, pp 6339–6343. https://doi.org/10.1109/IEMBS.2011.6091565

13. Aggarwal S, Chugh N (2022) Review of machine learning techniques for EEG based brain computer interface. Archiv Comput Methods Eng 29(5):3001–3020. https://doi.org/10.1007/s11831-021-09684-6

14. Cohen MX (2014) Analyzing neural time series data: theory and practice. https://doi.org/10.7551/mitpress/9609.001.0001

15. Abiri R, Borhani S, Sellers EW, Jiang Y, Zhao X (2019) A comprehensive review of EEG-based brain–computer interface paradigms. J Neural Eng 16(1):011001. https://doi.org/10.1088/1741-2552/aaf12e

16. Xie Y, Oniga S (2020) A review of processing methods and classification algorithm for EEG signal. Carpathian J Electron Comp Eng 13(1):23–29. https://doi.org/10.2478/cjece-2020-0004

17. Overman JJ, Carmichael ST (2014) Plasticity in the injured brain: more than molecules matter. Neuroscientist 20(1):15–28. https://doi.org/10.1177/1073858413491146

18. Stinear CM, Lang CE, Zeiler S, Byblow WD (2020) Advances and challenges in stroke rehabilitation. Lancet Neurol 19(4):348–360. https://doi.org/10.1016/S1474-4422(19)30415-6

19. Beuter A, Balossier A, Trofimchuk S, Volpert V (2018) Modeling of post-stroke stimulation of cortical tissue. Math Biosci 305:146–159. https://doi.org/10.1016/j.mbs.2018.08.014

20. Beuter A, Balossier A, Vassal F, Hemm S, Volpert V (2020) Cortical stimulation in aphasia following ischemic stroke: toward model-guided electrical neuromodulation. Biol Cybern 114(1):5–21. https://doi.org/10.1007/s00422-020-00818-w

21. Leonardi G, Ciurleo R, Cucinotta F, Fonti B, Borzelli D, Costa L, Tisano A, Portaro S, Alito A (2022) The role of brain oscillations in post-stroke motor recovery: an overview. Front Syst Neurosci 16:947421. https://doi.org/10.3389/fnsys.2022.947421

22. Kwakkel G, Veerbeek JM, van Wegen EEH, Wolf SL (2015) Constraint-induced movement therapy after stroke. Lancet Neurol 14(2):224–234. https://doi.org/10.1016/S1474-4422(14)70160-7

23. Tung SW, Guan C, Ang KK, Phua KS, Wang C, Zhao L, Teo WP, Chew E (2013) Motor imagery BCI for upper limb stroke rehabilitation: an evaluation of the EEG recordings using coherence analysis. In: 2013 35th Annual International Conference of the IEEE Engineering in Medicine and Biology Society (EMBC), pp 261–264. https://doi.org/10.1109/EMBC.2013.6609487

24. Adadi A, Berrada M (2018) Peeking inside the black-box: a survey on explainable artificial intelligence (XAI). IEEE Access 6:52138–52160. https://doi.org/10.1109/ACCESS.2018.2870052

25. Pinto M, Leal A, Lopes F, Pais J, Dourado A, Sales F, Martins P, Teixeira CA (2022) On the clinical acceptance of black-box systems for EEG seizure prediction. Epilepsia Open 7(2):247–259. https://doi.org/10.1002/epi4.12597

# Real-Time Decoding of Leg Motor Function and Dysfunction from the Subthalamic Nucleus in People with Parkinson's Disease

Kyuhwa Lee, Yohann Thenaisie, Charlotte Moerman, Stefano Scafa, Andrea Gálvez, Elvira Pirondini, Morgane Burri, Jimmy Ravier, Alessandro Puiatti, Ettore Accolla, Benoit Wicki, André Zacharia, Mayte Castro Jiménez, Julien F. Bally, Grégoire Courtine, Jocelyne Bloch, and Eduardo Martin Moraud

**Abstract** We developed a real-time decoding framework that can accurately predict leg motor functions, as well as key aspects of walking, from local field potentials (LFP) recorded from the subthalamic nucleus of patients with Parkinson's disease.

---

Kyuhwa Lee and Yohann Thenaisie contributed equally with all other contributors.

K. Lee (✉)
Wyss Center for Bio and Neuroengineering, Geneva, Switzerland
e-mail: kyuhwa.lee@wysscenter.ch

Y. Thenaisie · C. Moerman · E. M. Moraud
Department of Clinical Neurosciences, Lausanne University Hospital (CHUV) and University of Lausanne (UNIL), Lausanne, Switzerland

NeuroRestore, Defitech Centre for Interventional Neurotherapies, CHUV, UNIL, and Ecole Polytechnique Fédérale de Lausanne (EPFL), Lausanne, Switzerland

S. Scafa
Department of Clinical Neurosciences, Lausanne University Hospital (CHUV) and University of Lausanne (UNIL), Lausanne, Switzerland

NeuroRestore, Defitech Centre for Interventional Neurotherapies, CHUV, UNIL, and Ecole Polytechnique Fédérale de Lausanne (EPFL), Lausanne, Switzerland

Institute of Digital Technologies for Personalized Healthcare (MeDiTech), University of Southern Switzerland (SUPSI), Lugano-Viganello, Switzerland

A. Gálvez · M. Burri · J. Ravier
NeuroRestore, Defitech Centre for Interventional Neurotherapies, CHUV, UNIL, and Ecole Polytechnique Fédérale de Lausanne (EPFL), Lausanne, Switzerland

Faculty of Life Sciences, EPFL, NeuroX Institute, Lausanne, Switzerland

E. Pirondini
Department of Clinical Neurosciences, Lausanne University Hospital (CHUV) and University of Lausanne (UNIL), Lausanne, Switzerland

Department of Physical Medicine and Rehabilitation, University of Pittsburgh, Pittsburgh, PA, USA

C. Guger et al. (eds.), *Brain-Computer Interface Research*, SpringerBriefs in Electrical and Computer Engineering, https://doi.org/10.1007/978-3-031-49457-4_9

83

Concretely, we designed decoders that can predict locomotor states, gait events, modulations in force during obstacle avoidance, and freezing of gait episodes while participants walked freely in unconstrained conditions. Our algorithms employed the full spectrum of LFP recorded bilaterally, either through externalized deep brain stimulation (DBS) leads connected to an external, high-resolution amplifier (six bipolar channels, Fs = 8 kHz), or wirelessly using a last-generation implantable stimulator with sensing capabilities (Percept PC, Medtronic, two bipolar channels, Fs = 250 Hz). These results represent the first neural decoding of leg motor function operating in real-time from therapeutically implanted DBS electrodes. Considering the large number of patients treated worldwide with DBS implants, as well as the capabilities of newest commercial stimulators, our results pave the way for the design and widespread deployment of closed-loop neuromodulation therapies that address gait deficits with new closed-loop approaches.

**Keywords** Real time · Decoding · Deep learning · Convolutional network · Random forest · Machine learning · Motor · Movement · LFP · DBS · Subthalamic nucleus · STN

Rehabilitation and Neural Engineering Labs, University of Pittsburgh, Pittsburgh, PA, USA

A. Puiatti
Institute of Digital Technologies for Personalized Healthcare (MeDiTech), University of Southern Switzerland (SUPSI), Lugano-Viganello, Switzerland

E. Accolla
Department of Neurology, Hôpital Fribourgeois, Fribourg University, Fribourg, Switzerland

B. Wicki
Department of Neurology, Hôpital du Valais, Sion, Switzerland

A. Zacharia
Clinique Bernoise, Crans-Montana, Switzerland

Department of Neurology, Lausanne University Hospital (CHUV) and University of Lausanne, Lausanne, Switzerland

Department of Medicine, University of Geneva, Geneva, Switzerland

M. C. Jiménez · J. F. Bally
Department of Neurology, Lausanne University Hospital (CHUV) and University of Lausanne, Lausanne, Switzerland

G. Courtine · J. Bloch
Department of Clinical Neurosciences, Lausanne University Hospital (CHUV) and University of Lausanne (UNIL), Lausanne, Switzerland

NeuroRestore, Defitech Centre for Interventional Neurotherapies, CHUV, UNIL, and Ecole Polytechnique Fédérale de Lausanne (EPFL), Lausanne, Switzerland

Faculty of Life Sciences, EPFL, NeuroX Institute, Lausanne, Switzerland

Department of Neurosurgery, Lausanne University Hospital (CHUV) and University of Lausanne, Lausanne, Switzerland

## 1   Introduction

Every year, more than 10,000 patients with Parkinson's disease undergo surgical implantation of electrodes in the Subthalamic Nucleus (STN) [1]. These electrodes not only enable the delivery of deep brain stimulation to treat motor symptoms, but also allow recording of neuronal activity to study the encoding of functional and dysfunctional movements [2, 3]. Despite impressive therapeutic advances, gait and balance deficits remain little understood and hard to treat. Biomarkers of leg motor dysfunction are critically missing to guide the development of novel therapies that specifically target locomotor impairments. Furthermore, pharmacotherapies and deep brain stimulation (DBS) interventions have limited efficacy in the current form for late-stage Parkinson's disease patients suffering from gait and balance deficits, when compared to patients suffering from upper limb movement deficits [4].

To address these issues, we conceived a neurorobotic platform that allowed us to deconstruct and isolate key components of walking while patients were sitting. This deconstruction of movements made it possible to study the encoding of leg motor function in the STN under well-controlled conditions. These experiments exposed direct links between STN modulations and the amplitude of leg muscle activation and force, which opened the intriguing possibility to predict modulations in leg force production from STN dynamics.

We leveraged this platform to elucidate the principles that determine the encoding of leg muscle activations during active and passive movements. These conditions revealed that the STN encodes sensory feedback as well as the initiation, termination, and amplitude of leg muscle activation during isometric force production and single joint movements. We observed that the same principles apply to the encoding of bilateral leg muscle synergies during walking. These observations suggested that the activity of the STN is linked to the vigor of walking. To confirm this principle, we designed paradigms that required sudden or sustained increase in muscle synergy activation, such as avoiding obstacles and stair climbing. We identified robust links between STN activity and the modulation of muscle synergies during the performance of these paradigms. We translated this understanding into machine learning decoders that detected functional and dysfunctional features of gait in real-time across activities of daily living in individuals with PD.

## 2   Method

### 2.1   Study Design

The study was designed to uncover how the STN correlates with locomotor functions and develop decoders to predict different locomotor states of humans. Experiments were approved by the Ethical Committee of the Canton de Vaud, Switzerland (no. PB_2017-00064). All 18 participants received bilateral Medtronic 3389 DBS

leads and were recorded within the 5 days after the surgery. Local field potentials (LFP) were recorded from eight externalized patients (six channels, 8192 Hz sampling frequency, downsampled to 2048 Hz), and ten patients with Percept PC (two channels, 250 Hz sampling frequency) [5]. For both groups of patients, signals were 50-Hz notch filtered. The spatial locations of DBS leads were confirmed using tridimensional anatomical reconstructions [6].

## 2.2 Leg Force and Locomotor State Classifications

The isolated conditions of experiments performed while seated allowed us to expose a link between STN modulations and the amplitude of sustained leg muscle activation. This opened the intriguing possibility of predicting the intensity of leg force production from STN dynamics. To decode the leg force levels in real time, we used a non-linear machine-learning framework based on Random Forests classification algorithms using spectral features, as implemented in [7, 8]. Algorithms were trained to predict one of three classes: "strong force", "weak force" or "rest" (66%, 33%, or 0% of maximal voluntary contraction respectively, for each patient, N = 16 patients). Our decoders used the entire power spectrum of bilateral LFP modulations (range: 5–120 Hz), and automatically extracted patient-specific spectral features that contributed to the encoding of muscle activation. The decoder ran at approximately 30 classifications per second including feature computation time. Figure 1a shows the overall setup of the leg force classification experiment.

We then applied the same decoding framework to discriminate gait states directly from STN LFP. We defined the three gait states ("standing", "walking", "initiation/termination" of gait, N = 12 patients, Fig. 2), and trained using the same machine learning algorithms as used in the leg force classification condition. Participants were instructed to stand for 3 s before initiating a sustained walking bout, after which they had to stand for another 3 s.

## 2.3 Leg Force Regression

We then asked ourselves whether we can predict the continuous levels of force instead of discrete levels of force from the STN. To facilitate the analysis, we grouped the complex patterns of muscle activity during walking into muscle synergies. These synergies captured the concurrent activation of multiple muscles that are functionally linked [9]. We computed synergies across all the recorded muscles from the left and right leg [10]. We restricted the number of synergy components to four, which sufficiently captured muscle activations (~90% of explained variance). Then, we used these four-dimensional time-series synergy values as target values of our regression model.
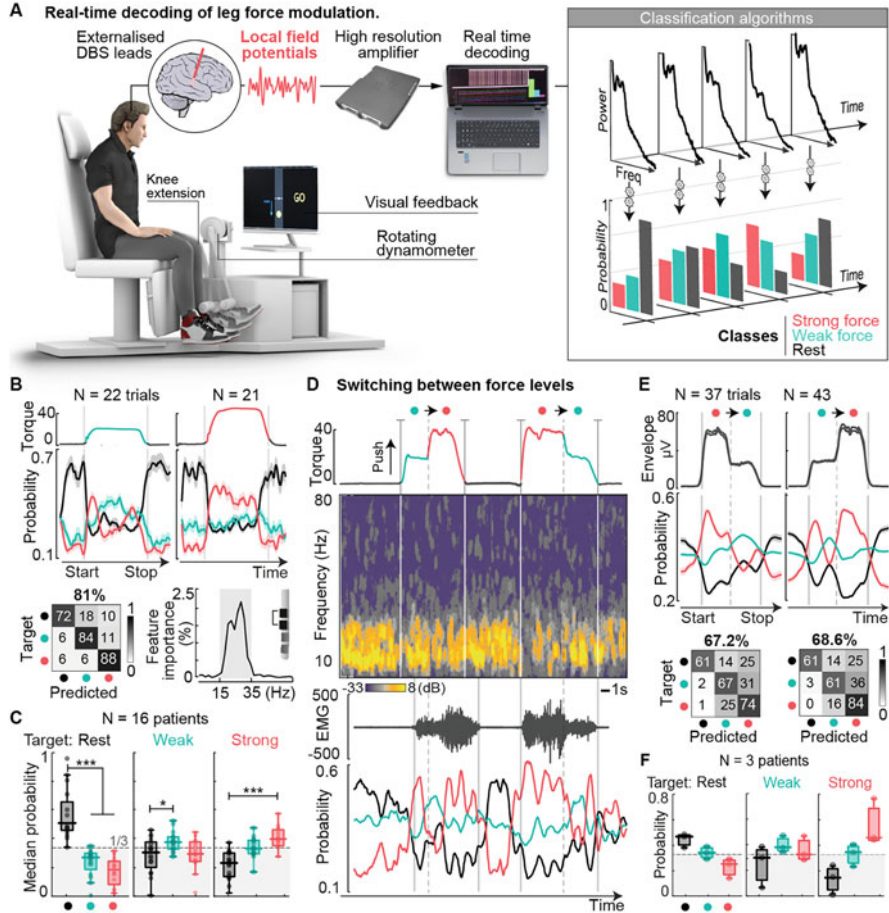
**Fig. 1** Real-time decoding of leg force modulation

For this purpose, we designed a convolutional neural network (CNN) to model the continuous amplitude modulations of leg muscle synergies from STN LFP (Fig. 3a). Bilateral raw LFP are pre-processed and used to compute a spectrogram for each contact pair using multitaper spectral analysis. For each time point (10 ms resolution), a sliding window (500 ms) is isolated and fed into a convolutional neural network (CNN) that processes their image properties. The CNN is composed of three consecutive convolutional layers with increasing receptive fields. Each layer identifies the spectro-temporal features that best predict the output at their specific resolution and pass them on to the next layer. The final layer (fully connected neural network) combines all features to predict synergy activations (one or four synergies). The idea behind this design is that there is unknown latency between the neuromodulation patterns (LFP) and synergy responses of EMGs, and we let the
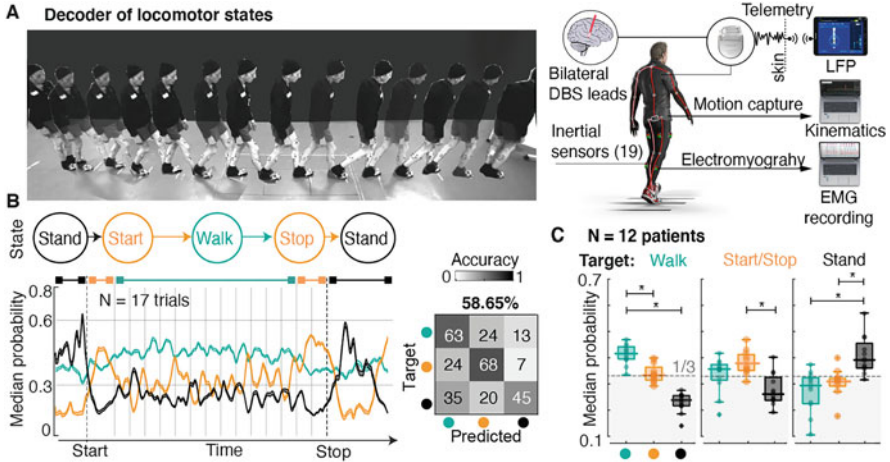
**Fig. 2** Real-time decoding of locomotor states from STN LFP

CNN learn the mapping between the LFP and synergy responses by searching for relevant dynamical features within this short time window.

Training and testing of the CNN are performed using leave-one-out cross-validation on all short and long walking sequences combined. We compared the performance when predicting an individual synergy (unilateral) versus predicting the sum of all four synergies (bilateral).

# 3    Results

## 3.1    Leg Force and Locomotor State Classifications

Decoder performance during the first force task (Externalized participant E4) can be seen in Fig. 1b. Probability (median $\pm$ SEM) for each class over time and confusion matrix (accuracy $= 0.81$, F-score $= 0.79$) are also shown in the lower row. Feature contribution traces display the frequencies that are automatically identified as being more relevant for the decoder, showing low- and high-beta range to be predominantly informative for this patient (shaded box). The feature importance distribution closely matched the relevant frequency bands modulated during movement for each participant (Fig. 1b, Feature Importance).

Figure 1c shows the performance of all patients who performed this task (one-way ANOVA with Bonferroni correction, n $= 16$, *p $< 0.05$, ***p $< 0.001$). It can be seen that strong force epochs were more distinguishable from the rest epochs. Figure 1d shows an illustrative example of real-time recording during the second task, which involves switching between two levels of force. Average performance traces (EMG envelope, top, and probability traces, bottom) and confusion
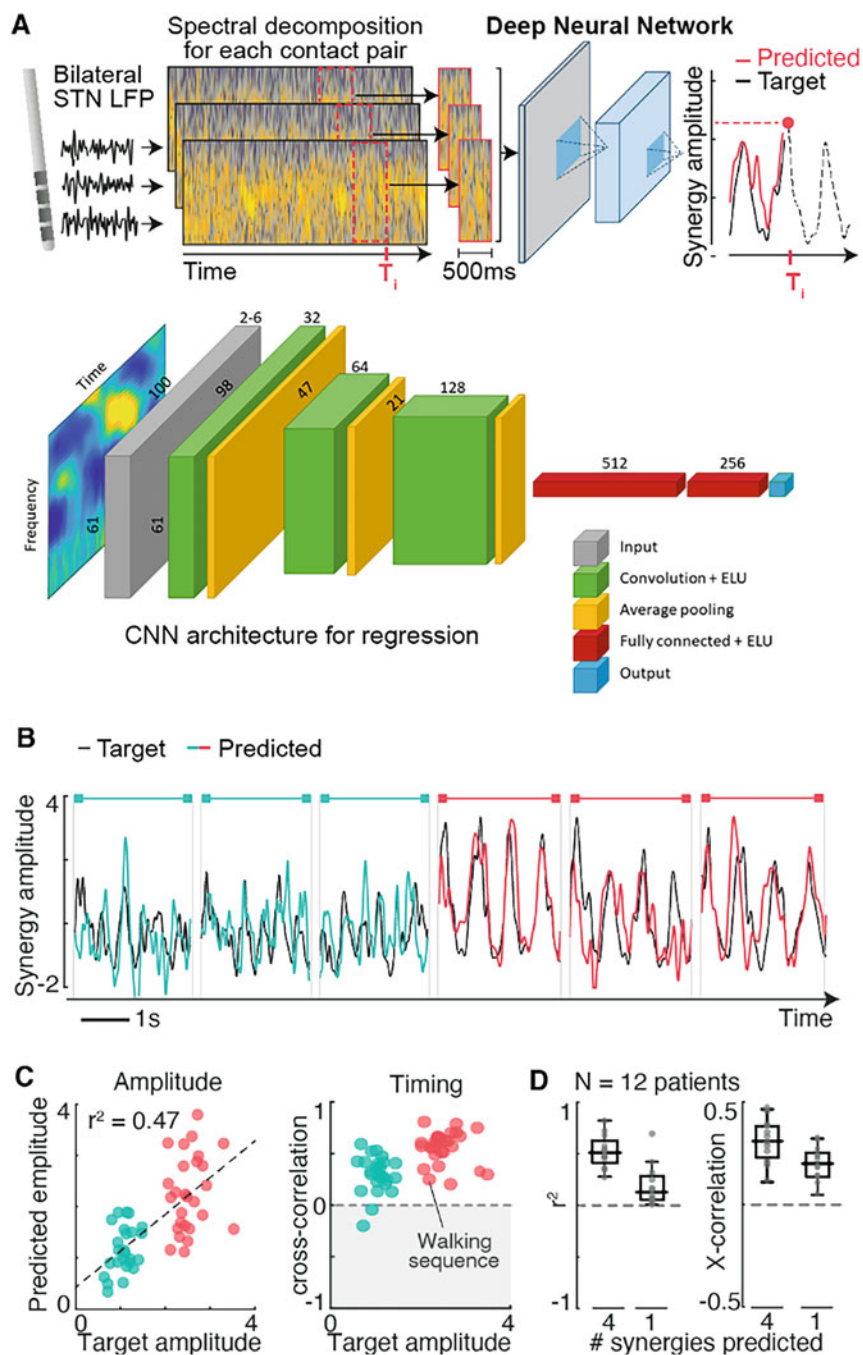
**Fig. 3** Prediction of muscle synergy activation during walking using a deep learning model

matrices for both cases can be seen in Fig. 1e. Finally, Fig. 1f shows the cross-patient performance achieved for the three patients who were tested in real-time.

For the locomotor state classification, we ran the decoder offline, but the data were replayed in real time to mimic the online performance. Figure 2b shows the average probability traces of each class ("standing", "walking" and "start/stop" transitions) over time, and confusion matrix of one example patient. The cross-patient performance (N = 12, *p < 0.05 ANOVA with Bonferroni post-hoc correction) is shown in Fig. 2c. Importantly, comparable decoding performances were achieved regardless of whether data were recorded through DBS leads that were externalized and connected to high-resolution amplifiers (operating at 8 kHz, six bipolar channels) or wirelessly through implantable systems endowed with telemetry capabilities (250 Hz, two channels only), further emphasizing the flexibility and robustness of our approach.

## 3.2  Leg Force Regression

The regression performance was computed using the $r^2$ score and cross-correlation. Figure 3b shows illustrative examples of target versus predicted synergy traces of six walking sequences (three sequences of small steps and three sequences of big steps) for an externalized participant E2. Figure 3c shows the quantification of performance for predicting the amplitude and timing (cross-correlation between target and prediction) of synergy profiles for each walking sequence (same patient). The boxplots show the cross-participant accuracy when modelling the sum of all (four, bilateral) synergy profiles vs predicting a single synergy (*p < 0.05). The model predicted the amplitude (average $r^2$ score = 0.51) and timing (average cross-correlation = 0.30) of synergy values of all participants (Fig. 3d). Training the model to predict only one synergy led to lower accuracy, both in amplitude (average $r^2$ score = 0.21) and timing (average cross-correlation = 0.24), compared to the prediction of all four synergies combined.

## 4  Discussion

We conceived a neurorobotic platform that allowed us to uncover fundamental principles of leg movement encoding in the STN. We translated this understanding into machine learning algorithms that predicted leg force levels, locomotor states, and the vigor of walking from STN LFP. We used all frequency components (in the ranges of 10–120 Hz) from all recorded contact pairs to predict walking states, gait events and muscle synergies with accuracy. Interestingly, the feature importance distribution closely matched the relevant frequency bands modulated during movement for each participant, which coincides with the literature [11, 12]. While each algorithm was trained and tested separately on individually defined classes, they

could easily operate in parallel as part of an integrative platform for real-life applications.

The decoding results confirm that human STN LFP signals may be leveraged to predict the initiation, termination and amplitude of leg muscle activation and loco-motor functions in real-time, which holds promises to regulate neuromodulation therapies in closed-loop to specifically address gait deficits in PD. However, these results also document the limitations in the robustness of gait features that may be decoded from STN LFP to control closed-loop therapies. For example, spatiotem-poral stimulation of the lumbar spinal cord [13] has the potential to alleviate gait deficits in people with PD. This intervention requires real-time control of stimulation bursts targeting specific joint movements. Our results suggest that this spatial resolution is not accessible from STN LFP. Other brain regions may complement STN decoders for applications that require muscle- or joint-specificity. Increasing the resolution of STN recordings may resolve this issue. For instance, single-cell recordings reported preferential firing of STN neurons with different joystick direc-tions in intra-operative conditions [14], as well as with detailed kinematics in animal models [15].

We implemented a comprehensive set of tasks to assert the robustness of our observations and of our decoding framework across conditions of daily life. How-ever, not all patients were able to perform all the described tasks, which restricted the conclusions that could be drawn for some conditions. Reproducing our results on a wider population may allow further identification of differences in the frequency bands, force levels or temporal phases reported in this work. Similarly, decoding accuracy may be improved by explicitly accounting for long-term temporal depen-dencies or prior knowledge of state sequences, which would better capture the dynamics that intrinsically underlie walking. Decoder behavior will also need to be validated once integrated within a closed-loop stimulation framework.

More details of the results, including a force regression model based on convolutional neural networks, can be found in [16]. Our open-source decoding framework can be found in [17].

# References

1. Ponce F et al (2010) Deep brain stimulation. Prog Brain Res 184:311–324
2. Lozano AM et al (2013) Probing and regulating dysfunctional circuits using deep brain stimulation. Neuron 77:406–424
3. Krauss JK et al (2020) Technology of deep brain stimulation: current status and future directions. Nat Rev Neurol:1–13
4. Fasano A et al (2015) Axial disability and deep brain stimulation in patients with Parkinson disease. Nat Rev Neurol 11:98–110
5. Thenaisie Y et al (2021) Towards adaptive deep brain stimulation: clinical and technical notes on a novel commercial device for chronic brain sensing. medRxiv
6. Horn A et al (2019) Lead-DBS v2: towards a comprehensive pipeline for deep brain stimulation imaging. NeuroImage 184:293–316

7. Lee K et al (2017) A brain-controlled exoskeleton with cascaded event-related desynchronization classifiers. Robot Auton Syst 90:15–23
8. Huggins J et al (2019) Workshops of the seventh international brain-computer interface meeting: not getting lost in translation. Brain-Comp Interfaces 6(3):71–101
9. Ivanenko Y et al (2006) Motor control programs and walking. Neuroscientist 12(4):339–348
10. Dominici N et al (2011) Locomotor primitives in newborn babies and their development. Science 334(6058):997–999
11. Hammond C et al (2007) Pathological synchronization in Parkinson's disease: networks, models and treatments. Trends Neurosci 30:357–364
12. Bouthour W et al (2019) Biomarkers for closed-loop deep brain stimulation in Parkinson disease and beyond. Nat Rev Neurol 15:343–352
13. Wagner F et al (2018) Targeted neurotechnology restores walking in humans with spinal cord injury. Nature 563(7729):65–71
14. Williams Z et al (2005) Timing and direction selectivity of subthalamic and pallidal neurons in patients with Parkinson disease. Exp Brain Res 162:407–416
15. Dhawale A et al (2021) The basal ganglia control the detailed kinematics of learned motor skills. Nat Neurosci 24(9):1256–1269
16. Thenaisie Y et al (2022) Principles of gait encoding in the subthalamic nucleus of people with Parkinson's disease. Sci Transl Med 14(661):eabo1800
17. https://github.com/dbdq/neurodecode

# Designing Touch: Intracortical Neurohaptic Feedback in Virtual Reality

**Courtnie J. Paschall, Jason S. Hauptman, Rajesh P. N. Rao, Jeffrey G. Ojemann, and Jeffrey Herron**

**Abstract** Touch sensation offers complex and innate biological feedback that underlies dexterous interactions with our environments, making the restoration of touch an important component of functional brain computer interface (BCI). To advance synthetic touch research, I developed a virtual reality (VR) platform for use with human patients receiving intracranial neural implants for epilepsy evaluation (Fig. 1) [Paschall et al. (An immersive virtual reality platform integrating human ECOG & sEEG: implementation & noise analysis, 2022]. Following validation, noise, and user studies with this VR research platform, I designed a BCI experiment in which tactile information about contact with a virtual object was delivered to the brain through direct cortical stimulation (DCS). I recoined the term neurohaptics to describe this use of DCS for haptic feedback [Paschall et al. (2022 IEEE International Conference on Systems, Man, and Cybernetics (SMC). IEEE, 2022)]. I also developed a new way to deliver neurohaptic feedback using amplitude modulated DCS to evoke distinct and discriminable sensory percepts that better mimicked natural touch sensation [Paschall et al. (2022 IEEE International Conference on Systems, Man, and Cybernetics (SMC). IEEE, 2022)]. This work demonstrates the intrinsic interpretability of dynamic temporal structure in DCS and its utility in the restoration of touch sensation. It paves the way for further first-person VR-BCI

C. J. Paschall (✉)
Department of Bioengineering, University of Washington, Washington, DC, USA
e-mail: copa2894@uw.edu

J. S. Hauptman
Seattle Children's Hospital, Neurological Surgery, Seattle, WA, USA

R. P. N. Rao
Paul G. Allen School of Computer Science, University of Washington, Washington, DC, USA

J. G. Ojemann
Seattle Children's Hospital, Neurological Surgery, Seattle, WA, USA

Department of Neurological Surgery, University of Washington, Washington, DC, USA

J. Herron
Department of Neurological Surgery, University of Washington, Washington, DC, USA

neurohaptic design and brings a novel bidirectional BCI and cognitive neuroscience platform into the clinic for work with implanted neural devices in patient populations.

**Keywords** BCI · ECoG · sEEG · Virtual reality · Neurohaptic

Touch sensation offers complex and innate biological feedback that underlies dexterous interactions with our environments, making the restoration of touch an important component of functional brain computer interface (BCI) [1, 2]. To advance synthetic touch research, I developed a virtual reality (VR) platform for use with human patients receiving intracranial neural implants for epilepsy evaluation (Fig. 1) [3]. Following validation, noise, and user studies with this VR research platform, I then designed a BCI experiment in which tactile information about contact with a virtual object was delivered to the brain through direct cortical stimulation (DCS). I recoined the term **neurohaptics** to describe this use of DCS for haptic feedback [4]. I also developed a new way to deliver neurohaptic feedback by using amplitude-modulated DCS to evoke sensory percepts with distinct and discriminable temporal structure that better mimicked natural touch sensation [4]. This work demonstrated the innate interpretability of dynamic temporal structure in DCS and its utility in the restoration of touch sensation. It paves the way for first-person VR-BCI development and neurohaptic design and unlocks access to the



**Fig. 1** *In vivo* virtual reality experimentation. A clinical neural recording patient completes an immersive virtual reality (VR) task, reaching out beyond the confines of the hospital bed to grasp a virtual object. VR offers a robust platform for human behavioral neuroscience, granting experimental control over every aspect of an immersive visual environment. This enables novel research in neuroscience, neurohaptic engineering, and brain computer interface (BCI)

in-patient neural implant population for functional BCI development and new approaches to cognitive neuroscience research.


# 1   Introduction

Neuroprosthetics controlled by brain computer interface (BCI) hold tremendous promise to restore independence and quality of life to the more than 5 million people in the United States with paralysis and sensorimotor deficit due to neurological disease disorder, and injury [5–10]. BCI refers to any device that enables direct communication with the brain: either decoding neural activity into control signals over a neuroprosthetic robot or a virtual avatar, or encoding information directly to the brain in the form of direct electrical stimulation of neural tissue. Touch sensation may be restored by direct cortical stimulation (DCS) of the somatosensory cortex and is a key feature of functional BCI development. **Neurohaptics** refers to the design of this synthetic touch using DCS [1, 2, 4].

While multiple technologies promising touch sensory restoration exist, only direct cortical stimulation (DCS) is able to elicit artificial touch sensations independent of peripheral sensory channels [10–16]. This technique uses small pulses of electrical current (Fig. 2) to evoke touch sensations, or percepts, at locations that correspond with the somatic representation of the sensory (S1) cortex being stimulated [16]. If DCS is applied to the part of the cortex that represents touch sensation along the right thumb, hand, or arm, for example, a reliable percept can be felt in that right thumb, hand, or arm, respectively.

Traditionally, DCS in humans has been delivered as a train of constant-amplitude, biphasic, charge-matched, square-wave pulses (Fig. 2). Although the resultant percepts have been shown to be reliably localizable [14, 16], they are most often described as artificial, strange, and unfamiliar—essentially, traditional DCS evokes
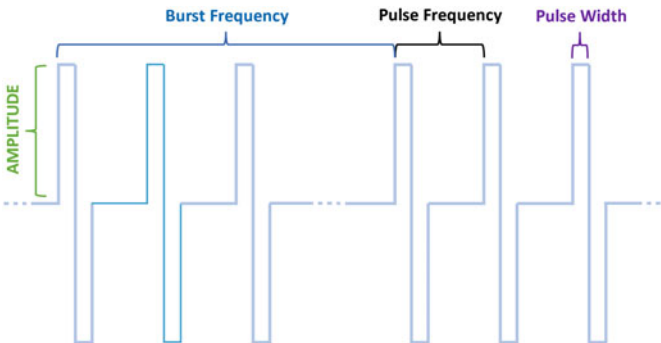


**Fig. 2**  In classic DCS, biphasic square-wave pulses (a single pulse is highlighted in bright blue) are delivered with constant amplitude (green) and pulse width (purple), at a particular pulse frequency (blue) for a burst of a given number of pulses (e.g., n = 3) at a set burst frequency (black)

precepts that you can point to but that feel distinctly unnatural [14, 17]. Nonetheless, DCS percepts have been useful as feedback because of this reliable localization and some innate discriminability [1, 14, 15, 17, 18]. Specifically, the intensity of a DCS percept has been shown to modulate with changes to pulse-width, frequency, or amplitude in humans [15–17, 19, 20] and burst frequency (i.e., the time between groups of stimulation pulses) in monkeys [11]. In humans, the ability to discriminate between different S1-DCS parameter levels by intensity has been exploited as graded neurohaptic feedback to guide movement behavior [1]. DCS percepts have also been shown to be distinguishable from concurrent natural touch at the same location [21, 22].

Research has continued to search for ways to enhance the utility of DCS feedback by evoking more natural, sensorimimetic percepts [23] and by defining ways to improve discriminability. It has been suggested that DCS which replicates the oscillatory structure of neural signals during natural touch may evoke more natural percepts. Moreover, it has been demonstrated in monkeys [11] that simple temporal structure in DCS is interpretable and could provide a new axis for discriminable DCS design. My research implemented and evaluated the interpretability of a continuous amplitude-modulation approach to dynamic DCS in humans.

Additionally, human DCS studies have historically relied on "passive" stimulation protocols, meaning that the DCS was supplied to the patient independent of any actions taken by the patient. This has prevented self-administration, expectation and neural preparation for DCS, and integration of sensory DCS with naturalistic behaviors. The lack of "active" stimulation protocols is largely due to the difficulty of real-world experimental setups that both enable object interaction and suppress or disentangle natural touch as a confound. To overcome this, pioneering studies in non-human primates have integrated DCS with natural object exploration within 2D virtual object interactions [11, 13, 24], and a recent study in humans delivered DCS sensory feedback based on the interaction of a third-person robotic arm and target object [2]. Modern VR systems overcome the limitations of real-world experimental design.

Using binocular visual displays and camera- and sensor-based tracking of real-world objects, VR creates immersive three-dimensional alternate realities with which humans can naturally interact and over which experimenters have near complete control (Fig. 1). While VR technology has been quickly leveraged by research teams using non-invasive neural recording modalities such as electroencephalography (EEG) and functional MRI (fMRI) [25, 26], it had been limitedly integrated with out-patient intracranial recording [26, 27] and not incorporated at all with in-patient intracranial recording. The work acknowledged by the BCI Award committee presented the first VR integration solution with in-patient subjects, developed during my PhD.

While the in-patient clinical setting presented unique challenges, it also granted unique access to the broad cortical and subcortical coverage with electrocorticography (ECoG) and stereo-electroencephalography (sEEG) electrodes (Fig. 3) that are implanted in children and adults for medical evaluation of refractory epilepsy. For a week to 2 weeks, these patients undergo continuous clinical
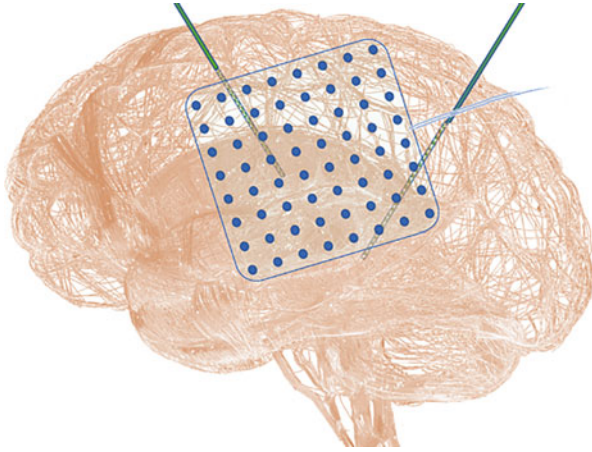
**Fig. 3** Intracranial arrays. Electrocorticography (ECoG) are strips or grids of flat, circular electrodes [8, 11] implanted subdurally or epidurally to record directly from the cortex. Stereo-EEG (sEEG) are vertical probes of cylindrical electrodes [11] stereotactically implanted to deeper, subcortical structures. Superficial sEEG contacts may also record from the cortex, and both arrays can deliver DCS for clinical mapping of eloquent neural tissue or for research purposes, to excite or inhibit neural activity [12]

monitoring and invasive neural recording to precisely characterize and map seizure activity. This presents a chronic neural recording research opportunity with dozens of subjects a year, per site. Additionally, ECoG and sEEG offer significant improvements in spatiotemporal resolution of neural signals over non-invasive recording modalities, and also permit direct electrical stimulation of the human brain—requisite for both pre-surgical mapping of eloquent cortex, and BCI and neurohaptic DCS research [28].

The remaining pages of this chapter outline the design and validation of this first in-patient, intracranial VR experimental platform [3] and the methods and results from the first VR-BCI neurohaptic study [4]. The goal of this chapter is to outline the VR system and clinical approaches useful to immersive VR research, to present advances in neurohaptic DCS design, and to encourage VR adoption for advanced neuroscience and BCI research with in-clinic patient populations.

## 2 Virtual Reality Experimental Platform

### 2.1 Hardware and Software

An HTC Vive Pro Eye Virtual Reality system was selected for immersion and interaction within virtual environments. These "scenes" were designed with the
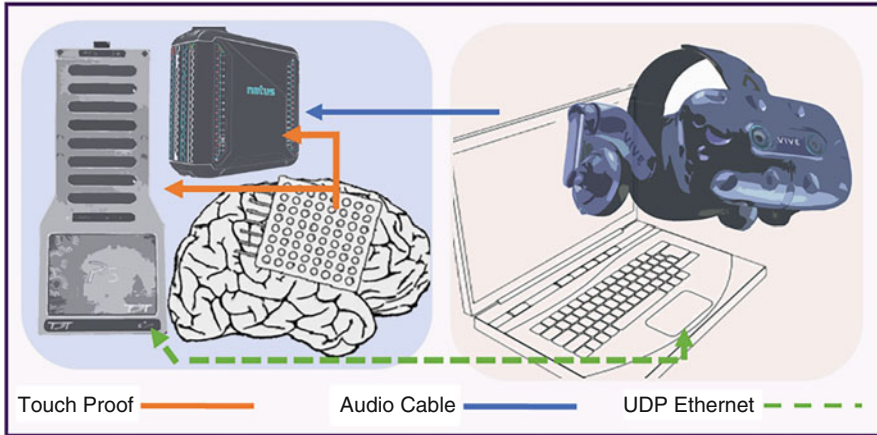
**Fig. 4** System diagram: hardware connectivity and synchronization. An HTC VIVE Pro Eye virtual reality system links to a Tucker Davis Technologies (TDT) neural recording and stimulation suite and a Natus Quantum clinical recording suite. Data synchronization between neural recording hardware and the VR hosting laptop was completed by UDP (dashed green) or audio inputs (solid blue)

Unity game engine and hosted by an Alienware m15 R4 (32GB RAM NVIDIA GeForce RTX 3070 8GB) gaming laptop (Fig. 4).

Audio cues were used to align VR task data with the neural signals recorded by a clinical Natus Quantum biosignal recording system (at 1024 or 2048 Hz). An additional neural recording system, the Tucker Davis Technologies (TDT) neurophysiology suite, was used to both record neural signals at a higher sampling rate (up to 12 kHz) and deliver direct cortical stimulation (DCS). UDP packets were used to synchronize experimental VR data and trigger neurohaptic DCS.

Custom control circuits were built in Synapse, proprietary TDT software, to manage near simultaneous neural recording and precise neural stimulation (circuits available on request). An independent Synapse-Unity API was also developed in the course of this work and is available on Github [29]. All data were collected in accordance with protocols approved by the University of Washington Institutional Review Board (IRB) and included neural signals, in-room sound and video, kinematic tracking variables and object interaction flags, ocular tracking, and subjective descriptions of experimental events acquired by both questionnaire and free response. Direct electrical stimulation of neural tissue was conducted within known standards of charge density safety [30] and at electrical current magnitudes below 15 mA, the maximum used by clinical stimulators.

## 2.2   Validation Studies

A benchtop validation study [29] of the VR experimental platform was conducted, using function generators and clinical electrode arrays in a saline tank. With this setup, the time delay between the occurrence of a tracked event in VR (e.g. object collision) and the onset of S1-DCS delivered by the TDT was shown to be 6.8 ms ± 1.7 ms across 217 collision-stimulation trials, with a maximum delay of 16.8 ms. These results place the delay between a touch event registered in VR and the delivery of neurohaptic DCS at well below the 45 ms for a detectable visuohaptic separation [31], though potential cognitive delays in processing DCS as touch [21, 22] will need to be evaluated in future VR-based neurohaptic studies.

Following benchtop validation, a human subject noise and feasibility study was conducted [3]. To evaluate signal quality during a VR study, neural signals were evaluated during unstructured activity in VR (with headset on) and unstructured activity with the headset off, over more than 20 min in two subjects, and across both ECOG and sEEG electrodes, analyzed independently. Results from this study revealed an increase in line noise power (57–63 Hz) with the VR headset on but no significant change in the noise floor band power (125–240 Hz). Following simple common average referencing (CAR), no significant difference in line noise or broadband noise floor existed between the headset on and off conditions [3]. These results confirm preserved neural signal integrity recorded by both ECOG and sEEG electrode configurations during the use of a VR headset for immersive task presentation. This contrasts previous studies which demonstrated significant signal perturbation from VR hardware when using noninvasive, electro-encephalography (EEG) electrodes [25].

I also published guidelines for VR task design and patient protocols to don and doff the VR headset, introduce VR hardware, and facilitate comfortable VR immersion [3]. Summarized: use high-end VR hardware and design scenes with distant horizons, simple backgrounds, and low visual complexity to reduce the chance of virtual reality sickness (VRS). Also, limit head movement and avoid camera translation within the VR scene ("Don't walk when you can teleport"). To improve immersion and professional design esthetic, *always add a skybox* and use visually comfortable lighting intensity and angles. While I describe specific protocols in the paper, my general advice is to incorporate the subject in all forms of headset positioning and have the subject tighten and adjust the fit of the headset themselves. Subjects will tighten the headset more snugly than the researchers, and a good fit is paramount for comfort. In total, we have completed VR studies in nearly a dozen intracranial neural recording patients and have not had a subject experience VRS or related symptoms, nor express discomfort with the headset that precluded experiment completion, nor decline additional sessions and days of VR tasks due to discomfort with VR immersion or headset fit. If anything, the opposite was found: we witnessed unexpectedly strong task engagement and performance, willingness to remain in VR for extended periods of time to explore commercial VR gameplay, and

eagerness for additional sessions and days of VR experience. VR is a powerful platform for researchers, and, in our experience, a very enjoyable way to pass the time for our intracranial subjects.

## 3 Neurohaptic Design

### 3.1 Virtual Object Discrimination Tasks

Two object discrimination tasks were designed with a throw-to-target game mechanic. Subjects were instructed to throw an object delivering any DCS neurohaptic feedback towards a target in the binary HapticSort task, and to throw different objects delivering unique DCS neurohaptic feedback towards the correct target in the ternary HapticSort_ABØ task (Fig. 5). Neurohaptic DCS was only delivered while a neurohaptic object was grasped, and ended when the object was released. In these tasks, a subject was able to interact with a virtual object using natural exploration behavior to determine (1) whether neurohaptic feedback was occurring (binary discrimination) and then (2) which neurohaptic sensation was being felt (ternary discrimination). Each subject first completed the binary HapticSort task with controller-based vibrotactile haptic feedback prior to completing the task with DCS to ensure task comprehension and to serve as a baseline of discrimination performance [4].

Within each discrimination task, distinct training and testing scenes were created (Fig. 5). In training scenes, objects delivering neurohaptic feedback were visually-encoded—meaning, the object was visually identifiable as either a neurohaptic or a "null" object. In the testing scenes, objects were visually identical. This was done to allow the subject to organically "train themselves" to identify distinct neural stimulation patterns in the training scene, and then test object discrimination in the testing scene.

In the binary task (Fig. 5, top), the training scene was limited to 13 trials, from 6 nonhaptic and 7 neurohaptic objects. In the ternary task, however (Fig. 5, bottom), subjects were free to complete any desired number of training trials, in which objects were visually encoded to indicate neurohaptic feedback. In both the binary and ternary testing scenes, pushing down on a simple, brown button would generate a visually non-descript object. All objects in the testing scene were visually identical and could only be discriminated by neurohaptic profile. Subjects were asked to complete at least 15 testing trials but encouraged to complete as many as they were willing to do. Additionally, after training in the ternary task, subjects were asked to select a single word to describe the neurohaptic profile that corresponded to each target. This word was added to the corresponding target during testing (Fig. 5, bottom) to remove a memory confound in target selection. This was done after the first subject stated that remembering which object went to which target was a significant factor in the accuracy of their object sorting. Additionally, while the
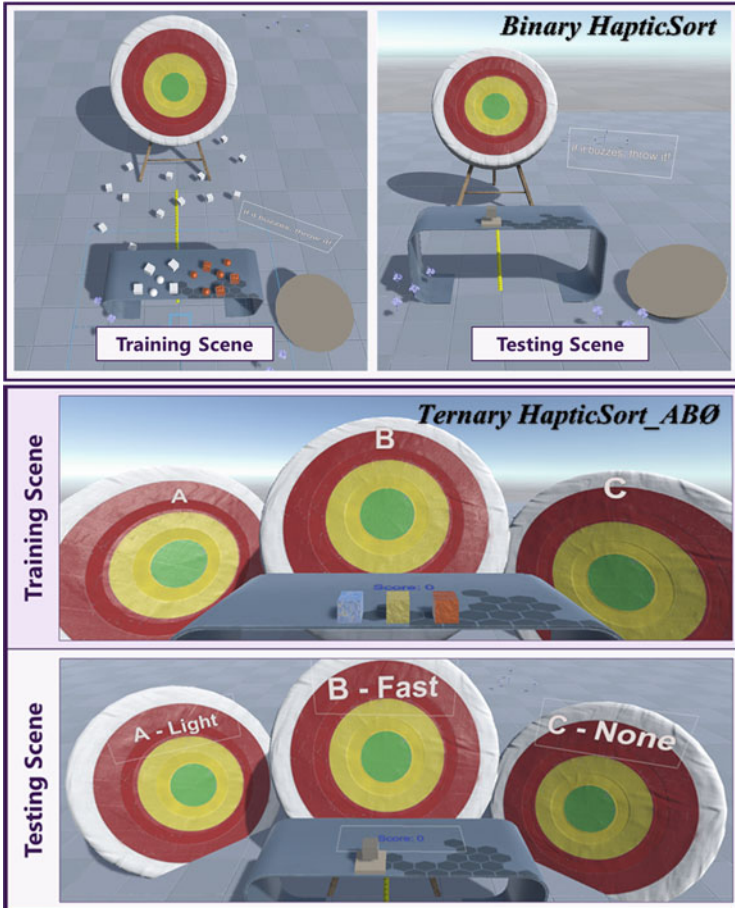
**Fig. 5** Virtual object discrimination scenes. Neurohaptic objects are thrown towards a bullseye target. During binary HapticSort training (top left), six visually encoded objects deliver no feedback when grasped (matte white) and seven deliver neurohaptic feedback (metallic orange). In the testing scene, a button is depressed to generate a visually identical cube for neurohaptic discrimination (top right). During ternary HapticSort_ABØ training (middle panel), two neurohaptic cubes and one non-haptic cube are visually encoded and must be thrown to own bullseye target. During testing (bottom panel), the button again generates an identical object for ternary neurohaptic discrimination (bottom panel), the button again generates an identical object for ternary neurohaptic discrimination. To mitigate the confound of "remembering" which percept belongs to which target, targets were labelled with subject-determined single descriptors

throw-to-target game mechanic provided an entertaining and kinematically dynamic task, the accuracy of neurohaptic discrimination was determined based on target intent. Meaning, that regardless of whether the subject hit the target they intended to hit, the "trial" would be counted as accurate if an object was thrown *towards* the correct target.

## 3.2 Electrode Localization for DCS Candidates

Electrode localization by published methods [4] was used to identify candidate stimulation electrodes and their likely somatic coverage along the somatosensory (S1) cortex. The presence, strength, location, and character of any evoked percept was determined by subjective report. Stimulation between 1 mA and 6.5 mA with pulse counts of 1, 5 or 20 pulses at 30 Hz were evaluated. DCS perception and required stimulation thresholds were assessed for each subject prior to each day's first neurohaptic task (Fig. 6).

## 3.3 Complex Stimulation Design

Neurohaptic feedback by DCS was delivered as biphasic square wave pulses of 200 μs pulse width at a 50 Hz maximum pulse frequency during grasp of neurohaptic objects. Stimulation was continuous during object grasp and ceased as soon as the object was released. Novel, DCS sequences were constructed to create distinct amplitude-modulated stimulation patterns (Fig. 7) which were evaluated for subjective description and discriminability.
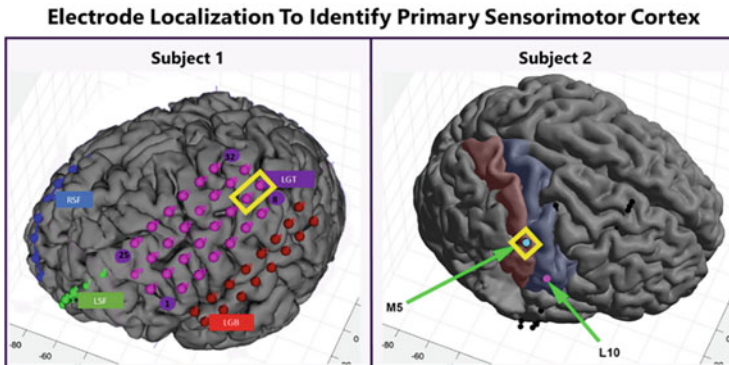


**Fig. 6** Electrode localization. (Left) In Subject 1, S1-DCS at left somatosensory hand electrodes (yellow box) elicited a percept in the right thumb and index filter. (Right) In Subject 2, Surface sEEG electrodes in the right somatosensory hand (M4:6) (yellow box) induced a sensorimotor percept of clenching despite pre-existing paralysis in that hand and no actual movement
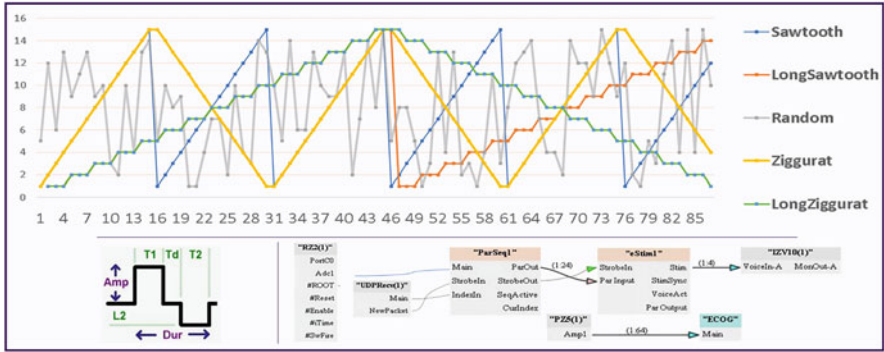
**Fig. 7** Amplitude-modulated sequences. Five distinct templates of amplitude-modulated DCS were designed. Templates were built as sequences of indices (1:15) that were sent by Unity to the TDT neural stimulation hardware. By sending indices to ensure DCS safety, the VR task triggered complex DCS during object interaction across a subject-specific range of amplitudes that were tuned to the percept thresholds of each subject before each new day of neurohaptic stimulation [4]

## 4 Behavioral Results

### 4.1 Subjective Descriptions

Subject 1 described the evoked percept from constant amplitude DES in the hand areas of the left somatosensory cortex as "maybe buzzing." This response may have been influenced by both the preceding controller-based vibrational haptics and the use of the word "buzz" in the task description. The Sawtooth amplitude-modulated S1-DCS pattern was described as having a "pulsing effect" with a quick, ~2 Hz rhythm. The LongSawtooth and LongZiggurat sequences were both described as "bumpy" with "different bumpiness"—specifically that the bumps of the LongSawtooth sequence were "sharper." The Random sequence was described as "smoother" in comparison to the LongSawtooth pattern. After the amplitude-modulated sequences, constant amplitude stimulation was described as "flatter." In a direct comparison, the LongSawtooth pattern was described as "slow" and the Sawtooth pattern as "fast." Multiple days later, LongSawtooth was again described as "bumpy" compared to constant amplitude stimulation described as "smooth, no bumps."

In Subject 2, a short 20-pulse burst of S1-DCS over the hand area of the right somatosensory cortex evoked a phantom motor sensation without actual muscle activation in a paralyzed left hand (motor deficit, sensation intact): "I felt like I was clenching," Subject 2 said while demonstrating a gripping gesture with the right hand, opening and closing in a regular rhythm. Perhaps this reflects the induction of a motor intention through S1-DCS or a unique interaction with neural tissue that may have undergone some level of cortical remapping following functional paralysis of the left hand. The Sawtooth sequence was described as having an irregular "pulsing" rhythm, with the LongSawtooth was clearly (and unexpectedly) felt as "a little

faster." The Random pattern evoked a lingering perceptual effect that seemed to persist with decaying intensity for more than 3 s. This was initially concerning as evidence of potential after-discharge activity, but the clinical team confirmed no irregular or epileptiform neural activity. Later, the LongZiggurat sequence was barely perceptible with no distinct character, but the Ziggurat sequence was perceived as a regular "bump, bump, bump, bump" percept. In comparison, the Sawtooth felt "faster" and the LongSawtooth was "pulsing" but was "not clearly different" from Sawtooth. The Random sequence, cautiously evaluated, was perceived as "just fast pulsing" with no lingering percept.

## 4.2  Discrimination Accuracy

Task accuracy was evaluated as: (1) binary stimulation accuracy (AB-Ø), the accuracy of neurohaptic vs. nonhaptic discrimination; (2) ternary percept accuracy (A-B-Ø), the overall accuracy of discriminating between one nonhaptic and two distinct neurohaptic sequences of feedback; and (3) binary percept accuracy (A-B), the accuracy of discriminating between the two neurohaptic sequences.

[a]Training scene: visual encoding of objects

[b]Testing scene: no visual encoding

Subject 1 completed three non-consecutive days of neurohaptic VR experiments with binary and ternary HapticSort accuracies shown in Table 1. Results from first round of HapticSort_ABØ Testing (Table 1, row 7) demonstrate the confounding

**Table 1**  Percent accuracy (%) of HapticSort trials

| Stimulation details | Stim binary AB − Ø | Percept ternary A − B − Ø | Percept binary A − B |
|---|---|---|---|
| *Subject 1* | | | |
| 13 trials, 200 µs, 3 mA[a] | 88.1 | – | – |
| 28 trials, 200 µs, 3 mA[b] | 92.9 | – | – |
| 3 trials, 200 µs, 2 mA[b] | 0 | – | – |
| 48 trials, 150 µs, 3 mA[b] | 95.8 | – | – |
| 52 trials, 400 µs, 4–6.1 mA[b] *LongSawtooth* | 100 | – | – |
| 32 trials, 400 µs, 4–6.1 mA[a] *Sawtooth—LongSawtooth* | 86.2 | 84.4 | 87 [of 23] |
| 20, 400 µs, 4–6.1 mA[b] *Sawtooth—LongSawtooth* | 90 | 50 | 57.1 [of 14] |
| 46 trials, 400 µs, 4–6.1 mA[b] *LongSawtooth— 3.85 mA* | 86.9 | 73.9 | 77.8 [of 27] |
| *Subject 2* | | | |
| 6 trials, 400 µs, 2–3.4 mA[a] *Sawtooth—Ziggurat* | 100 | 100 | 100 [of 5] |
| 16 trials, 400 µs, 2–3.4 mA[b] *Sawtooth—Ziggurat* | 81.3 | 68.8 | 80 [of 10] |
| 29 trials, 400 µs, 2–3.4 mA[b] *Sawtooth—Ziggurat* | 89.7 | 72.4 | 79.2 [of 24] |
| 50 trials, 400 µs, 2–3.4 mA[b] *Sawtooth—2 Hz Burst* | 98 | 82 | 79.5 [of 39] |

impact of memory in the first implementation of this task: while A-B-Ø and A-B were both quite low (50% and 57.1%, respectively), simple AB-Ø was quite high, at 90%. In this round, multiple discrimination mistakes were made *not* because A and B were indistinguishable, but because recalling the target assignment of A verses B was difficult. Learning from this task implementation error, the targets in subsequent HapticSort_ABØ testing scenes were labelled with the subjective description of the associated stimulation sequence, as described earlier and shown in Fig. 5.

Subject 2 also completed 3 days of neurohaptic VR experiments, with results shown in the bottom section of Table 1. In the final round of the ternary HapticSort_ABØ task (Table 1, last row), the Ziggurat sequence was contrasted with a new 2 Hz burst frequency stimulation condition that more closely replicated a published approach used in a non-human primate object discrimination task [11]. Specifically, a 5-pulse burst of stimulation at 50 Hz was repeated at a 2 Hz burst frequency. The A-B-Ø of 82% over 50 trials reveals improved performance compared to previous rounds, with stim binary AB-Ø of 98% and percept binary A-B at 79.5% across 39 detected stimulation trials (Table 1, last row).

## 5   Discussion

The VR experimental platform presented here enables advanced BCI development and cognitive neuroscience in a unique, important, and previously challenging-to-access clinical in-patient research population [3]. The validation and noise analysis studies demonstrated maintained signal integrity and strong participant enjoyment, and can facilitate the broader adoption of VR for research with this intracranial research population. The subsequent integration of DES with naturalistic motor behavior during object exploration, termed neurohaptics, demonstrated robust binary and ternary discrimination. This suggests the innate interpretability of temporally dynamic DCS stimuli in the brain. Additionally, the HapticSort task was the first demonstration of DCS during active object manipulation in humans and enabled the first first-person, self-directed, and spontaneously natural human interaction with "tangible" virtual objects—the first to enable a human to "feel" a virtual reality through an implanted, neurohaptic BCI. Finally, this work expands upon existing DCS approaches by exploring novel stimulation protocols with amplitude modulated pulse-train shape. Across subjects, amplitude modulated DCS was shown to be more reliably discernable than constant amplitude stimulation. It was also able to elicit stable, distinct, and discriminable percepts in two subjects. The subjective descriptions of amplitude-modulated S1-DES include rhythms with variable "bumpiness". While I would not suggest these percepts are yet "natural" feeling, they were described with more natural sensorimimetic language and interpretable as dynamic sensation.

Understanding how the brain interprets and integrates DCS with behavior will continue to refine the naturalness and utility of DCS neurohaptic feedback. This work encourages a virtual route forward for neurohaptics design with implications

for BCI and neuroprosthetics. Future research directions include the identification of the neural features of the sensory expectation of DCS, the neural dynamics of DCS processing, and the neural state that may predict successful DCS identification.

# References

1. Cronin JA et al (2016) Task-specific somatosensory feedback via cortical stimulation in humans. IEEE Trans Haptics **9**:515–522
2. Flesher SN et al (2021) A brain-computer interface that evokes tactile sensations improves robotic arm control. Science 372:831–836
3. Paschall C, Rao RPN, Hauptman J, Ojemann G, Herron J (2022) An immersive virtual reality platform integrating human ECOG & sEEG: implementation & noise analysis
4. Paschall CJ, Hauptman JS, Rao RPN, Ojemann JG, Herron J (2022) Touching the void: intracranial stimulation for NeuroHaptic feedback in virtual reality. In: 2022 IEEE International Conference on Systems, Man, and Cybernetics (SMC). IEEE. https://doi.org/10.1109/smc53654.2022.9945366
5. Collinger JL et al (2013) High-performance neuroprosthetic control by an individual with tetraplegia. Lancet 381:557–564
6. Ajiboye AB et al (2017) Restoration of reaching and grasping movements through brain-controlled muscle stimulation in a person with tetraplegia: a proof-of-concept demonstration. Lancet 389:1821–1830
7. Ethier C, Oby ER, Bauman MJ, Miller LE (2012) Restoration of grasp following paralysis through brain-controlled stimulation of muscles. Nature 485:368–371
8. Collinger JL, Gaunt RA, Schwartz AB (2018) Progress towards restoring upper limb movement and sensation through intracortical brain-computer interfaces. Curr Opin Biomed Eng 8:84–92
9. Paralysis statistics. Reeve Foundation. https://www.christopherreeve.org/living-with-paralysis/stats-about-paralysis.
10. Bensmaia SJ, Miller LE (2014) Restoring sensorimotor function through intracortical interfaces: progress and looming challenges. Nat Rev Neurosci 15:313–325
11. O'Doherty JE et al (2011) Active tactile exploration using a brain-machine-brain interface. Nature 479:228–231
12. Armenta Salas M et al (2018) Proprioceptive and cutaneous sensations in humans elicited by intracortical microstimulation. Elife 7
13. O'Doherty JE, Lebedev MA, Li Z, Nicolelis MAL (2012) Virtual active touch using randomly patterned intracortical microstimulation. IEEE Trans Neural Syst Rehabil Eng 20:85–93
14. Caldwell DJ, Cronin JA, Levinson LH, Rao PN (2021) Chapter 14 – Touch restoration through electrical cortical stimulation in humans. In: Güçlü B (ed) Somatosensory feedback for neuroprosthetics. Academic Press, pp 443–478. https://doi.org/10.1016/B978-0-12-822828-9.00021-6
15. Cronin, J. A. Human psychophysics of direct cortical stimulation of somatosensory cortex. (2018).
16. Libet B et al (1964) Production of threshold levels of conscious sensation by electrical stimulation of human somatosensory cortex. J Neurophysiol 27:546–578
17. Johnson LA et al (2013) Direct electrical stimulation of the somatosensory cortex in humans using electrocorticography electrodes: a qualitative and quantitative report. J Neural Eng 10: 036021

18. Leuthardt EC, Miller KJ, Schalk G, Rao RPN, Ojemann JG (2006) Electrocorticography-based brain computer interface–the Seattle experience. IEEE Trans Neural Syst Rehabil Eng 14:194–198
19. Libet B et al (1993) Production of threshold levels of conscious sensation by electrical stimulation of human somatosensory cortex. In: Libet B (ed) Neurophysiology of consciousness. Birkhäuser, Boston, pp 1–34. https://doi.org/10.1007/978-1-4612-0355-1_1
20. Hiremath SV et al (2017) Human perception of electrical stimulation on the surface of somatosensory cortex. PLoS One 12:e0176020
21. Caldwell DJ et al (2019) Direct stimulation of somatosensory cortex results in slower reaction times compared to peripheral touch in humans. Sci Rep 9:3292
22. Caldwell DJ et al (2019) Publisher Correction: Direct stimulation of somatosensory cortex results in slower reaction times compared to peripheral touch in humans. Sci Rep 9:20317
23. Bjånes DA et al (2022) Multi-channel intra-cortical micro-stimulation yields quick reaction times and evokes natural somatosensations in a human participant. bioRxiv. https://doi.org/10.1101/2022.08.08.22278389
24. O'Doherty JE, Shokur S, Medina LE, Lebedev MA, Nicolelis MAL (2019) Creating a neuroprosthesis for active tactile exploration of textures. Proc Natl Acad Sci U S A 116:21821–21827
25. Tauscher J-P et al (2019) Immersive EEG: evaluating electroencephalography in virtual reality. In: 2019 IEEE Conference on Virtual Reality and 3D User Interfaces (VR), pp 1794–1800. https://doi.org/10.1109/VR.2019.8797858
26. Georgiev DD, Georgieva I, Gong Z, Nanjappan V, Georgiev GV (2021) Virtual reality for neurorehabilitation and cognitive enhancement. Brain Sci 11
27. Topalovic U et al (2020) Wireless programmable recording and stimulation of deep brain activity in freely moving humans. Neuron 108:322–334.e9
28. Caldwell DJ, Ojemann JG, Rao RPN (2019) Direct electrical stimulation in electrocorticographic brain–computer interfaces: enabling technologies for input to cortex. Front Neurosci
29. Montag M, Paschall C, Ojemann J, Rao R, Herron J (2021) A platform for virtual reality task design with intracranial electrodes. Conf Proc IEEE Eng Med Biol Soc 2021:6659–6662
30. Cogan SF, Ludwig KA, Welle CG, Takmakov P (2016) Tissue damage thresholds during therapeutic electrical stimulation. J Neural Eng 13:021001
31. Vogels IMLC (2004) Detection of temporal delays in visual-haptic interfaces. Hum Factors 46:118–134

# May the Force Be with You: Biomimetic Grasp Force Decoding for Brain Controlled Bionic Hands

**Elizaveta V. Okorokova, Anton R. Sobinov, John E. Downey, Qinpu He, Ashley van Driesche, David Satzer, Peter C. Warnke, Nicholas G. Hatsopoulos, and Sliman J. Bensmaia**

**Abstract** Intracortical brain-computer interfaces (iBCIs) have achieved remarkable progress in restoring arm and hand movement by inferring motor intent from neural signals in primary motor cortex (M1) and realizing the intended movements in a bionic limb. However, manual interactions with objects require not only restoration of movement but also the precise application of forces on objects, which implies a different mode of limb control that has been largely overlooked. One of the major obstacles in incorporating force control is the lack of understanding of how manual forces are encoded in M1 during object interactions. To fill this gap, we recorded the neural activity in M1 as monkeys grasped sensorized objects with varying levels of force. We found that static decoders could not reliably extract force information from M1 activity, suggesting a dynamic relationship between force and neural activity. Consistent with this hypothesis, a recurrent neural network could exploit these dynamics to accurately decode time-varying forces. Next, we applied the insights gleaned from our experiments with able-bodied macaques to build decoders of manual force in a human participant with tetraplegia. First, we found that the patterns

E. V. Okorokova (✉) · Q. He
Committee on Computational Neuroscience, University of Chicago, Chicago, IL, USA
e-mail: lizok@uchicago.edu

A. R. Sobinov · J. E. Downey · A. van Driesche
Department of Organismal Biology and Anatomy, University of Chicago, Chicago, IL, USA

D. Satzer
Department of Neurological Surgery, University of Chicago, Chicago, IL, USA

P. C. Warnke
Department of Neurological Surgery, University of Chicago, Chicago, IL, USA

Neuroscience Institute, University of Chicago, Chicago, IL, USA

N. G. Hatsopoulos · S. J. Bensmaia
Committee on Computational Neuroscience, University of Chicago, Chicago, IL, USA

Department of Organismal Biology and Anatomy, University of Chicago, Chicago, IL, USA

Neuroscience Institute, University of Chicago, Chicago, IL, USA

of responses in human M1 during imagined force application were similar to those in monkey M1 during physical force application. We then applied recurrent neural networks to decode force from M1 activity and showed that these allow the participants to accurately exert forces with a (brain-controlled) virtual hand.

**Keywords** Intracortical brain-computer interface (iBCI) · Primary motor cortex · Bionic hand · Recurrent neural network · Force decoding

## 1   Sliman Bensmaia: A Tribute to an Exceptional Scientist and Mentor

With heavy hearts, we begin this paper by acknowledging the recent and unexpected passing of our senior author, Sliman Bensmaia. Sliman was a brilliant scientist and mentor whose expertise in somatosensation and brain-computer interfaces transformed our understanding of sensory perception and its underlying mechanisms, bringing hope to patients who have suffered amputations or spinal cord injuries. Sliman left a deep impact on his colleagues, the broader scientific community, and most notably, on his mentees, profoundly shaping their training, careers, and personal development. We are dedicating this paper to Sliman's memory, honoring his remarkable contributions to science and our lives.

## 2   Introduction

Intracortical brain-computer interfaces (iBCI) show great promise for restoring hand function in patients with tetraplegia through the use of bionic hands [1–5]. Current approaches to restoring hand and arm function are restricted to decoding kinematics, enabling users to control the position or speed of the arm and hand [3–5]. A hallmark of manual behavior, however, is interactions with objects that require precise regulation of forces exerted on them [6]. While motor cortical (M1) activity related to force has been identified in studies with non-human primates [7–15] and humans [16–19], the precise relationship between neuronal activity and force is still poorly understood. Accordingly, harnessing these signals to decode grasp force in iBCI has proven challenging. To date, M1 signals were used to decode one or a few discrete force levels [18–21], but not the online control of graded forces, critical for achieving seamless object manipulation. To fill this gap, we conducted two experiments. First, we recorded the neural activity in M1 as monkeys grasped sensorized objects, characterized the force signal in this population, and tested various force decoders. We found that, while static linear or non-linear decoders yielded poor force decoding performance, a recurrent neural network could accurately reconstruct the forces exerted by monkeys. Second, we investigated the degree to which we could leverage insights gleaned from the monkey experiments to enable force control in a real-time

iBCI. We found that the M1 activity associated with attempted force exertion in tetraplegic humans resembles that associated with actual force exertion in able-bodied monkeys. We then show that a recurrent neural network, which supports high-performance force decoding in monkeys, enables highly accurate force exertion with a brain-controlled virtual hand.

# 3  Results

## 3.1  Non-human Primate Grasp Force Task

On each trial, a manipulandum—consisting of two thin metal plates, covered with high-resolution sensor sheets (Tekscan) that enabled real-time monitoring of grasp force—was placed in the monkey's workspace by a motorized stage. The monkey's task was to reach to and squeeze the manipulandum at a force level cued by an LED to obtain a water reward (Fig. 1a). On each trial, an auditory tone cued the monkey to reach for and grasp the manipulandum. Another LED provided the animal with online feedback of the force exerted on the manipulandum (the summed output of all the force sensors, Fig. 1a). Monkeys received a juice reward for maintaining force within a range of forces for a specified duration (0.8–1 s). Monkeys exerted a variety of force profiles for each target condition (Fig. 1b). Neural activity was recorded with Utah electrode arrays (Blackrock Neurotech) implanted in the hand representation of M1.

### 3.1.1  Force Representation in Monkey Motor Cortex

First, we examined the dependence of M1 activity on force level by plotting the peri-stimulus time histograms (PSTH) in each recorded unit for each grasp force level, aligned to grasp onset and reward. Most recorded units (81%, Wilcoxon sign rank test, $p < 0.01$) were modulated by the task and showed a variety of response profiles. The most common pattern included a large response transient at contact with the manipulandum, followed by a weak sustained response (example unit 3 in Fig. 1c), sometimes followed by a transient at the release of the object (example unit 32 in Fig. 1c). Surprisingly, few units exhibited responses that were significantly modulated by force level (25% of recorded units, ANOVA, $p < 0.01$), with some responses enhanced at higher force levels (example unit 65 in Fig. 1c) and others suppressed (example unit 48 in Fig. 1c).

### 3.1.2  Force Can Be Decoded from Neural Population Responses

Next, we assessed the degree to which we could decode time-varying force from the response of the M1 population on individual trials. To this end, we implemented
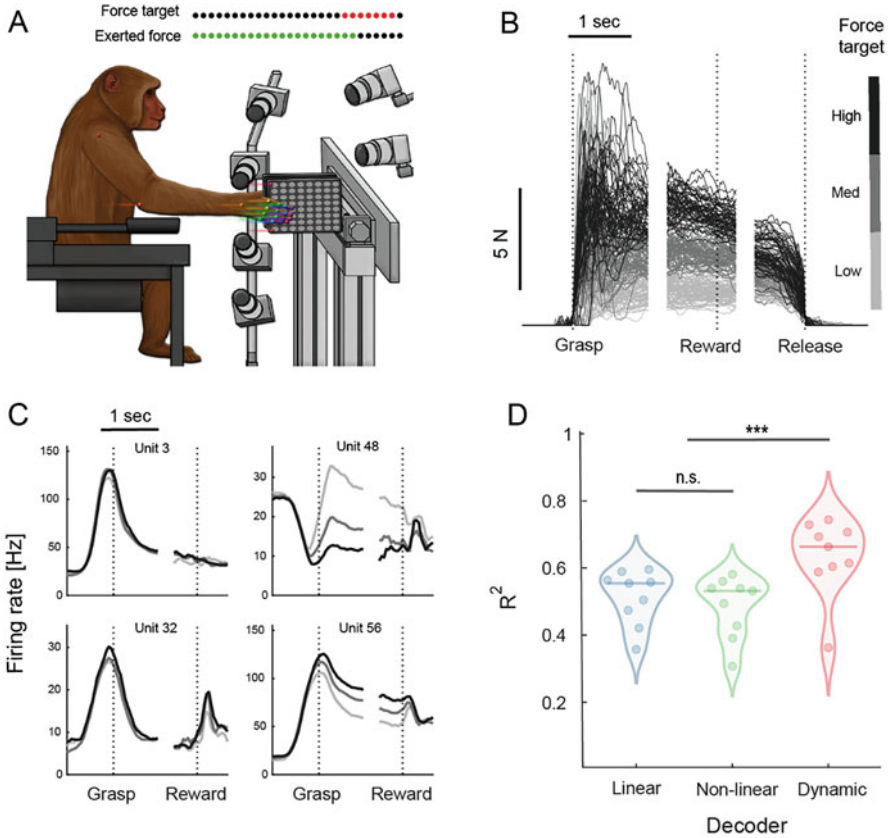
**Fig. 1** Non-human primate grasp force task. (**a**) Two monkeys were trained to reach for and grasp an object with an instructed amount of force. (**b**) Single trial force profiles shaded by force target. (**c**) Average neural responses (peristimulus time histograms) of four example neurons to each of the three force targets, shaded like panel (**b**). (**d**) Comparison of force decoder performance for the three classes of models: linear, non-linear, and dynamic. Each point is coefficient of determination ($R^2$) between actual and predicted force in one session. Horizontal bars indicate median performance of all sessions. ***Significant at alpha of 0.001, *n.s.* not significant

three types of decoders of increasing complexity. The first was a linear decoder (linear regression), which assumes an instantaneous linear relationship between neural response and force. The second was a non-linear decoder with static non-linearity (ANN—artificial neural network), which assumes an instantaneous non-linear relationship between neural response and force. The third model was a non-linear decoder with recurrence (LSTM—long short-term memory model) that could accommodate a dynamical non-linear relationship between neural activity and force.

We found that the linear decoder could capture coarse force fluctuations, but often failed to account for force adjustments throughout the hold period (median

$R^2 = 0.55$, Fig. 1d, blue). Decoder performance did not improve with the addition of static nonlinearity (median $R^2 = 0.53$, Fig. 1d, green), suggesting that the relationship between neural activity and force is dynamic. Consistent with this interpretation, a recurrent neural network (Long Short-Term Memory network or LSTM), which can accommodate a non-linear and dynamic relationship between input and output, substantially outperformed all other decoders (median $R^2 = 0.66$, Wilcoxon signed rank test $p < 0.01$, Fig. 1d, red). Our results are consistent with the hypothesis that force signals are encoded in non-linear dynamical patterns of activity in M1 and can only be harnessed by decoders that can accommodate or exploit those dynamics.

## 3.2 Human iBCI Grasp Force Task

Having discovered force signals in the motor cortex of able-bodied monkeys, we assessed whether the same signals were present in a human participant with a C4-level spinal cord injury that affected his ability to control his right hand. The participant was implanted with two Utah electrode arrays (Blackrock Neurotech) in the hand representation of the motor cortex (M1) (Fig. 2a). The participant controlled a limb avatar in a physics engine platform (MuJoCo, [22]) (Fig. 2b), which he experienced through a virtual reality headset (Valve Index). He used the virtual limb to grasp virtual objects at one of four force levels, cued by the color of the object and verbal instruction (Fig. 2c). Initially, virtual limb movements and force feedback were under computer control and the participant observed and attempted to perform the actions of the virtual limb. The neural activity during this observation phase was used to construct decoders—linear, static non-linear, or dynamic—of hand closing velocity and grasp force. The participant then used these decoders to perform the task in virtual reality.

### 3.2.1 Force Representation in Human Motor Cortex

First, we assessed the degree to which signals in human M1 were modulated by the task. To this end, we compared each neuron's firing rate during attempted movement (from data used for decoder training) before and after cue onset. We found that the firing rates changed significantly at cue onset on 61% of the active motor channels (Wilcoxon sign rank test, $p < 0.01$). Many M1 channels exhibited a strong transient at the onset of grasp (Fig. 2d) and a weaker transient upon object release. A few channels were also visibly modulated by force, exhibiting either increases (Fig. 2d, middle plot) or decreases in response at higher forces (Fig. 2d, right plot). Of all active motor channels, only 26% produced responses that were significantly modulated by force (ANOVA, $p < 0.01$). Overall, the force signal in human M1 resembles its counterpart in monkey M1.
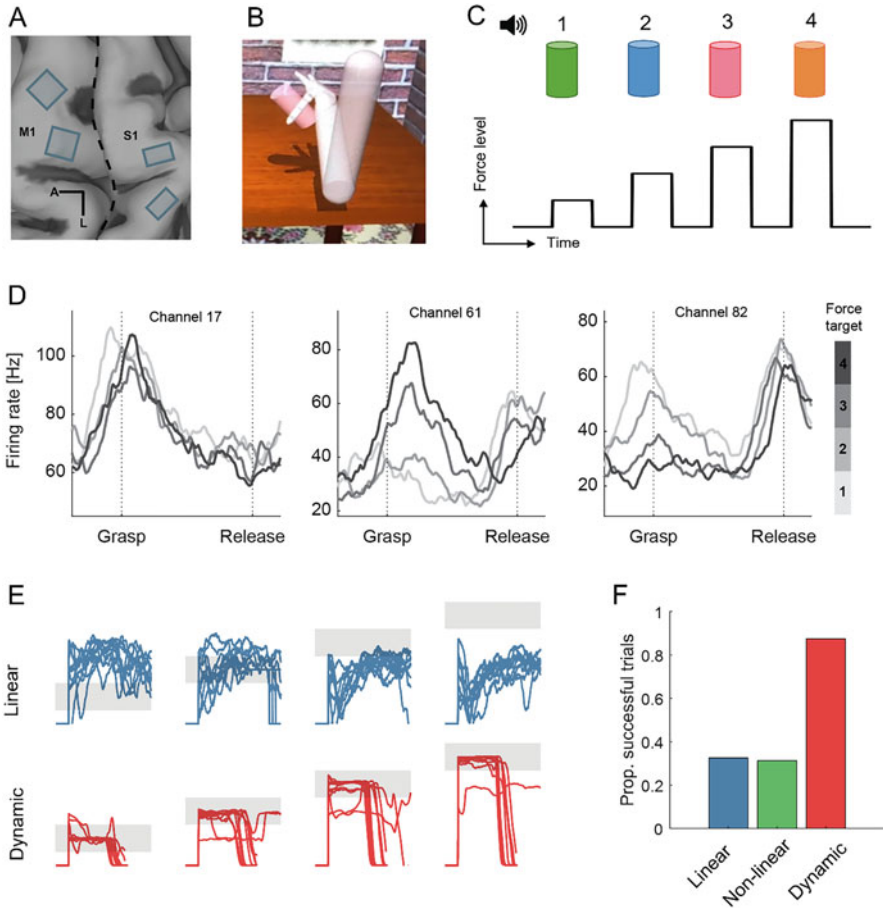
**Fig. 2** Human iBCI grasp force task. (**a**) Array (blue rectangles) placement. M1—motor cortex, S1—sensory cortex. (**b**) MuJoCo virtual environment. The participant controlled an avatar limb that grasped a virtual cylindrical object. (**c**) Example of force command sequence with four force levels. Force target was indicated by a verbal cue and a color of an object. (**d**) Mean response profiles (peristimulus time histograms) to four levels of grasp force on three motor channels, shaded by force target. (**e**) Example reconstructed force traces with linear (top, blue) and dynamic (bottom, red) decoders. Shaded grey areas indicate the acceptance boundary for each target force. Several trials are superimposed and aligned to first contact. (**f**) Proportion of successful trials performed using linear, non-linear, or dynamic decoders online

### 3.2.2  Dynamic Decoder Allows Accurate Force Decoding

Having established that a subpopulation of M1 neurons was modulated by attempted force, we gauged the degree to which time-varying force could be decoded from M1 responses. We tested the same decoders as with the monkeys: a standard linear decoder often used for real-time prosthetic control (linear regression), a decoder with

a static non-linearity (ANN), and a dynamic decoder (recurrent neural network—LSTM). For all sessions, the dynamic decoder significantly outperformed both linear and non-linear methods offline (median $R^2$ = 0.58, 0.59, and 0.73, for linear, non-linear, and dynamic models, respectively), suggesting that there is a non-linear dynamic relationship between target force and neural responses in motor cortex.

While the dynamic decoder outperformed other decoders offline, good offline performance does not always translate into improved online performance [23, 24]. With this in mind, we assessed the participant's ability to perform the force task with the dynamic decoder. As in the offline case, the participant was cued to exert one of four levels of force on the virtual object. Both the hand closure and the level of force were decoded from M1 signals with decoders, trained on the observation data as described above. We found that the dynamic decoder enabled outstanding performance on the task, yielding an average performance of 87.5%, far surpassing the performance of the other two decoders (32.5% and 31.3% for linear and non-linear, respectively), mirroring the results of the offline decoding analysis (Fig. 2e, f). Thus, a recurrent neural network is well suited to extract force signals from the M1 population response, presumably because it can accommodate the dynamic representation of force in M1, while the other decoder types cannot.

## 4 Conclusions

We showed that the force signals in the motor cortex of able-bodied monkeys squeezing an object are comparable to those found in the motor cortex of a human with spinal cord injury attempting to squeeze an object. In particular, force signals in M1 peak around grasp onset, and then decay rapidly, with a second burst at grasp offset. The mapping between the M1 response and force is thus highly dynamic throughout the grasp and cannot be captured with a linear model in contrast to relationship between M1 response and kinematics, which can be well captured using a linear model [3–5, 25, 26]. While models with a static non-linearity can account for the relationship between time-averaged M1 responses and force [11], these models cannot capture the dynamics of the M1 force signal. We show that recurrent neural networks, which can accommodate a dynamical mapping between input and output, can accurately decode intended force from the M1 response in both offline and online settings, implying a different approach for force decoding than is typically employed for kinematics decoding.

## 5   Methods

### 5.1   Non-human Primate Experiment

#### 5.1.1   Animals and Surgery

Neural recordings were collected from two male rhesus macaques (M and P, ages 11 and 9 years at the time of surgery). They were each chronically implanted with a single Utah electrode array in the right primary motor cortex (Brodmann area 4, M1). The electrode lengths were 1.5 mm, with uniform spacing of 400 μm aligned on a 10 by 10 grid. Arrays were placed in the arm and hand representation of the motor cortex, as confirmed by electrically stimulating the cortex during surgery with surface electrodes and observing corresponding muscle twitches before array implantation. Surgical procedures consisted of the implantation of a head-fixing post onto the skull, craniotomy, intraoperative electrical stimulation of the brain surface, and implantation of the array. All procedures were performed under aseptic conditions and anesthesia induced with ketamine HCl (20 mg kg$^{-1}$, IM) and maintained with isoflurane (10–25 mg kg$^{-1}$ h$^{-1}$, inhaled). Handling of animals was performed in accordance with the rules and regulations of the University of Chicago Animal Care and Use Committee. Monkeys received care from a full-time husbandry staff, and a full-time veterinary staff monitored the animals' health.

#### 5.1.2   Behavioral Task

We trained two monkeys (M and P) to perform a visually guided grasping task, in which they were required to grasp an object with a visually cued amount of force to receive a juice reward. Each trial was initiated when an LED display came on to indicate the target force level to the animal. The animal then reached for the object, and, upon contact, another LED display tracked the total forces exerted on the plates in real-time. Monkeys received a juice reward when the target force was maintained for 0.8–1 consecutive seconds. Monkeys performed at least 150 trials on each session. In this paper we report data from 10 sessions: 8 performed by monkey M and 2 performed by monkey P.

#### 5.1.3   Forces

Grasp force was monitored continuously using two dense sensor sheets mounted on the outer surface of the object. Each sensor sheet (Tekscan, Sensor 5076, Tekscan, Boston, MA) consists of 1936 'sensels' arranged in a square grid of size (83.8 mm$^2$). We recorded force values from each 'sensel' on the two sensor sheets at 300 Hz. We used total force, computed as a sum of all sensel values from both plates for continuous feedback to the monkey throughout the experiment. For offline analyses,

we first denoised each sensel value by first subtracting its baseline activity (no touch condition). We then summed all 'sensel' values to get total force. Finally, we low-pass filtered the total force with third order Butterworth filter with a cutoff of 10 Hz.

### 5.1.4 Electrophysiology and Neural Data Preprocessing

Neural data was collected with a CerePlex Direct data acquisition system coupled with CerePlex E digital headstage (Blackrock Microsystems). For each channel, we bandpass filtered neural signals from 250 Hz to 3 kHz and extracted threshold crossing events at a $-4.5$ RMS value. We then used offline spike sorting (Offline Sorter, Plexon, Dallas, TX) to remove non-spike threshold crossings and isolate individual units.

## 5.2 Human BCI Experiment

### 5.2.1 Participant

The study involved one participant who provided informed consent as part of a multi-site clinical trial (NCT01894802). The participant was a 57-year-old male at the time of the implant who had a C4-level ASIA D spinal cord injury (SCI) 35 years prior. He had no control over the intrinsic or extrinsic muscles of his right hand but could move his arm with some weakness in upper limb muscles.

### 5.2.2 Array Implantation

We surgically implanted four Neuroport microelectrode arrays (Blackrock Neurotech, Salt Lake City, UT, USA) in the left hemisphere of the participant. In somatosensory cortex (S1), two arrays, measuring 2.4 mm × 4 mm, each had sixty 1.5-mm electrode shanks wired in a checkerboard pattern, allowing for 32 electrodes to be stimulated (not used in this study). In motor cortex (M1), the other two arrays measured 4 mm × 4 mm and had one hundred 1.5-mm electrode shanks, with ninety six wired (active), and four inactive shanks located at the corners of all arrays. All electrodes were coated with sputtered iridium oxide. The participant had two percutaneous connectors placed on his skull, with each connected to one sensory and one motor array. We used functional neuroimaging of the participant attempting to make movements of the hand and arm, and imagining feeling sensations on their fingertips during surgery, to target array placement within the constraints of anatomical features such as blood vessels and cortical topography.

### 5.2.3 Neural Recordings

Only data from M1 arrays were analyzed in this study. Neural signals were recorded at 30 kHz using the NeuroPort system (Blackrock Neurotech, Salt Lake City, UT, USA). The data were high-pass filtered with a third order Butterworth filter above 350 Hz. Whenever the signal crossed a threshold ($-4.5$ RMS, set at the start of each recording session), a spiking event was recorded, and a snippet of the waveform was saved. Spikes were binned in 20-ms bins for offline analyses and decoding. Only channels with firing rate above 0.5 Hz were used (active channels).

### 5.2.4 Virtual Environment Task

We used a physics engine platform (MuJoCo, DeepMind Technologies, London, UK) to simulate a virtual environment with an avatar hand and a rigid cylindrical object. The participants observed a virtual room through a VR headset (Valve Index, Valve Corporation, Bellevue, WA). Each trial began with the hand in a neutral open position next to a gray-colored cylindrical object. A verbal command was given to the participants indicating a number from 1 to 4, which corresponded to a specific amount of force to be applied when grasping the object. The color of the object changed based on the given target force. Participants then attempted to grasp the object with the instructed amount of force as they observed the virtual hand closing around the object. They were required to maintain the grasp for 1 s, before releasing it upon another verbal command. Force targets were randomized.

### 5.2.5 Online Decoder Training and Control

The experiment was conducted in two stages: observation and full brain control. During the observation stage, the physics engine controlled the movement of the hand and the force exerted on the object. The participant was required to attempt the task as he watched it being performed. In the control stage, an online decoder, trained on data collected during the observation stage, was employed to direct the hand's movement and the force applied to the object. In each session, the participant performed 40–80 trials of observation, followed by 20–60 trials of using the decoder. The three types of decoders (linear, non-linear, or dynamic) used in this study were trained on the same observation data, and tested online in random order, keeping the subject blinded to the type of decoder he was using. The trial was considered successful if the subject could maintain grasp force within the target zone for 1 s. No visual, auditory, or tactile feedback was given to the subject. In this paper, we report data from 10 sessions.

## 5.3 Data Analysis

### 5.3.1 Alignment and PSTHs

Since trial duration varied, especially in the non-human primate dataset, we used multiple alignment events when averaging data for illustration purposes. For non-human primate data, we used three alignment events labeled as 'grasp', 'reward', and 'release'. 'Grasp' and 'release' were defined based on the total force profile as the first and last time point when total force exceeded 0.5 N, respectively. 'Reward' was the time point when the monkey received a juice reward for maintaining the force for the instructed amount of time. For human data, we aligned the neural responses to first and last contact of an avatar limb with the virtual object, labelled 'grasp' and 'release', respectively. For peristimulus time histogram (PSTH) plots, we found trials that belong to the same force target and took median-smoothed neural responses around the three alignment events.

### 5.3.2 Task and Force Modulation

We evaluated task modulation in each channel by computing a paired sample Wilcoxon signed rank test on the mean neural responses in two windows. For the non-human primate data, we compared a window of 1 s prior to object presentations, to a window of 2 s centered on the hand contact with an object. In human iBCI data we compared 2 s prior to cue presentation and 4 s after cue presentation. We assumed the channel was task modulated if p-value of the test was below 0.01. We also selected force-modulated channels using ANOVA test grouped by target force in a window of 2 s following first contact with an object. Channels with a p-value below 0.01 were deemed force-dependent.

### 5.3.3 Decoding Models

We used three models to decode continuous grasp force: linear regression (referred to as linear model), a feedforward artificial neural network (non-linear model), and a recurrent neural network (dynamic model). All decoders were restricted to be causal to accommodate the online regime, in which we only used neural data no later than 20 ms prior to the current time stamp, and spikes were smoothed with a 440-ms long exponential kernel.

Linear model assumes that a force signal can be represented as a weighted sum of neural inputs. The coefficients of the model were inferred using ordinary least squares estimation. The non-linear model was constructed as a feedforward neural network with one fully connected layer of 150 units. The dynamic model consisted of a layer of 150 LSTM nodes. Hyperparameters of both networks were optimized to achieve the best cross-validation fit.

We used a fivefold cross-validation procedure in which we split the observation data pseudo-randomly (keeping the number of trials in each condition balanced) into five testing sets. For each test set, we trained the model on the remaining 80% of the data. We used the coefficient of determination ($R^2$) to assess decoder performance in the test set.

# References

1. Ajiboye AB, Willett FR, Young DR, Memberg WD, Murphy BA, Miller JP, Walter BL, Sweet JA, Hoyen HA, Keith MW, Peckham PH, Simeral JD, Donoghue JP, Hochberg LR, Kirsch RF (2017) Restoration of reaching and grasping movements through brain-controlled muscle stimulation in a person with tetraplegia: a proof-of-concept demonstration. Lancet 389(10081):1821–1830. https://doi.org/10.1016/S0140-6736(17)30601-3

2. Blabe CH, Gilja V, Chestek CA, Shenoy KV, Anderson KD, Henderson JM (2015) Assessment of brain–machine interfaces from the perspective of people with paralysis. J Neural Eng 12(4): 043002. https://doi.org/10.1088/1741-2560/12/4/043002

3. Collinger JL, Wodlinger B, Downey JE, Wang W, Tyler-Kabara EC, Weber DJ, McMorland AJ, Velliste M, Boninger ML, Schwartz AB (2013) High-performance neuroprosthetic control by an individual with tetraplegia. Lancet 381(9866):557–564. https://doi.org/10.1016/S0140-6736(12)61816-9

4. Hochberg LR, Bacher D, Jarosiewicz B, Masse NY, Simeral JD, Vogel J, Haddadin S, Liu J, Cash SS, van der Smagt P, Donoghue JP (2012) Reach and grasp by people with tetraplegia using a neurally controlled robotic arm. Nature 485(7398):Article 7398. https://doi.org/10.1038/nature11076

5. Wodlinger B, Downey JE, Tyler-Kabara EC, Schwartz AB, Boninger ML, Collinger JL (2014) Ten-dimensional anthropomorphic arm control in a human brain−machine interface: difficulties, solutions, and limitations. J Neural Eng 12(1):016011. https://doi.org/10.1088/1741-2560/12/1/016011

6. Sobinov AR, Bensmaia SJ (2021) The neural mechanisms of manual dexterity. Nat Rev Neurosci 22(12):741–757. https://doi.org/10.1038/s41583-021-00528-7

7. Evarts EV (1968) Relation of pyramidal tract activity to force exerted during voluntary movement. J Neurophysiol 31(1):14–27. https://doi.org/10.1152/jn.1968.31.1.14

8. Gardner EP, Ro JY, Babu KS, Ghosh S (2007) Neurophysiology of prehension. II. Response diversity in primary somatosensory (S-I) and motor (M-I) cortices. J Neurophysiol 97(2): 1656–1670. https://doi.org/10.1152/jn.01031.2006

9. Georgopoulos AP, Ashe J, Smyrnis N, Taira M (1992) The motor cortex and the coding of force. Science 256(5064):1692–1695. https://doi.org/10.1126/science.256.5064.1692

10. Hendrix CM, Mason CR, Ebner TJ (2009) Signaling of grasp dimension and grasp force in dorsal premotor cortex and primary motor cortex neurons during reach to grasp in the monkey. J Neurophysiol 102(1):132–145. https://doi.org/10.1152/jn.00016.2009

11. Hepp-Reymond M-C, Kirkpatrick-Tanner M, Gabernet L, Qi H-X, Weber B (1999) Context-dependent force coding in motor and premotor cortical areas. Exp Brain Res 128(1):123–133. https://doi.org/10.1007/s002210050827

12. Intveld RW, Dann B, Michaels JA, Scherberger H (2018) Neural coding of intended and executed grasp force in macaque areas AIP, F5, and M1. Sci Rep 8(1):Article 1. https://doi.org/10.1038/s41598-018-35488-z

13. Kalaska JF, Cohen DA, Hyde ML, Prud'homme, M. (1989) A comparison of movement direction-related versus load direction-related activity in primate motor cortex, using a two-dimensional reaching task. J Neurosci Off J Soc Neurosci 9(6):2080–2102. https://doi.org/10.1523/JNEUROSCI.09-06-02080.1989

14. Maier MA, Bennett KM, Hepp-Reymond MC, Lemon RN (1993) Contribution of the monkey corticomotoneuronal system to the control of force in precision grip. J Neurophysiol 69(3): 772–785. https://doi.org/10.1152/jn.1993.69.3.772

15. Wannier TM, Maier MA, Hepp-Reymond MC (1991) Contrasting properties of monkey somatosensory and motor cortex neurons activated during the control of force in precision grip. J Neurophysiol 65(3):572–589. https://doi.org/10.1152/jn.1991.65.3.572

16. Branco MP, de Boer LM, Ramsey NF, Vansteensel MJ (2019) Encoding of kinetic and kinematic movement parameters in the sensorimotor cortex: a Brain-Computer Interface perspective. Eur J Neurosci 50(5):2755–2772. https://doi.org/10.1111/ejn.14342

17. Branco MP, Geukes SH, Aarnoutse EJ, Vansteensel MJ, Freudenburg ZV, Ramsey NF (2019) High-frequency band temporal dynamics in response to a grasp force task. J Neural Eng 16(5): 056009. https://doi.org/10.1088/1741-2552/ab3189

18. Downey JE, Weiss JM, Flesher SN, Thumser ZC, Marasco PD, Boninger ML, Gaunt RA, Collinger JL (2018) Implicit grasp force representation in human motor cortical recordings. Front Neurosci 12. https://www.frontiersin.org/articles/10.3389/fnins.2018.00801

19. Rastogi A, Willett FR, Abreu J, Crowder DC, Murphy BA, Memberg WD, Vargas-Irwin CE, Miller JP, Sweet J, Walter BL, Rezaii PG, Stavisky SD, Hochberg LR, Shenoy KV, Henderson JM, Kirsch RF, Ajiboye AB (2021) The neural representation of force across grasp types in motor cortex of humans with tetraplegia. ENeuro 8(1):ENEURO.0231-20.2020. https://doi.org/10.1523/ENEURO.0231-20.2020

20. Carmena JM, Lebedev MA, Crist RE, O'Doherty JE, Santucci DM, Dimitrov DF, Patil PG, Henriquez CS, Nicolelis MAL (2003) Learning to control a brain–machine interface for reaching and grasping by primates. PLoS Biol 1(2):e42. https://doi.org/10.1371/journal.pbio.0000042

21. Dekleva BM, Weiss JM, Boninger ML, Collinger JL (2021) Generalizable cursor click decoding using grasp-related neural transients. J Neural Eng 18(4):0460e9. https://doi.org/10.1088/1741-2552/ac16b2

22. Todorov E, Erez T, Tassa Y (2012) MuJoCo: A physics engine for model-based control. In: 2012 IEEE/RSJ International Conference on Intelligent Robots and Systems, pp 5026–5033. https://doi.org/10.1109/IROS.2012.6386109

23. Glaser JI, Benjamin AS, Chowdhury RH, Perich MG, Miller LE, Kording KP (2020) Machine learning for neural decoding. arXiv. https://doi.org/10.48550/arXiv.1708.00909

24. Pandarinath C, Bensmaia SJ (2022) The science and engineering behind sensitized brain-controlled bionic hands. Physiol Rev 102(2):551–604. https://doi.org/10.1152/physrev.00034.2020

25. Menz VK, Schaffelhofer S, Scherberger H (2015) Representation of continuous hand and arm movements in macaque areas M1, F5, and AIP: A comparative decoding study. J Neural Eng 12(5):056016. https://doi.org/10.1088/1741-2560/12/5/056016

26. Okorokova EV, Goodman JM, Hatsopoulos NG, Bensmaia SJ (2020) Decoding hand kinematics from population responses in sensorimotor cortex during grasping. J Neural Eng 17(4): 046035. https://doi.org/10.1088/1741-2552/ab95ea

# Real-Time Intraoperative Sensorimotor Cortex Localization and Consciousness Assessment with the Spatial and Spectral Profile of the Median Nerve Somatosensory Evoked Potentials

**Priscella Asman, Giuseppe Pellizzer, Sujit Prabhu, Sudhakar Tummala, Shreyas Bhavsar, Israt Tasnim, Matthew J. Hall, and Nuri F. Ince**

**Abstract** Mapping the sensorimotor cortex is a critical first step in various applications, including awake craniotomies and invasive brain-computer interface systems. Usually, during surgery, the sensorimotor area is defined using the conventional phase reversal of the somatosensory evoked potentials (SSEPs) originating from median nerve stimulation. The approach relies on the subjective interpretation of the phase reversal amplitude captured with a strip electrode. However, the localized nature of the SSEP around the hand area, location, size of the craniotomy, and changes in brain activity due to tumor invasion or lesion can cause misconstrued interpretation of the phase reversal. In this study, using a high-density grid, we recorded electrocorticogram (ECoG) from the sensorimotor cortex of patients in the anesthetized and awake states. We used the spatial distributions of SSEPs in the temporal and spectral domain and employed an unsupervised machine learning approach to delineate the central sulcus in real time. In Simulink/Matlab, we visualized instantaneous signal amplitude and power modulations in the gamma band over the 3D cortical surface rendered from individual patient MRIs. Furthermore, we showed that the temporal and spectral features of the SSEPs can serve as a

P. Asman · I. Tasnim · M. J. Hall · N. F. Ince (✉)
Clinical Neural Engineering Lab, Biomedical Engineering Department, University of Houston, Houston, TX, USA
e-mail: nfince@uh.edu

G. Pellizzer
Research Service, Minneapolis VA Health Care System, Departments of Neurology and Neuroscience, University of Minnesota, Minneapolis, MN, USA

S. Prabhu · S. Tummala
Department of Neurosurgery, University of Texas MD Anderson Cancer Center, Houston, TX, USA

S. Bhavsar
Department of Anesthesiology, University of Texas MD Anderson Cancer Center, Houston, TX, USA

valuable tool for assessing consciousness. Specifically, using the long latency gamma modulations in the SSEP trace and the cortical interpeak latency, we show that we can differentiate between the anesthetized and awake states. Our findings have various potential implications ranging from intraoperative surgical planning to assessing the consciousness status of patients with disorders of consciousness.

**Keywords** Somatosensory evoked potentials · Real-time cortical mapping · ECoG · Gamma activity · Cortical interpeak latency

## 1   Introduction

Cortical mapping during awake craniotomies for gliomas located within or adjacent to the Rolandic cortex provides the necessary guidance for minimizing the risk of transient or permanent neurologic compromise [1–3]. In addition, cortical mapping is essential for various brain-computer interface (BCI) applications, such as for sensorimotor rehabilitation or control of prosthetics [4–6].

Clinical practice for sensorimotor cortex mapping generally relies on the rapid subjective interpretation of median nerve-induced short-latency somatosensory evoked potentials (SSEPs), such as the conventional N20 (posterior) and P20 (anterior) components, to delineate the central sulcus (CS) [7, 8]. However, common factors such as the complexity of the exposed brain during surgery and the potential distortion of normal anatomy and function caused by the tumor or tumor-related edema can lead to misinterpreted results, requiring multiple electrode placements or relocation to confirm the CS delineation [9, 10]. When there is unsolvable doubt, direct cortical electrical stimulation is employed, which is time-consuming and can trigger seizures [11, 12]. Studies have shown that the SSEPs' spatial distributions in the temporal (N20/P20) and spectral (60–200 Hz) domains can define the primary sensorimotor areas [13–16]. Fusing the activation profiles of these features with the brain anatomy of individual subjects as a heat map might provide an unambiguous view of the CS in a short time and can be strategically used as a feedback signal intraoperatively to guide the surgery.

Intraoperative assessment of neural activity is also widely used to monitor the consciousness of patients by investigating the cortical background activity [1]. Earlier studies have shown the use of SSEPs peak amplitudes to assess the effects of anesthesia, but with contradicting results. While some studies have observed significant alterations in N20 amplitude between anesthetized and awake states [17, 18], other studies did not find any significant differences in N20 amplitude [19–21]. This study demonstrates that the temporal and spectral features of the SSEPs can serve as a valuable tool for assessing consciousness in the operating room (OR). We established an intraoperative visualization system that converts the SSEPs' spatial-temporal and spectral features into heat maps [22]. It also clusters the regional channels of the grid with unsupervised machine learning [14]. We further assessed the feasibility of using the induced temporal and spectral modulations to assess consciousness.

Intraoperatively, we provided a clear view of the CS by visualizing the spatial-temporal features of the SSEPs at N20 and spatial-spectral response in the gamma range up to 250 ms post median nerve stimulation as a heat map on a 2D grid. We projected these images on the OR screen for subjective interpretation by the neurosurgeon. We also grouped the anterior and posterior channels in an automated fashion using the entire SSEP trace rather than depending on individual time points. Consistently in all subjects, we observed late gamma power increase starting 50 ms after the stimulation onset in the awake/conscious state. In conjunction, we noted a difference in peak latency in the primary somatosensory area (S1) between states. Our findings could increase information for intraoperative surgical planning and assess the consciousness of patients from awake to comatose states.

## 2 Methods

### 2.1 Subject Recruitments

We recruited eight patients (four males and four females, ages 25–68 years) who were diagnosed with a brain tumor and scheduled for resection surgeries requiring an awake craniotomy. The protocol included high-density ECoG recording for real-time cortical mapping and CS delineation by assessing the median nerve SSEPs during the anesthetized and awake states. The Institutional Review Boards (IRB) of the University of Texas MD Anderson Cancer Center and the University of Houston reviewed and approved the study protocol. Each patient was made aware of the characteristic thumb twitching they would experience from the median nerve stimulation a day before their surgery. They consented to undergo the cortical mapping and participate in this study per the Declaration of Helsinki.

### 2.2 3D Cortical Rendering

We obtained pre-operative thin slice MRI scans of each patient based on a Fluid Attenuated Inversion Recovery (FLAIR) sequence (repetition time of 6.8 s, echo time of 101.6 ms, slice thickness of 1 mm with 262,144 pixels) to create a 3D cortical rendering of the brain surface in MATLAB (MathWorks, Natick, MA, USA) [23]. Incorporating a pipeline from our previous study [22, 24], we generated the segmented gray matter and white matter with Statistical Parametric Mapping (SPM12) [25]. After surface extraction from SPM, additional artifact removal and object conversion was done using Surf-Ice [26].

## 2.3 Anesthesia Administration and Surgical Procedure

The anesthetic management based on the asleep-awake-asleep technique [27] started with administering general anesthesia. The neurosurgeon opened the dura and marked the presumed location of the somatosensory and motor area based on the standard phase reversal technique with a 2×4 clinical subdural electrode grid (10 mm spacing), crossing the presumed location of the CS and hand knob. The 2×4 grid was then flipped and placed under the dura, serving as the reference and ground for the high-density grid (Fig. 1a). We stimulated the median nerve (Fig. 1b) to record the ECoG SSEPs with the high density grid and electromyogram (EMG) data (Fig. 1c) and conducted cortical mapping with the visualization system.
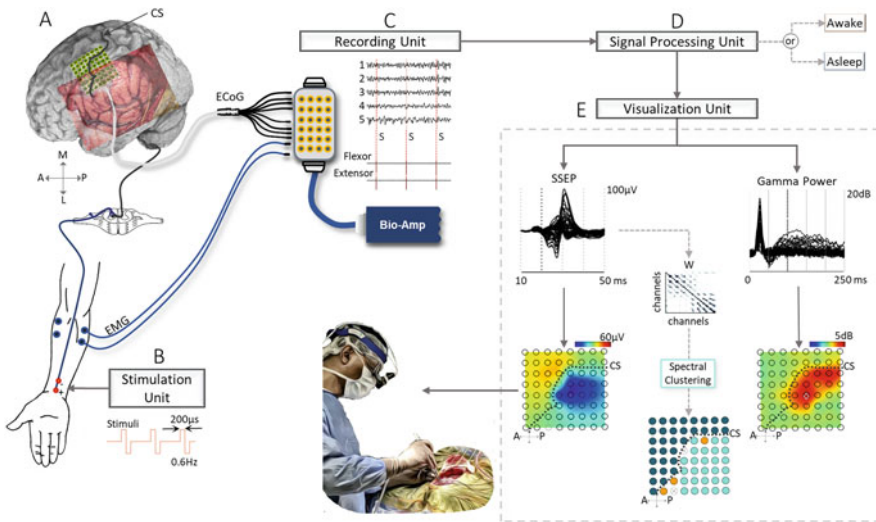


**Fig. 1** Pipeline of analysis. (**a**) The 3D cortical rendering from the preoperative MRI shows the location of the central sulcus (CS) (a gray line) with the overlapped image of the craniotomy and the high-density ECoG grid. (P) Posterior, (A) anterior, (M) medial, (L) lateral. (**b**) (Left) The electrical stimulus pathway from the periphery. (Right) The electrical stimulation at a low frequency applied to the median nerve. (**c**) (Left) Recording system setup used in the operating room. (Right) ECoG from selected channels and recorded EMG from flexor and extensor muscles, showing the stimulation onset as spike artifact (S). (**d**) Real time signal processing in MATLAB Simulink. The patient's consciousness is assessed with time frequency analysis. (**e**) Visualization by the neurosurgeon. (Left) The generated overlapping plot of the SSEP trace and the spatial temporal behavior as a heat map at 20 ms. The CS is represented with a gray dotted line. (Middle) The unsupervised clustering of the SSEP trace applied to the second smallest eigenvector of the normalized Laplacian derived from the adjacency matrix (W). The clustering results are visualized on the 2D grid by marking each contact with a color representing its membership (deep blue is anterior, light blue is posterior and orange is a misclassified channel). (Right) The generated overlapping plot of the temporal gamma power (60–250 Hz). The spatial spectral activity of the gamma power is shown as a heat map on the 2D grid at 100 ms

Each patient emerged from the general anesthesia by discontinuing all the anesthesia agents. After the patient was deemed ready to begin neurological testing by the anesthesiologist, we repeated the real-time mapping with the visualization system. Once we evaluated the SSEPs in the anesthetized and awake state and tumor resection was complete, the patient was then administered general anesthesia again until the completion of surgery.

## 2.4   Hardware Interface Module

For patients 1–3, we used a 32-64 channel high-density grid with 5 mm spacing and 2.3 mm contact exposure, Fig. 1a. For patients 4–8, we used a 25-53 channel hybrid grid (Cortec-Hybrid grid) with 10 mm spacing and 1–2.7 mm contact exposure. Two disposable conductive solid-gel electrodes were attached to the contralateral median nerve at the wrist in the OR (Fig. 1b). Using the clinical 2 or 4-channel EMG/EP Measuring System (Neuropack S1 MEB-9400), we stimulated with a frequency of 0.6 Hz, a square wave electric pulse of 200 μs, and a current intensity adjusted between 5 and 15 mA. The stimulation caused small twitches of their thumb abductor pollicis brevis, as stated in the standard protocol (American Clinical Neurophysiology Society (ACNS), 2015). We recorded the neural data from the ECoG grids and bipolar surface EMG from the forearm with a multichannel bio amplifier (gHIamp: 256 channels, g.tec medical engineering GmbH, Graz Austria) at a sampling frequency of 2.4 KHz with a 24 bit A/D resolution. We used recorded bipolar EMG to capture the stimulation onset as spikes (S) (Fig. 1c). We also re-referenced the ECoG data with common averaging (Fig. 2a, left). All the acquired data was synchronized, processed, and visualized in real-time intraoperatively using Simulink/Matlab, Fig. 1d, and gHIsys block sets (g.tec medical engineering GmbH, Graz Austria).

## 2.5   Online Spatial-Temporal and Spectral Analysis of SSEPs

### 2.5.1   Real-Time Preprocessing

The raw neural data was streamed through the universal serial bus (USB) into the Simulink/MATLAB environment (MathWorks 2022b, Inc. USA) and recorded. Simulink is a graphical programming environment comprising a rich set of signal processing and visualization libraries for modeling, simulating, and analyzing dynamic systems. We removed the power line noise at 60 Hz with a second-order infinite impulse response (IIR) notch filter (Fig. 2a). The ECoG data was then observed online with 'g.Scope' (gHIamp driver block of gHIsys library, gTec, Graz, Austria) to assess the data clarity and exclude corrupted channels (channels

with high variances and distortions) during the spatial visualization (Figs. 1d and 2a, left).

### 2.5.2 Spatial-Temporal and Spatial-Spectral Heat Map

The real-time mapping of the sensorimotor area with the spatial features of SSEP is described in detail by Asman et al. [14].

Using the gHIsys library and digital signal processing (DSP) toolboxes in MATLAB/Simulink, we computed the overlapping plot of the average SSEP trace and gamma power trace in Fig. 1e (top-left and top-right). We high-pass filtered the incoming data at a cut-off frequency of 30 Hz using a second-order Butterworth filter. We further band-pass filtered the ECoG between 60 and 250 Hz and computed the gamma power as another data stream. We used a "Trigger" block that receives the incoming ECoG data and trigger onset (S) from the EMG channel to create an epoch of the data up to 500 ms, with 150 ms as the baseline. Then the epoch was transmitted to an "Averaging" block to calculate the average SSEPs or gamma power, thus creating the SSEPs or gamma power waveform (g.tec Simulink Highspeed Library user manual v3.16.01) (Fig. 2a, middle). We investigated the SSEPs up to 50 ms and the gamma power up to 250 ms following the stim onset. A MATLAB Level-II S function was programmed to pick up the SSEPs/Gamma power from the online averaging block. Using the S-function, at a particular time point along the SSEP/Gamma power trace, we projected the waveform's instantaneous amplitude onto a 2D grid as a heat map (Fig. 1e, middle). We also simultaneously animated the heat map on the cortical surface rendered from each patient's preoperative MRI using the 'Interpolation Scope' available through g.tec Suite 2020 (g.tec Suite 2020, g.tec, Graz, Austria). The block allowed a rapid electrode co-registration based on the neurosurgeon's confirmed CS delineation by the heatmap in the OR (Fig. 2a, right).

### 2.5.3 Unsupervised Identification of Central Sulcus

We further employed spectral clustering, an unsupervised machine-learning technique, to group the channels of the ECoG grid, which are anterior and posterior to the CS [22]. First, we applied a Savitzky-Golay filter with a polynomial degree of 3 to smooth the SSEP trace without distorting it and estimated its derivative [28]. We then smoothed the derivative trace and normalized it to retain the waveform morphology. We applied a Gaussian similarity function (1) to create the adjacency

and posterior (blue) channels (right). (**c**) Confusion matrix for all eight patients showing the clustering accuracy. *A* anterior, *P* posterior. (**d**) Gamma power after common averaging showing the suppression after 0.6 ms in the anesthetized state and enhancement in the awake state. The heat map of the average power from 1 to 1.5 ms is projected on the 3D surface. Results shown here for P10

matrix, $W_{ij}$ (Fig. 1e, middle), whose entries represented the connectivity network between the different ECoG channels. We then derived the Laplacian matrix (L) (2) from the adjacency matrix based on the random walk method. We applied k-means to the second smallest eigenvector of the normalized Laplacian matrix to group anterior and posterior channels (Fig. 1e, bottom).

$$W_{ij} = e^{-\left(\left|x_i - x_j\right|^2\right)/2\sigma^2} \tag{1}$$

$$L = I - \left(\sum\nolimits_j W_{ij}\right)^{-1} W_{ij} \tag{2}$$

## 2.6 Offline Spectral and Temporal Analysis of SSEPs

We visually examined the ECoG recordings to remove corrupted channels and artifacts. We removed the power line noise and high-pass filtered the recording at a cut-off frequency of 30 Hz using a second-order Butterworth filter.

### 2.6.1 Electrode Coregistration

Two neurosurgeons, blinded to electrophysiology, defined the CS and sensorimotor borders on the 3D-rendered cortical surface. We used all the electrode channels anterior and posterior to the CS as the ground truth for accessing the clustering accuracy. We co-registered the electrodes on the rendered surface. We used the image of the craniotomy with electrode placements taken in the OR as a reference (Fig. 1a). The electrodes within the primary somatosensory (S1) and motor area (M1) borders were labeled accordingly and selected for further analysis.

### 2.6.2 Time-Frequency Maps and Spectral and Temporal Power

We extracted data segments around the median nerve stimulation onset ($-150$ ms to 250 ms) and applied time-frequency (TF) analysis at each channel using Stockwell transform. We averaged the spectrogram across trials and then normalized it using the same baseline power $-150$ ms before the stimulation onset to obtain the smooth spectrograms. We then transformed the averaged spectrograms into a decibel (dB) scale to yield the centered spectrograms. The TF maps were visible for frequencies up to 900 Hz. We averaged the time-frequency maps across S1 and M1 channels separately in the anesthetized and awake states to assess the average spectral modulations in each cortical region and state.

   To assess the temporal power modulations in the gamma range (60–250 Hz) for each patient in each state, we filtered the epochs using a second-order Butterworth

IIR zero-phase filter (forward and backward). We then squared the filtered signals to compute the temporal power trace and normalized it against the baseline preceding the stimulation onset.

## 2.7   Interpeak Latencies

To estimate the SSEP temporal profile in each state, we aligned the ECoG traces concerning the stimulation pulse onset (S) and then averaged them across trials in individual channels. We computed the average SSEP trace for each patient for the M1 and S1 separately. The averaged SSEP trace revealed the posterior negative deflection (N20) and anterior positive peak (P22), defined between +17 and +25 ms, followed by a posterior large positive deflection (P30) and anterior negative bend (N35) between +27 and +40 ms. We extracted the peak latencies from these averaged SSEP waveforms and estimated the peak latencies at the posterior N20-P30 and anterior P25-N35. We defined the interpeak latencies (IPL) as the latency difference between peaks at 20 ms (N20, P20) and 30 ms (P30, N35) after stimulation onset.

## 2.8   Statistical Analysis

We used the area under the curve (AUC) of the receiver operating characteristic (ROC) curve to determine the accuracy in distinguishing the anterior and posterior channels based on the peak amplitude at N20 and gamma power from 50 to 250 ms. We evaluated the spectral clustering performance from the confusion matrix based on the ground truth. We applied paired t-tests to compare the gamma oscillations and interpeak latencies between the anesthetized and awake states.

## 3   Results

### 3.1   Real-Time Delineation of the Central Sulcus

In each patient, we recorded SSEPs in the anesthetized state and then in the awake state. We delivered about $100 \pm 20$ trials of electrical stimulation to the median nerve. Using the real-time visualization system in Simulink, we generated the 2D heat map and projected it onto the OR screen during the surgery. We could also generate the heatmaps on the 3D rendering of each patient in real-time. We designed a MATLAB graphic user interface (GUI) to control the Simulink model for variables like running and stopping the model, excluding corrupted channels, adjusting the heat map amplitude, and the time point where the most negative peak is noted (N20).

The GUI also allowed us to choose which feature of the SSEP to view as a heat map and whether to enable spectral clustering.

### 3.1.1 Spatial-Temporal Feature

As we recorded the neural data, we generated the SSEP waveform in the OR. We computed the heat map of the spatial profile at the 20 ms timepoint along the SSEP trace for each channel on the 2D grid, Fig. 2b. A color map was then applied to visualize the amplitude, and interpolated values allowed continuous color throughout the grid map. The red patches showed the P20, and the blue patches showed the N20. The neurosurgeon confirmed which channels were in the anterior and posterior regions by comparing them to the anterior and posterior channels estimated by the standard phase reversal technique with the 2×4 grid. We created a montage with the verified grid placement using gtec's iEEG Montage Creator [g.tec medical engineering GmbH, Graz Austria] and the cortical surface. We observed the heatmap on the 3D cortical surface, as shown in Fig. 2b (bottom). The color contrast revealed the delineated CS, correlating with the sulcus in the 3D rendering. Using the amplitude of the heatmap at the N20, we noted a consistently high separation accuracy of $93.6 \pm 14.9\%$ in the anesthetized and $89.9 \pm 14.4\%$ in awake states across all patients, estimated offline.

### 3.1.2 Spectral Clustering

Using a cluster assignment of 2 [22], we applied spectral clustering for an unsupervised delineation of the CS (Fig. 2b, right). The k-means clustering applied to the second smallest eigenvector provided a color-coded classification. We assigned the anterior and posterior channels with two contrasting colors on the 2D electrode grid on the OR screen. We assessed the clustering accuracy in the anesthetized state and observed an average overall accuracy of $89.96 \pm 17\%$, estimated offline (Fig. 2c).

### 3.1.3 Spatial-Spectral Feature

We generated the gamma power waveform (60–250 Hz) in real-time. Using the S-function, we projected the spatial-spectral profile of the SSEPs on the 2D grid and 3D rendering on the OR screen (Fig. 2d). The yellow to deep orange-red regions represented the primary somatosensory area (S1). Within the time points between +10 to +50 ms, we could define S1 in both the anesthetized and awake states. We observed a delineation accuracy of $91 \pm 10.3\%$ in the anesthetized and $91 \pm 13.4\%$ in the awake state estimated offline. Within the +60 to +200 ms time points, we observed enhanced late gamma activity in S1 after the subjects were awake, which was previously suppressed in the anesthetized state (Fig. 2d). The spatial-spectral

map revealed late gamma activity (red patches) for all patients in the awake state, mainly predominant on channels near the CS and S1. In contrast, we saw late gamma suppression (blue patches) in the anesthetized state in S1.

## 3.2 State-Specific Characteristics of Induced Spectral Modulations

We assessed the stimulus-aligned, baseline-normalized group average time-frequency maps for S1 and M1 channels in the awake and anesthetized states (Fig. 3a, top). Figure 3a (bottom) shows the temporal profile power change in the gamma (60–250 Hz) band concerning baseline. We noted that the late gamma modulation was temporarily isolated, occurring from +50 ms to +250 ms in M1 and S1, and was the most prominent in S1 in the awake state than in other cases. Interestingly, we observed suppressed late gamma activity in the anesthetized state in both M1 (independent t-test $t (7) = -4.1194$, $p < 0.01$) and S1 (independent t-test $t (7) = -3.2519$, $p = 0.0140$). While in the awake state, the late gamma power increased significantly relative to baseline both in M1 (independent t-test $t (7) = 4.6057$, $p < 0.01$) and S1 (independent t-test $t (7) = 6.0072$, $p < 0.01$; Fig. 3a). Furthermore, the difference in late gamma power between the anesthetized and the awake state was highly significant for M1 (paired t-test $t (7) = -5.8103$, $p < 0.01$) and for S1 (paired t-test $t (7) = -5.8868$, $p < 0.01$) and consistent across all subjects.

## 3.3 State-Specific Characteristics of Induced Temporal Features

We averaged the anterior (A) and posterior (P) channels in the anesthetized and awake states and marked the anterior P22-N25 and the posterior N20-P30 peaks on the average waveform (Fig. 3b). Across all subjects, we noticed a consistent decrease in latency from anesthetized to awake state for N20 (group latency difference; 1.51 ms $\pm$ 0.74 ms, independent t-test (7) $p < 0.01$, $t = 5.8000$) and P30 (group latency difference; 3.33 ms $\pm$ 1.11 ms, independent t-test (7) $p < 0.01$, $t = 8.4664$). The assessment of the interpeak latencies (IPL) between posterior N20 and P30 showed a significant decrease from the anesthetized to the awake state (IPL N20-P30: An: 8.54 ms $\pm$ 0.54 ms, Aw: 6.72 ms $\pm$ 1.14 ms, paired t-test $p < 0.01$, $t = 4.9427$) (Fig. 3b, bottom). This decrease in the awake state was consistent in all patients. However, we observed no difference in latency between states for anterior P22 and N35. The IPL between P22 and N35 also showed no difference between states (IPL P22-N35: An: 9.17 ms $\pm$ 2.47 ms, Aw: 9.42 ms $\pm$ 3.96 ms, paired t-test $p = 0.7942$, $t = -0.2710$).
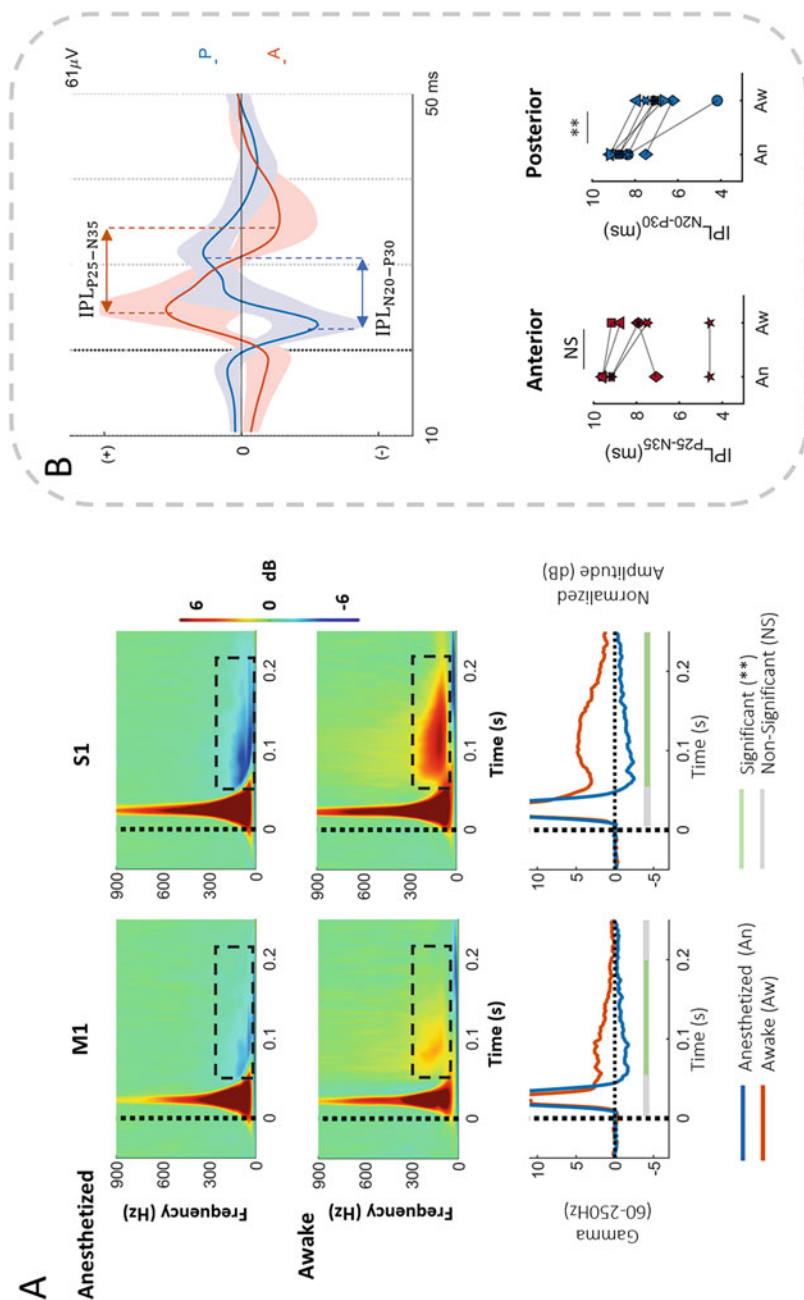
**Fig. 3** Offline state analysis. (**a**) Spectral assessment of somatosensory evoked potential: (Top) The average time-frequency map matrix across all patients showing the spectral modulation in the anesthetized and awake states in the primary somatosensory (S1) and motor (M1) regions. The dashed rectangle shows the late gamma modulation. (Bottom) Group Gamma power modulation is shown for S1 and M1 compared between the awake and anesthetized states. (**b**) (Top) The average SSEP waveform shown for P1 shown for the anterior (A) (red) and posterior (P) (blue) regions, where the interpeak latencies are derived. The

## 4    Discussion

This study aims to (i) delineate the CS with the spatial heat maps assessed from the temporal and spectral profile of the SSEPs with ECoG grids in real-time, (ii) cluster the anterior and posterior channels without manual supervision, and (iii) assess the level of consciousness.

### 4.1    Clinical Approach to CS Delineation

The electrical activity originating from the peripheral nerve stimulation measured with ECoG grids placed over the sensorimotor cortex reflects the cerebral impulse response's bombardments that generate the complex SSEP waveform [9, 10, 13, 29]. The routine clinical assessment of SSEPs relies on phase reversal to locate the somatosensory and motor area on the cortical surface using electrode strips. However, the conventional N20/P20 can be ambiguous due to the strip electrode misplacement or poor spatial resolution, usually requiring multiple relocations with DCS to achieve delineation success [1, 3, 7, 10, 30–34]. Neurosurgeons also use intraoperative MRI (iMRI) to define the sensorimotor area in the OR. While intraoperative navigation presents real-time intuitive tumor detection, it is time-consuming and inevitably affected by brain drift [35]. iMRI may be good at detecting tumor boundaries and avoiding brain shifts. However, it substantially lengthens operation time.

### 4.2    CS Delineation with SSEPs Spatial Features

With a single placement of the ECoG grid, we identified the spatial orientation of the sensorimotor area with the spatial heat map in real-time on the 2D grid and 3D cortical surface and delineated the CS (Fig. 2b). The SSEPs' spatial-temporal profile at N20 was first implemented in 1989 by Allison et al. and adopted by several investigators over time [13, 15, 16, 36]. We, to our knowledge, are the first to apply this approach in real-time in the OR (Fig. 2a). We also observed a clear primary somatosensory area definition with the evoked gamma activity up to 50 ms post-stimulation in each state. Studies have shown that early gamma oscillations can achieve accurate CS delineation [15, 37–39]. We also saw late-gamma activity suppressed in the anesthetized state and enhanced in the awake state after 60 ms in real time. Ray et al. found that significant gamma responses (60–150 Hz) occurring

shaded region represents the variance. (Bottom) The scatter plot showing the change in M1 IPL P22-N35IPL and S1 -N20-P30 between states . A ** represents a paired t-test, **p < 0.01, *NS* non-significant, *An* anesthetized, *Aw* awake

in the somatosensory area at longer latencies (300–800 ms) were enhanced when the respective tactile stimuli were attended [40]. We also observed focal enhanced gamma activity in the primary somatosensory area (Fig. 2d).

## 4.3   Unsupervised Regional Clustering

We applied spectral clustering to the derivative trace of the SSEPs to separate the anterior and posterior channels in a short time (Fig. 2b, right). Spectral clustering uses subspace decomposition on high dimensionality to achieve data clustering [41]. Some studies adopted spectral clustering to characterize the connectivity between cortical areas based on fluctuations in high gamma power [42]. Others clustered channels at different seizure stages and determined epileptic focus by extracting features in different brain regions based on their functional dependencies. [43, 44]. Based on the morphology of SSEPs, we observed a high anterior and posterior clustering accuracy in each state in less than 10 stimulations (Fig. 2c). The large ECoG grid enabled a better estimation of the connectivity matrix (and the Laplacian) that depended on the waveform morphology of different cortical areas. Our previous study also assessed the influence of the electrode size on clustering accuracy by resampling the channels of the large grid to form $1 \times N$ or $2 \times N$ electrodes and observed a systematic increase in accuracy from $1 \times N$ to $2 \times N$ to a larger grid (see [14] for more details).

## 4.4   State Characteristics of the Spectral Features of SSEPs

We found two temporally distinct gamma components in response to median nerve stimulation (Fig. 3a) in M1 and S1. The early component (15–50 ms) occurred in both the anesthetized and awake states. The late component was more temporally widespread (50–250 ms), suppressed in the anesthetized state, and enhanced in the awake state (Fig. 3a). Studies have reported that a consciously perceived external stimulus results in neural responses comprising an early event-related component accompanied by a late sustained one [45–47]. MEG studies have also shown that the prolonged event-related high gamma (60–90 Hz) power increase in the somatosensory cortex, from 100 ms to 500 ms, was due to tactile attention [48]. In this study, we asked each patient to pay attention to their thumb twitching in the awake state. We believe that the increase in late gamma activity was associated with the conscious processing of the somatosensory sensations induced by median nerve stimulation. We observed a significant late gamma power suppression in the anesthetized state both in S1 and M1 (Fig. 3a). Studies have shown that anesthetics block or depress the cortical somatosensory responses. This suppression occurs by enhancing the inhibitory effect of gamma-aminobutyric acid (GABA) and blocking the excitatory effect of glutamate [49–51]. We also believe that the significant late gamma

suppression was due to the impact of the anesthetic on the complex inhibitory mechanisms. These mechanisms were mediated by the GABA-modulated connectivity within the sensorimotor cortex, blocking the excitatory effects of glutamatergic synapses.

## 4.5 Interpeak Latency

The interpeak latencies between N20 and P30 and between P22 and N35 represent transit times of action potentials from areas 3b to the cortical Broadman area 1 [52, 53]. We overserved a significant change in IPL N20-P30 from the anesthetized to the awake state, consistent in all our patients (Fig. 3b). Numerous studies have found that longer latency SSEPs waves, which represent further neural processing of somatosensory inputs, are highly sensitive to anesthetic drugs [54–56]. We saw that the difference in posterior IPL was due to a significant change in P30 latency. We believe that the apparent change in P30 latency conforms with the previous studies, and the IPL may provide a good evaluation of wakefulness.

## 5 Conclusion

The spatial distribution of the SSEP's temporal and spectral features are readily detectable in real-time, which can be used in the OR to define the contours of the CS and the sensorimotor area in a short time. This high-dimensional data can be efficiently processed and visualized with modern, portable computers to assist clinical decision-making and surgical planning. The late gamma difference in the sensorimotor area and the interpeak latency difference in S1 between the anesthetized and awake states can monitor the state of consciousness in patients undergoing awake craniotomy and can help with the assessment of consciousness for subjects who have a disorder of consciousness.

## References

1. Jahangiri FR, Pautler K, Watters K, Anjum SS, Bennett GL (2020) Mapping of the somatosensory cortex. Cureus 12(3)
2. Pondal-Sordo M, Diosy D, Téllez-Zenteno JF, Girvin JP, Wiebe S (2006) Epilepsy surgery involving the sensory-motor cortex. Brain 129(12):3307–3314
3. Sheth SA, Eckhardt CA, Walcott BP, Eskandar EN, Simon MV (2013) Factors affecting successful localization of the central sulcus using the somatosensory evoked potential phase reversal technique. Neurosurgery 72(5):828–834
4. Borton D, Micera S, Millán JDR, Courtine G (2013) Personalized neuroprosthetics. Sci Transl Med 5(210):210rv2

5. Gilja V, Pandarinath C, Blabe CH, Nuyujukian P, Simeral JD, Sarma AA, Sorice BL, Perge JA, Jarosiewicz B, Hochberg LR, Shenoy KV (2015) Clinical translation of a high-performance neural prosthesis. Nat Med 21(10):1142–1145

6. Schwartz AB, Cui XT, Weber DJ, Moran DW (2006) Brain-controlled interfaces: movement restoration with neural prosthetics. Neuron 52(1):205–220

7. Celix JM, Silbergeld DL (2016) Intraoperative cortical mapping techniques and limitations. In: Functional mapping of the cerebral cortex. Springer, Cham, pp 63–76

8. Lim SH, Park SB, Moon DY, Kim JS, Choi YD, Park SK (2019) Principles of intraoperative neurophysiological monitoring with insertion and removal of electrodes. Korean J Clin Lab Sci 51(4):453–461

9. Iwasaki M, Nair D, Lüders HO (2003) Cortical somatosensory evoked potential mapping. Handb Clin Neurophysiol 3:287–295

10. Wood CC, Spencer DD, Allison T, McCarthy G, Williamson PD, Goff WR (1988) Localization of human sensorimotor cortex during surgery by cortical surface recording of somatosensory evoked potentials. J Neurosurg 68(1):99–111

11. Desmurget M, Sirigu A (2015) Revealing humans' sensorimotor functions with electrical cortical stimulation. Phil Trans R Soc B Biol Sci 370(1677):20140207

12. Weiss Lucas C, Nettekoven C, Neuschmelting V, Oros-Peusquens AM, Stoffels G, Viswanathan S, Rehme AK, Faymonville AM, Shah NJ, Langen KJ, Goldbrunner R (2020) Invasive versus non-invasive mapping of the motor cortex. Hum Brain Mapp 41(14): 3970–3983

13. Allison TRUETT, McCarthy GREGORY, Wood CC, Darcey TM, Spencer DD, Williamson PD (1989) Human cortical potentials evoked by stimulation of the median nerve. II. Cytoarchitectonic areas generating short-latency activity. J Neurophysiol 62(3):694–710

14. Asman P, Pellizzer G, Tummala S, Tasnim I, Bastos D, Bhavsar S, Prabhu S, Ince NF (2023) Long-latency gamma modulation after median nerve stimulation delineates the central sulcus and contrasts the states of consciousness. Clin Neurophysiol 145:1–10

15. Fukuda M, Nishida M, Juhasz C, Muzik O, Sood S, Chugani HT, Asano E (2008) Short-latency median-nerve somatosensory-evoked potentials and induced gamma-oscillations in humans. Brain 131(7):1793–1805

16. Maegaki Y, Najm I, Terada K, Morris HH, Bingaman WE, Kohaya N, Takenobu A, Kadonaga Y, Lüders HO (2000) Somatosensory evoked high-frequency oscillations recorded directly from the human cerebral cortex. Clin Neurophysiol 111(11):1916–1926

17. Banoub M, Tetzlaff JE, Schubert A (2003) Pharmacologic and physiologic influences affecting sensory evoked potentials: implications for perioperative monitoring. J Am Soc Anesthesiol 99(3):716–737

18. Burnos S, Fedele T, Schmid O, Krayenbühl N, Sarnthein J (2016) Detectability of the somatosensory evoked high frequency oscillation (HFO) co-recorded by scalp EEG and ECoG under propofol. NeuroImage Clin 10:318–325

19. Bala E, Sessler DI, Nair DR, McLain R, Dalton JE, Farag E (2008) Motor and somatosensory evoked potentials are well maintained in patients given dexmedetomidine during spine surgery. J Am Soc Anesthesiol 109(3):417–425

20. Hasan MS, Tan JK, Chan CYW, Kwan MK, Karim FSA, Goh KJ (2018) Comparison between effect of desflurane/remifentanil and propofol/remifentanil anesthesia on somatosensory evoked potential monitoring during scoliosis surgery—A randomized controlled trial. J Orthop Surg 26(3):2309499018789529

21. Tobias JD, Goble TJ, Bates G, Anderson JT, Hoernschemeyer DG (2008) Effects of dexmedetomidine on intraoperative motor and somatosensory evoked potential monitoring during spinal surgery in adolescents. Pediatr Anesth 18(11):1082–1088

22. Asman P, Prabhu S, Bastos D, Tummala S, Bhavsar S, McHugh TM, Ince NF (2021) Unsupervised machine learning can delineate central sulcus by using the spatiotemporal characteristic of somatosensory evoked potentials. J Neural Eng 18(4):046038

23. Ashikaga R, Araki Y, Ishida O (1997) MRI of head injury using FLAIR. Neuroradiology 39(4): 239–242. https://doi.org/10.1007/s002340050401

24. Jiang T, Liu S, Pellizzer G, Aydoseli A, Karamursel S, Sabanci PA, Sencer A, Gurses C, Ince NF (2018) Characterization of hand clenching in human sensorimotor cortex using high-, and ultra-high frequency band modulations of electrocorticogram. Front Neurosci 12:110

25. Ashburner J, Barnes G, Chen CC, Daunizeau J, Flandin G, Friston K, Kiebel S, Kilner J, Litvak V, Moran R, Penny W (2014) SPM12 manual, vol 2464. Wellcome Trust Centre for Neuroimaging, London, p 4

26. Rorden C et al (2021) Surf ice: main page. In: NITRC, Neuroimaging Informatics Tools and Resources Clearinghouse v2. pp 1–57

27. Huncke K, Van de Wiele B, Fried I, Rubinstein EH (1998) The asleep-awake-asleep anesthetic technique for intraoperative language mapping. Neurosurgery 42(6):1312–1316

28. Savitzky A, Golay MJ (1964) Smoothing and differentiation of data by simplified least squares procedures. Anal Chem 36(8):1627–1639

29. Markand ON (2020) Somatosensory evoked potentials. In: Clinical evoked potentials. Springer, Cham, pp 139–207

30. Cedzich C, Taniguchi M, Schäfer S, Schramm J (1996) Somatosensory evoked potential phase reversal and direct motor cortex stimulation during surgery in and around the central region. Neurosurgery 38(5):962–970

31. Grant GA, Farrell D, Silbergeld DL (2002) Continuous somatosensory evoked potential monitoring during brain tumor resection: report of four cases and review of the literature. J Neurosurg 97(3):709–713

32. MacDonald DB (2020) Monitoring somatosensory evoked potentials. Neurophysiol Neurosurg:35–51

33. Selner AN, Stone JL (2016) Somatosensory-and motor-evoked potentials in surgery of eloquent cortex under general anesthesia: advantages and limitations. In: Functional mapping of the cerebral cortex. Springer, Cham, pp 115–139

34. Towle VL, Dai Z, Zheng W, Issa NP (2016) Mapping cortical function with event-related electrocorticography. In: Functional mapping of the cerebral cortex. Springer, Cham, pp 91–104

35. You H, Qiao H (2021) Intraoperative neuromonitoring during resection of gliomas involving eloquent areas. Front Neurol 12:952

36. Romstöck J, Fahlbusch R, Ganslandt O, Nimsky C, Strauss C (2002) Localisation of the sensorimotor cortex during surgery for brain tumours: feasibility and waveform patterns of somatosensory evoked potentials. J Neurol Neurosurg Psychiatry 72(2):221–229

37. Fukuda M, Juhász C, Hoechstetter K, Sood S, Asano E (2010) Somatosensory-related gamma-, beta-and alpha-augmentation precedes alpha-and beta-attenuation in humans. Clin Neurophysiol 121(3):366–375

38. Kisley MA, Cornwell ZM (2006) Gamma and beta neural activity evoked during a sensory gating paradigm: effects of auditory, somatosensory and cross-modal stimulation. Clin Neurophysiol 117(11):2549–2563

39. Schubert R, Blankenburg F, Lemm S, Villringer A, Curio G (2006) Now you feel it—now you don't: ERP correlates of somatosensory awareness. Psychophysiology 43(1):31–40

40. Ray S, Niebur E, Hsiao SS, Sinai A, Crone NE (2008) High-frequency gamma activity (80–150 Hz) is increased in human cortex during selective attention. Clin Neurophysiol 119(1):116–133

41. Von Luxburg U (2007) A tutorial on spectral clustering. Stat Comput 17(4):395–416

42. Ko AL, Weaver KE, Hakimian S, Ojemann JG (2013) Identifying functional networks using endogenous connectivity in gamma band electrocorticography. Brain Connect 3(5):491–502

43. Hegde A, Erdogmus D, Principe JC (2006) Spatio-temporal clustering of epileptic ECOG. In: 2005 IEEE Engineering in Medicine and Biology 27th Annual Conference. IEEE, pp 4199–4202

44. Hegde A, Erdogmus D, Shiau DS, Principe JC, Sackellares CJ (2007) Clustering approach to quantify long-term spatio-temporal interactions in epileptic intracranial electroencephalography. Comput Intell Neurosci 2007
45. Avanzini P, Abdollahi RO, Sartori I, Caruana F, Pelliccia V, Casaceli G, Mai R, Lo Russo G, Rizzolatti G, Orban GA (2016) Four-dimensional maps of the human somatosensory system. Proc Natl Acad Sci 113(13):E1936–E1943
46. Fisch L, Privman E, Ramot M, Harel M, Nir Y, Kipervasser S, Andelman F, Neufeld MY, Kramer U, Fried I, Malach R (2009) Neural "ignition": enhanced activation linked to perceptual awareness in human ventral stream visual cortex. Neuron 64(4):562–574
47. Sergent C, Baillet S, Dehaene S (2005) Timing of the brain events underlying access to consciousness during the attentional blink. Nat Neurosci 8(10):1391–1400
48. Bauer M, Oostenveld R, Peeters M, Fries P (2006) Tactile spatial attention enhances gamma-band activity in somatosensory cortex and reduces low-frequency activity in parieto-occipital areas. J Neurosci 26(2):490–501
49. Sloan TB, Heyer EJ (2002) Anesthesia for intraoperative neurophysiologic monitoring of the spinal cord. J Clin Neurophysiol 19(5):430–443
50. Sloan TB (2002) Anesthetics and the brain. Anesthesiol Clin North Am 20(2):265–292
51. Wang HY, Eguchi K, Yamashita T, Takahashi T (2020) Frequency-dependent block of excitatory neurotransmission by isoflurane via dual presynaptic mechanisms. J Neurosci 40(21):4103–4115
52. Muengtaweepongsa S (2019) General principles of somatosensory evoked potentials
53. Muzyka IM, Estephan B (2019) Somatosensory evoked potentials. Handb Clin Neurol 160: 523–540
54. Koht A, Schütz W, Schmidt G, Schramm J, Watanabe E (1988) Effects of etomidate, midazolam, and thiopental on median nerve somatosensory evoked potentials and the additive effects of fentanyl and nitrous oxide. Anesth Analg 67(5):435–441
55. Porkkala T, Kaukinen S, Häkkinen V, Jäntti V (1997) Median nerve somatosensory evoked potentials during isoflurane anaesthesia. Can J Anaesth 44(9):963–968
56. Sloan TB (1998) Anesthetic effects on electrophysiologic recordings. J Clin Neurophysiol 15(3):217–226

# A Summary of the 2022 BCI Award with Discussion of BCI Trends

**Christoph Guger, Sanaz Rezvani, Nuri Firat Ince, Milena Korostenskaja, and Brendan Z. Allison**

**Abstract** The first chapter of this book readers introduced BCIs, the BCI Award Foundation and 2022 jury, the procedures and criteria of the awards, and the 12 nominees in 2022. Most chapters described projects that were nominated for a BCI Research Award. This is the last chapter of the book. Here, we provide more information about the awards ceremony and the winners. We then present some trends reflected in the awards involving BCI input devices and applications. This chapter ends with discussion and future directions. While we expected three winners, we had a tie for second place in 2022 and thus had four winners this year.

**Keywords** Brain-computer interface · EEG · ECoG · BCI research awards · BCI foundation

## 1 The 2022 Awards Ceremony

In October 2022, we held the Awards Ceremony in tandem with the virtual IEEE Systems, Man, and Cybernetics conference. We reviewed the 12 nominees and gave each group a certificate. Next, we announced the first, second, and third place winners. These winning teams each earned a Pfurtscheller bread knife and a cash prize (first place: $3000; second place: $2000; third place: $1000) along with the honor of winning. The main sponsor g.tec medical engineering GmbH, donated most

C. Guger (✉) · S. Rezvani
g.tec Medical Engineering GmbH, Schiedlberg, Austria
e-mail: guger@gtec.at

N. F. Ince
Department of Biomedical Engineering, University of Houston, Houston, TX, USA

M. Korostenskaja
The Institute of Neuroapproaches, Orlando, FL, USA

B. Z. Allison
Cognitive Science Department, University of California at San Diego, San Diego, CA, USA

of the awards, and we also thank IEEE Brain for donating the cash award for third place.

The BCI Award Foundation[1] has organized all of the BCI Research Awards since 2017, including the 2022 Award. The BCI Award Foundation is a non-profit organization whose main purpose is to manage the awards. g.tec medical engineering GmbH[2] is a for-profit company that produces and sells hardware and software to record and process biosignals, especially EEG, with a strong emphasis on BCIs. IEEE Brain is also a non-profit organization. According to its website,[3] its goal "is to facilitate cross-disciplinary collaboration and coordination to advance research, standardization, and development of engineering and technology to improve understanding of the brain in order to treat diseases and improve the human condition."

## 2 The 2022 Winners

Like all other BCI Awards, the 2022 nominees and winners were decided by a jury. In 2022, the head of the jury was Nuri Firat Ince. The other jury members were Nicholas Opie (winner 2021), Cynthia Chestek, Dora Hermes, Guiseppe Pellizzer, David Moses, and Abdelkader N. Belkacem. We announced the winners in October 2022, who were:

**First Place Winner:**
**Digital Bridge To Restore Voluntary Control Of Leg Movements After Paralysis**

Andrea Galvez [1–3], Guillaume Charvet[4], Jocelyne Bloch[1–3], Grégoire Courtine[1–3], Henri Lorach[1–3]

*1 NeuroX Institute, School of Life Sciences, Ecole Polytechnique Fédérale de Lausanne (EPFL), Geneve, Switzerland*
*2 Department of Clinical Neuroscience, Lausanne University Hospital (CHUV) and University of Lausanne (UNIL), Lausanne, Switzerland*
*3 .NeuroRestore, Defitech Center for Interventional Neurotherapies, EPFL/CHUV/ UNIL, Lausanne, Switzerland*
*4 University Grenoble Alpes, CEA, LETI, Clinatec, Grenoble, France*

**First Second Place Winner:**
**A High-Performance Intracortical Speech BCI**

Francis R. Willett[1, 2], Chaofei Fan[1], Erin Kunz[1], Donald T. Avansino[1], Foram Kamdar[1], Leigh R. Hochberg[3], Krishna V. Shenoy[1, 2], Jaimie M. Henderson[1]

---

1 Stanford University, USA

2 Howard Hughes Medical Institute, USA

3 Brown University, Harvard Medical School, Massachusetts General Hospital, Providence VA Medical Center, USA

**Second Second Place Winner:**
**Brain-Body Interfaces To Assist and Restore Motor Functions In People With Paralysis**

Elena Losanno[1], Marion Badi[2], Evgenia Roussinova[2], Andrew Bogaard[3], Maude Delacombaz[3], Solaiman Shokur[2], Silvestro Micera[1, 2]

1 The Biorobotics Institute and Department of Excellence in Robotics and AI, Scuola Superiore Sant'Anna, 56025 Pisa, Italy

2 Bertarelli Foundation Chair in Translational Neuroengineering, Center for Neuroprosthetics and Institute of Bioengineering, École Polytechnique Fédérale de Lausanne (EPFL), 1015 Lausanne, Switzerland

3 Department of Neuroscience and Movement Sciences, Platform of Translational Neurosciences, Section of Medicine, Faculty of Sciences and Medicine, University of Fribourg, 1700 Fribourg, Switzerland

**Third Place Winner:**
**Highly Generalizable Spelling Using a Silent-Speech BCI in a Person With Severe Anarthria**

Sean L. Metzger[1–3], Jessie R. Liu[1–3], David A. Moses[1, 2], Maximilian E. Dougherty[1], Margaret P. Seaton[1], Kaylo T. Littlejohn[1, 2, 4], Josh Chartier[1, 2], Gopala K. Anumanchipalli[1, 2, 4], Adelyn Tu-Chan[5], Karunesh Ganguly[2, 5], Edward F. Chang[1–3]

1 Department. of Neurological Surgery University of California, San Francisco (UCSF), USA

2 Weill Institute for Neurosciences UCSF, USA

3 University of California, Berkeley-UCSF Grad. Program in Bioengineering, USA

4 Department. of Electrical Engr. and C.S., University of California, Berkeley, USA

5 Department of Neurology, UCSF, USA

The 2022 Awards were slightly unusual because we had a tie for second place. Thus, we have four winning teams to congratulate instead of the usual three, along with the other nominees. With over 100 submissions to the 2022 BCI Award, getting nominated was especially challenging and reflects work that stood out to our jury. We are grateful to everyone who submitted a project, as well as our jury and sponsors. Across all four of the winning projects, one team member gave a talk at the g.tec BCI & Neurotechnology Spring School 2023 in front of over 5000 people, followed by discussion and Q&A with the attendees.

## 3 Directions and Trends Reflected in the Awards

The primary goal of the Awards is to recognize and encourage top-quality BCI research. The Awards also provide a lens to study BCI research trends. Each submission to each annual Award has different characteristics, such as the type of brain imaging approach used or the project's main intended application. Our discussion chapters have typically entailed review and discussion of what we can learn about overall trends in BCI R&D from these characteristics.

For example, one characteristic that has remained fairly consistent every year is that the EEG is the dominant imaging approach. This was even more pronounced in 2022; 77.6% of all submissions relied on the EEG, which is 5% more than the average of prior years. Among other non-invasive techniques, relative to prior years, NIRS was more prominent, whereas fewer submissions used MEG and fMRI. ECoG remained the most prominent invasive approach with a slight increase over the average of prior years. For the first time, stereo EEG was used in submissions. Three of the submissions used stereo EEG (which is an invasive technique). We also had one submission that relied primarily on spinal cord stimulation as well as other methods.

Another sustained trend since 2010 has been the combination of BCIs with other devices. The projects that were nominated in 2022 have combined BCI technology with exoskeletons, functional electrical stimulators, head-mounted displays, immersive avatars, transcranial magnetic stimulation, and other devices. BCIs may be hybridized with other devices even more often in the near future. This combination creates substantial extra challenges, but can lead to a complete system that is much more capable than a BCI by itself.

Submissions and nominees have usually involved groups from different countries. This hasn't changed much over the years, with many contributions involving the EU, US, Canada, China, and Japan. Similarly, most projects we saw for the BCI Awards came from groups with a range of different disciplines. These international and interdisciplinary features are also prominent elsewhere in the BCI community. Many of the most influential papers and projects have required extensive collaboration among different types of experts.

We have developed two tables to review the categories of the projects that were submitted. N reflects the number of submissions, and numbers in different cells present the percentage of submissions in a certain category. Each table both presents the average percentage of the last years' submissions under a certain category and that of the year 2022.

Table 1 shows that the input signals used for BCIs that were submitted to the BCI Research Awards haven't changed much over the past decade. EEG has remained the dominant tool to image the brain. Other non-invasive approaches—fMRI and NIRS—are used in some submissions but are much less common. Invasive methods like ECoG and Stereo EEG are also used in some submissions. While Stereo EEG is new in 2022, ECoG has been used in almost 10% of all submissions. All of these trends are also consistent with broader activity in BCI research and development.

**Table 1** Input signals for the BCI system

|  | Average of last years | BCI Award 2022, % (N = 103) |
|---|---|---|
| EEG | 72.6 | 77.6 |
| fMRI | 3.2 | 0.9 |
| ECoG | 9.1 | 11.6 |
| NIRS | 2.3 | 4.8 |
| Stereo EEG | – | 2.9 |
| MEG | 0.6 | 0.9 |
| Neural Control of Spinal Cord Stimulation | – | 0.9 |

Table 2 presents the outputs and applications submitted to the awards, both in 2022 and an average of all submissions. Some medical applications are more prominent in 2022, as are BCIs for art and creative applications. 2022 was the first year that projects were submitted that focused on BCIs for new electrodes/caps, neuromodulation, and assistive hearing. On the other hand, 2022 saw a decrease in BCIs centered on stroke or multiple sclerosis, with no submissions that centered on ethics or mechanical ventilation.

## 4 Overview of Other Changes with the Awards

What has and hasn't changed since the first BCI Research Award in 2010? We switched from one to three winners in 2014, increased the cash awards, and added other prizes. In the 2016 awards, we switched from 10 to 12 nominees each year. We established the BCI Foundation in 2017 to administer the awards.

We decided to switch to an online format for the BCI Research Awards ceremonies due to COVID.

The publisher of these books has been the same every year except the first year. InTech Open published the first book devoted to the BCI Research Awards [1], and its first chapter from that book is available online at no cost.[4] The second and subsequent BCI Research Awards were covered in books with Springer Publishing in this "A State-of-the-Art Summary" series [2].

Early books in this series just had an introduction, discussion, and chapters written by the nominees. We've tried some different chapter types over the years, such as interviews with winners [3]. We've also recorded interviews with nominees, which can be found on the BCI Award website.

We introduced some new components in 2022. Nominees from the 2022 Awards were invited to discuss their work on a NeuroCareers podcast hosted by author MK. This was the first year we did so, since these podcasts are new. The 2022

---

[4]https://www.intechopen.com/chapters/13501

**Table 2** Output systems and applications

|  | Average of last years | BCI Award 2022, % (N = 103) |
|---|---|---|
| Platform Technology Algorithm | 17.9 | 29.1 |
| Stroke Multiple Sclerosis | 11.4 | 3.9 |
| Wheelchairs Robots Prosthetics | 10.1 | 8.7 |
| Spelling Speech Decoding | 12.3 | 8.7 |
| Game Internet Surfing | 4.8 | 6.8 |
| Learning | 3.2 | 0.9 |
| Virtual Reality | 4.8 | 6.8 |
| Monitoring DOC | 4.7 | 1.9 |
| Stimulation | 2.3 | 7.8 |
| Authentication, Speech Assessment | 6.3 | 1.9 |
| Connectivity | 1.9 | 0.9 |
| Art (Installation, Dance, Painting, Music) | 2.2 | 13.6 |
| Designing new electrodes or caps for existing BCIs | – | 1.9 |
| Epilepsy, Parkinson, Tourette's, Autism, schizophernia | 2.6 | 10.7 |
| Depression, Fatigue, ADHD, pain, Substance use disorder | 2.8 | 3.9 |
| Neuromodulation | – | 1.9 |
| Emotion Recognition, Stress Management, Neuromarketing | 1.7 | 7.8 |
| Ethics | 1.4 | – |
| Attention | 4.2 | 0.9 |
| Mechanical ventilation | 1.6 | – |
| Assistive hearing device | – | 0.9 |

Awards were also first in that we invited all nominees to give a talk at GTEC's annual Spring School. The 2023 Spring School drew over 15,000 attendees from over 100 countries. It was thus not only the biggest Spring School but also the biggest event in the history of BCIs in terms of the number of attendees. In this discussion chapter, we also resumed our discussion of trends that we had in several earlier books.

On the other hand, the BCI Research Award hasn't changed many core components. The overall timing, we follow each year, judging criteria, jury selection procedure, and other elements haven't changed. The juries have always had 5–8
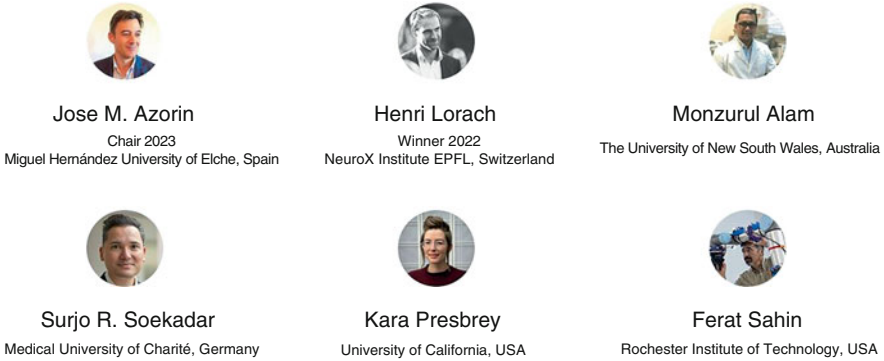
**Fig. 1** The jury for the 2023 BCI Research Awards

BCI experts with expertise in different facets of BCIs. We also haven't changed our goals with the BCI Research Awards. Since they began, the Awards were meant to recognize, publicize, and encourage high-quality BCI research from anywhere in the world.

## 5   Next Year's Award and Conclusion

As of this writing (August 2022), we have selected the jury for the 2023 BCI Research Awards. Figure 1 shows that the 2023 jury has six BCI practitioners, most of whom are experienced with BCI Research Awards.

Like most years, our jury includes a member of the team that won first place the preceding year. This time, that team member is Dr. Henri Lorach, who has a chapter in this book about his first place award. The chair of the jury, Jose M. Azorin, is a professor at the University of Elche in the Alicante region of Spain known for his outstanding work using BCIs and exoskeletons for gait rehabilitation with BCIs [4, 5].

We also announced the key dates for the 2023 awards:

1. Submission deadline: September 1st
2. Announcement of nominees: September 14th
3. Oral presentations from nominees and the BCI Award Ceremony: October 3rd

We will host the 2023 Award Ceremony online at an IEEE conference, like we did in 2020–2022. The 2023 conference will be organized through an IEEE Systems, Man, and Cybernetics conference. This conference[5] will be hosted virtually from Hawaii, United States from October 1–4. The conference will also feature numerous workshops and other activities involving BCI/BMI.

---

[5] https://ieeesmc2023.org/

Next year's BCI Research Award should also feature a new book with next year's projects. As more and more people study BCIs, awards and books like these should become more useful to broader audiences. Students, teachers, makers, medical experts, futurists, ethicists, and many other groups will want to learn more about different approaches to BCIs for new patient groups and applications.

## References

1. Guger C, Bin G, Gao X, Guo J, Hong B, Liu T (2011) State-of-the-art in BCI research: BCI Award 2010. INTECH Open Access Publisher
2. Guger C, Allison BZ, Edlinger G (2013) Brain-computer interface research: a state-of-the-art summary. Springer, Berlin
3. Guger C, Allison BZ, Miller K (2020) Highlights and interviews with winners. In: Brain–computer interface research. Springer, Cham, pp 107–121
4. He Y, Eguren D, Azorín JM, Grossman RG, Luu TP, Contreras-Vidal JL (2018) Brain–machine interfaces for controlling lower-limb powered robotic systems. J Neural Eng 15(2):021004
5. Ortiz M, Ferrero L, Iáñez E, Azorín JM, Contreras-Vidal JL (2020) Sensory integration in human movement: a new brain-machine interface based on gamma band and attention level for controlling a lower-limb exoskeleton. Front Bioeng Biotechnol 8:735